

# Neural Parameter Estimation with Incomplete Data

Matthew Sainsbury-Dale<sup>1</sup>, Andrew Zammit-Mangion<sup>2,3</sup>, Noel Cressie<sup>3</sup>, and  
Raphaël Huser<sup>1</sup>

<sup>1</sup>Statistics Program, Computer, Electrical and Mathematical Sciences and Engineering Division,  
King Abdullah University of Science and Technology (KAUST), Saudi Arabia

<sup>2</sup>School of Mathematics and Statistics, University of New South Wales, Australia

<sup>3</sup>School of Mathematics and Applied Statistics, University of Wollongong, Australia

## Abstract

Advances in artificial intelligence (AI) and deep learning have led to neural networks being used to generate lightning-speed answers to complex science questions, paintings in the style of Monet, or stories like those of Twain. Leveraging their computational speed and flexibility, neural networks are also being used to facilitate fast, likelihood-free statistical inference. However, it is not straightforward to use neural networks with data that for various reasons are incomplete, which precludes their use in many applications. A recently proposed approach to remedy this issue uses an appropriately padded data vector and a vector that encodes the missingness pattern as input to a neural network. While computationally efficient, this “masking” approach is not robust to the missingness mechanism and can result in statistically inefficient inferences. Here, we propose an alternative approach that is based on the Monte Carlo expectation-maximization (EM) algorithm. Our EM approach is likelihood-free, substantially faster than the conventional EM algorithm as it does not require numerical optimization at each iteration, and more statistically efficient than the masking approach. This research addresses a prototypical problem that asks how improvements could be made in AI by introducing Bayesian statistical thinking. We compare the two approaches to missingness using simulated incomplete data from a variety of spatial models. The utility of the methodology is shown on Arctic sea-ice data, analyzed using a novel hidden Potts model with an intractable likelihood.

**Keywords:** amortized inference, likelihood-free inference, Monte Carlo EM algorithm, neural Bayes estimator, simulation-based inference

## 1 Introduction

Artificial intelligence (AI) and deep learning have spurred significant advancements in recent years, revolutionizing fields ranging from image recognition to natural language processing, and enabling transformative technologies like ChatGPT (OpenAI, 2025). These breakthroughs are profoundly influencing how we work, communicate, and create, leaving

an indelible mark on society. In parallel, the last decade has seen growing interest in the adoption of neural networks for simulation-based inference, which is often used in statistical or physical models for which the likelihood function is unavailable or computationally intractable (Diggle and Gratton, 1984; Tavaré et al., 1997; Cranmer et al., 2020). Neural networks are being used to approximate the likelihood function (e.g., Papamakarios et al., 2019), the likelihood-to-evidence ratio (e.g., Hermans et al., 2020; Thomas et al., 2022; Walchessen et al., 2024), and the posterior distribution (e.g., Greenberg et al., 2019; Gonçalves et al., 2020; Radev et al., 2022); see Zammit-Mangion et al. (2025) for a recent review. In this work, we consider neural Bayes estimators (NBEs; Sainsbury-Dale et al., 2024), which are neural networks that map data to a point summary of the posterior distribution. These estimators are amortized, in the sense that, after an initial set-up cost, inference from observed data can be made in a fraction of the time required by conventional approaches. NBEs have been used to make fast inference with models for population genetics (Flagel et al., 2018), financial options (Hernandez, 2017; Horvath et al., 2021; Coloma and Kleiber, 2025), cognitive processes (Pan et al., 2025), point processes (Lambe et al., 2025), spatial processes (Gerber and Nychka, 2021; Banesh et al., 2021; Lenzi et al., 2023; Richards et al., 2024; Sainsbury-Dale et al., 2024, 2025; Tsyrlunikov and Sotskiy, 2024; Villazón et al., 2025; Wang and Genton, 2024), and spatio-temporal processes (Dell’Oro and Gaetan, 2025).

NBEs represent a promising approach to inference, yet significant challenges remain that hinder their widespread adoption. One of the key challenges is their application to the often-encountered “incomplete data” setting, where the structure of the available data renders the use of conventional neural networks problematic. Consider, for instance, remote-sensing data collected over a regular grid. If all pixels are observed (i.e., no data are missing), one can readily construct an NBE of a geophysical parameter using a standard convolutional neural network (CNN). However, this parsimonious, efficient architecture cannot be used directly if data are missing (e.g., due to cloud cover). Similarly, in medical and health applications, incomplete data often arise in electronic health records, where patients may have missing clinical or demographic information, or in clinical trials, where participants may drop out or miss scheduled evaluations. In these scenarios, the application of NBEs requires novel methods to handle incomplete data in a statistically principled manner.

A recently proposed method for handling missing data involves “masking” (Wang et al., 2024; Gloeckler et al., 2024). In this approach, the neural network takes as input the data completed with missing elements replaced by zero (or some other fixed constant) and a binary vector encoding the missingness pattern. Although computationally efficient, the masking approach has some drawbacks. For instance, incorporating the missingness pattern as an additional input results in a more challenging learning task. Further, the approach necessitates a stochastic model for the missingness mechanism and, as we will show, misspecification of this model can lead to biased and suboptimal inference.

Statistical efficiency is as important as computational efficiency, and in this research we consider both in a prototype problem that indicates where improvements could be made in AI by introducing statistical inferential tools. Specifically, we propose to facilitate the use of NBEs in the presence of missing data by leveraging methods developed for incomplete-data problems, where the data are challenging to analyze directly but their analysis becomes tractable through appropriate data augmentation. Several algorithms have been developed to address such problems, among which the most prominent are the expectation-

maximization (EM) algorithm for maximum-likelihood or maximum-a-posteriori (MAP) estimation (Dempster et al., 1977) and the data-augmentation algorithm for posterior sampling (Tanner and Wong, 1987). These approaches exploit likelihood functions or posterior distributions, respectively, that are intractable for the observed incomplete data but tractable under data augmentation. There is a strong parallel between the classical incomplete-data problem and that faced in neural inference: there are situations where neural-network architectures are complex or unavailable for observed incomplete data, but they are simpler, more parsimonious, and easier to train, under data augmentation. Note that in machine learning, “data augmentation” typically refers to methods that artificially increase the amount of data used to train neural networks; instead, we use it exclusively here to refer to the process of augmenting data with latent random variables.

Building on this connection between classical and neural inference, we introduce an implementation of NBEs for incomplete data using data augmentation. Specifically, we develop a type of Monte Carlo EM (MCEM) algorithm (Wei and Tanner, 1990) where, after conditional simulation of the missing data, the remaining components of the usual E- and M-steps are obtained almost instantaneously with an NBE trained to approximate the MAP estimator. MAP estimators are prominent in areas as diverse as image analysis (Hardie et al., 2004) and plant breeding (Montesinos-López et al., 2020). Our EM approach to neural Bayes estimation is likelihood-free, in the sense that it does not require evaluation of the likelihood function, and it does not require numerical optimization at each iteration, making it much faster than the classical EM algorithm. Critically, the NBE is trained on, and applied to, complete data only, which we show alleviates the drawbacks of the masking approach discussed above. Although our EM approach applies to a narrower class of models and is computationally slower than the masking approach, it provides stronger statistical guarantees; this trade-off clearly emerges in our simulation studies. Both methods have been incorporated into the user-friendly open-source software package **NeuralEstimators** (Sainsbury-Dale, 2024), which is available in `Julia` and `R`.

The remainder of this article is organized as follows. In Section 2, we review NBEs, discuss and give new insights into the masking approach of Wang et al. (2024), and introduce our EM approach. In Section 3, we conduct simulation studies to investigate the strengths and weaknesses of these two approaches for dealing with missing data. In Section 4, we apply our methodology to an analysis of Arctic sea-ice data. Finally, in Section 5 we give conclusions and outline avenues for future research. Supplementary material is also available that contains additional theoretical details, simulations, and figures. Code that reproduces all results in the manuscript is available from <https://github.com/msainsburydale/NeuralIncompleteData>.

## 2 Methodology

In Section 2.1, we review NBEs. (For a more comprehensive introduction, see Sainsbury-Dale et al., 2024, and Zammit-Mangion et al., 2025.) In Section 2.2, we present the masking approach for missing data and, in Section 2.3, we describe our novel approach based on MCEM.

## 2.1 Neural Bayes estimators

The goal of parametric point estimation is to estimate a  $d$ -dimensional parameter  $\boldsymbol{\theta} \in \Theta$  from data  $\mathbf{Z} \in \mathcal{Z}$  using an estimator,  $\hat{\boldsymbol{\theta}} : \mathcal{Z} \rightarrow \Theta$ . For ease of exposition, we let  $\Theta \subseteq \mathbb{R}^d$  and  $\mathcal{Z} \subseteq \mathbb{R}^n$ , although the approaches we describe generalize to other spaces. A ubiquitous decision-theoretic approach to the construction of estimators is based on average-risk optimality (e.g., [Lehmann and Casella, 1998](#), Ch. 4; [Robert, 2007](#), Ch. 4). Consider a loss function  $L : \Theta \times \Theta \rightarrow [0, \infty)$  and, for ease of exposition, assume that the prior measure for  $\boldsymbol{\theta}$  admits a density  $\pi(\cdot)$  with respect to Lebesgue measure on  $\mathbb{R}^d$ . Then the Bayes risk of the estimator  $\hat{\boldsymbol{\theta}}(\cdot)$  is

$$r(\hat{\boldsymbol{\theta}}(\cdot)) \equiv \int_{\Theta} \int_{\mathcal{Z}} L(\boldsymbol{\theta}, \hat{\boldsymbol{\theta}}(\mathbf{z})) p_{\mathbf{Z}|\boldsymbol{\theta}}(\mathbf{z} | \boldsymbol{\theta}) \pi(\boldsymbol{\theta}) d\mathbf{z} d\boldsymbol{\theta}, \quad (1)$$

where here and throughout, for generic random quantities  $A$  and  $B$ , we use  $p_{A|B}(\cdot | \cdot)$  to denote the conditional probability density or mass function of  $A$  given  $B$ , and  $p_A(\cdot)$  for the corresponding marginal. When clear from context, we omit subscripts for brevity. A minimizer of (1) is said to be a Bayes estimator with respect to  $L(\cdot, \cdot)$  and  $\pi(\cdot)$ .

Bayes estimators are functionals of the posterior distribution (e.g., the posterior mean under quadratic loss) and are often unavailable in closed form. However, since estimators are mappings from the sample space  $\mathcal{Z}$  to the parameter space  $\Theta$ , Bayes estimators could, in principle, be approximated well by a sufficiently flexible function. Recently, motivated by universal-function-approximation theorems (e.g., [Hornik et al., 1989](#); [Zhou, 2020](#)) and the speed at which they can be evaluated, neural networks have been used to approximate Bayes estimators (see, e.g., [Zammit-Mangion et al., 2025](#), Sec. 3.1). Let  $\mathbf{f} : \mathcal{Z} \rightarrow \Theta$  denote a neural network parameterized by  $\boldsymbol{\gamma}$ , that is,

$$\mathbf{f}(\mathbf{Z}; \boldsymbol{\gamma}) = (\mathbf{f}_J \circ \mathbf{f}_{J-1} \circ \cdots \circ \mathbf{f}_1)(\mathbf{Z}; \boldsymbol{\gamma}), \quad \mathbf{Z} \in \mathcal{Z}, \quad (2)$$

where  $\mathbf{f}_j(\cdot; \boldsymbol{\gamma}_j)$ ,  $j = 1, \dots, J$ , are nonlinear functions parameterized by  $\boldsymbol{\gamma}_j$ , and ‘ $\circ$ ’ denotes function composition. Throughout, we use  $\boldsymbol{\gamma} = (\boldsymbol{\gamma}_1^\top, \dots, \boldsymbol{\gamma}_J^\top)^\top \in \Gamma$  to denote generic neural-network parameters, although the number of parameters varies depending on context. Then, a Bayes estimator may be approximated by substituting

$$\boldsymbol{\gamma}^* \equiv \arg \min_{\boldsymbol{\gamma} \in \Gamma} \frac{1}{K} \sum_{k=1}^K L\{\boldsymbol{\theta}^{(k)}, \mathbf{f}(\mathbf{Z}^{(k)}; \boldsymbol{\gamma})\} \quad (3)$$

into (2) where, independently for each  $k$ ,  $\boldsymbol{\theta}^{(k)} \sim \pi(\boldsymbol{\theta})$  and  $\mathbf{Z}^{(k)} \sim p(\mathbf{Z} | \boldsymbol{\theta}^{(k)})$ . The process of performing the optimization task (3) on neural-network parameters  $\boldsymbol{\gamma}$  given in (2) is referred to as “training the network”, and this can be done efficiently using back-propagation and stochastic gradient descent ([Goodfellow et al., 2016](#)).

The trained neural network  $\mathbf{f}(\cdot; \boldsymbol{\gamma}^*)$  minimizes the approximate Bayes risk, and therefore it is called an NBE. Once trained, an NBE can be applied repeatedly to data sets that are realizations from the statistical model used for training, at a fraction of the computational cost of conventional inferential methods. It is therefore ideal to use an NBE in settings where inference needs to be made repeatedly; in this case, the initial training cost is said to be *amortized* over time.

Although (3) is written for a fixed training set of size  $K$ , in practice one often uses “on-the-fly” simulation, continually generating fresh parameter–data pairs  $\boldsymbol{\theta}^{(k)}$  and  $\mathbf{Z}^{(k)}$  during training. In that regime, the number  $K$  of such pairs need not be specified at all. However, with a fixed training set,  $K$  becomes an important hyperparameter that typically needs to be increased with the dimension  $d$  of  $\boldsymbol{\theta}$  and the tail-heaviness of the statistical model (Rödder et al., 2025). By contrast, when using parsimonious architectures that exploit the structure of the data (see below), the dimension  $n$  of  $\mathbf{Z}$  does not usually drive the choice of  $K$ , since parameter sharing and invariances in neural networks tend to reduce the effective dimensionality of the learning problem.

When constructing an NBE, a central consideration in designing the neural-network architecture (i.e., the functional form of (2)) is the underlying structure of the data. For example, if the data are gridded, a CNN is typically used, while for unstructured data, one typically adopts a classical multilayer perceptron (MLP). When the data are exchangeable, frameworks such as DeepSets (Zaheer et al., 2017) adapt these standard architectures in a manner that parsimoniously exploits exchangeability. However, beyond these general guidelines, the specific design of the network (e.g., depth, width, activation functions) and the choice of training-related hyperparameters (e.g., learning rate) typically require experimentation, tuning and, in some cases, automated search methods (see, e.g., Elsken et al., 2019). While Rödder et al. (2025) take important first steps in developing theory for the case of a single-layer perceptron applied to replicated data, extending such results to the richer classes of architectures commonly used in practice remains a challenge. Fortunately, once a suitable architecture is found, it often generalizes well across models, as demonstrated by our simulation experiments in Section 3.

As discussed in Section 1, the standard architectures outlined above do not naturally cater for missing data, and this has limited the applicability of neural Bayes estimation. Next, we discuss two approaches that address this challenge.

## 2.2 The masking approach for missing data

Data are often incomplete, and hence inference on  $\boldsymbol{\theta}$  is made using only a subset of  $\mathbf{Z}$ . For a given  $\mathbf{Z} \equiv (Z_1, \dots, Z_n)^\top$ , we denote the subvectors of observed and missing elements as  $\mathbf{Z}_1$  and  $\mathbf{Z}_2$ , respectively. We use  $\mathcal{I}_1 \equiv \{i : Z_i \text{ is observed}\}$  to denote the ordered set of indices corresponding to the observed component, so that  $\mathbf{Z}_1 \equiv (Z_i : i \in \mathcal{I}_1)^\top$ .

The masking approach we present in this section closely follows that of Wang et al. (2024), who applied it in the context of approximate posterior inference. Their approach consists of first constructing a masked version of  $\mathbf{Z}$ , denoted by  $\mathbf{U} \in \mathcal{U} \subseteq \mathbb{R}^n$ , with components

$$\begin{aligned} \mathbf{U}_1 &\equiv (U_i : i \in \mathcal{I}_1)^\top = \mathbf{Z}_1, \\ \mathbf{U}_2 &\equiv (U_i : i \in \mathcal{I}_2)^\top = c\mathbf{1}, \end{aligned} \tag{4}$$

where  $\mathcal{I}_2 \equiv \{1, \dots, n\} \setminus \mathcal{I}_1$ ,  $c \in \mathbb{R}$  is fixed (we set  $c = 0$  throughout), and  $\mathbf{1}$  denotes a vector of 1s of appropriate dimension. Now, define a vector of indicator variables,  $\mathbf{W} \in \mathcal{W} = \{0, 1\}^n$ , as follows:

$$\mathbf{W} \equiv (\mathbb{I}(i \in \mathcal{I}_1) : i = 1, \dots, n)^\top, \tag{5}$$

---

**Algorithm 1** The masking approach to neural Bayes estimation with missing data.

---

**Training stage** (slow, to be done only once offline)

**Require:** Prior  $\pi(\boldsymbol{\theta})$ , number of training samples  $K$ , probability models  $p(\mathcal{I}_1 \mid \boldsymbol{\theta})$  and  $p(\mathbf{Z} \mid \boldsymbol{\theta})$ ,  $c \in \mathbb{R}$  for use in (4), loss function  $L : \Theta \times \Theta \rightarrow [0, \infty)$ , neural network  $\mathbf{g} : \mathcal{U} \times \mathcal{W} \rightarrow \Theta$  parameterized by  $\gamma$ .

- 1: **for**  $k = 1, \dots, K$  **do**
- 2:   Sample parameters  $\boldsymbol{\theta}^{(k)} \sim \pi(\boldsymbol{\theta})$ .
- 3:   Simulate data  $\mathbf{Z}^{(k)} \sim p(\mathbf{Z} \mid \boldsymbol{\theta}^{(k)})$ .
- 4:   Sample indices  $\mathcal{I}_1^{(k)} \sim p(\mathcal{I}_1 \mid \boldsymbol{\theta}^{(k)})$ .
- 5:   Subset  $\mathbf{Z}_1^{(k)} \equiv (Z_i^{(k)} : i \in \mathcal{I}_1^{(k)})^\top$ .
- 6:   Compute  $\mathbf{U}^{(k)}$  using (4).
- 7:   Compute  $\mathbf{W}^{(k)}$  using (5).
- 8: **end for**
- 9: Solve  $\gamma^* \equiv \operatorname{argmin}_\gamma \sum_{k=1}^K L\{\boldsymbol{\theta}^{(k)}, \mathbf{g}(\mathbf{U}^{(k)}, \mathbf{W}^{(k)}; \gamma)\}$  to obtain the masking NBE,  $\mathbf{g}(\cdot, \cdot; \gamma^*)$ .

**Estimation stage** (fast, repeatable for arbitrarily many observed data sets)

**Require:** Observed data  $\mathbf{Z}_1$  and  $\mathcal{I}_1$ ,  $c \in \mathbb{R}$  for use in (4).

- 1: Compute  $\mathbf{U}$  using (4).
  - 2: Compute  $\mathbf{W}$  using (5).
  - 3: Return  $\mathbf{g}(\mathbf{U}, \mathbf{W}; \gamma^*)$ .
- 

where  $\mathbb{I}(\cdot)$  denotes the indicator function. While  $\mathbf{Z}_1$  and  $\mathcal{I}_1$  have a dimension that might vary across different observed data sets, the quantities  $\mathbf{U}$  and  $\mathbf{W}$  are each of fixed dimension  $n$ , which enables the use of parsimonious, efficient neural-network architectures.

An NBE based on the masking approach is constructed by first defining

$$\mathbf{g}(\mathbf{U}, \mathbf{W}; \gamma), \text{ for } \mathbf{U} \in \mathcal{U}, \mathbf{W} \in \mathcal{W}, \quad (6)$$

where  $\mathbf{g}(\cdot, \cdot; \gamma)$  is a neural network parameterized by  $\gamma \in \Gamma$ . Then, substitute

$$\gamma^* \equiv \operatorname{argmin}_{\gamma \in \Gamma} \sum_{k=1}^K L\{\boldsymbol{\theta}^{(k)}, \mathbf{g}(\mathbf{U}^{(k)}, \mathbf{W}^{(k)}; \gamma)\} \quad (7)$$

into (6), where  $\boldsymbol{\theta}^{(k)} \sim \pi(\boldsymbol{\theta})$  and, independently for each  $k$ ,  $\mathbf{U}^{(k)}$  and  $\mathbf{W}^{(k)}$  are constructed by first sampling indices  $\mathcal{I}_1^{(k)}$  from a model  $p(\mathcal{I}_1 \mid \boldsymbol{\theta}^{(k)})$  for the missingness mechanism, simulating complete data  $\mathbf{Z}^{(k)} \sim p(\mathbf{Z} \mid \boldsymbol{\theta}^{(k)})$ , subsetting  $\mathbf{Z}_1^{(k)} \equiv (Z_i^{(k)} : i \in \mathcal{I}_1^{(k)})^\top$ , and substituting these quantities into (4) and (5). We note that for some models it may be possible to directly simulate incomplete data. Further, as discussed in Section 2.1, rather than fixing  $K$ , one may simulate parameter–data pairs and missingness patterns on-the-fly. Once trained, the neural network can be used repeatedly to estimate parameters from new incomplete data sets. Algorithm 1 summarizes the approach, and Figure 1 illustrates its Estimation stage.

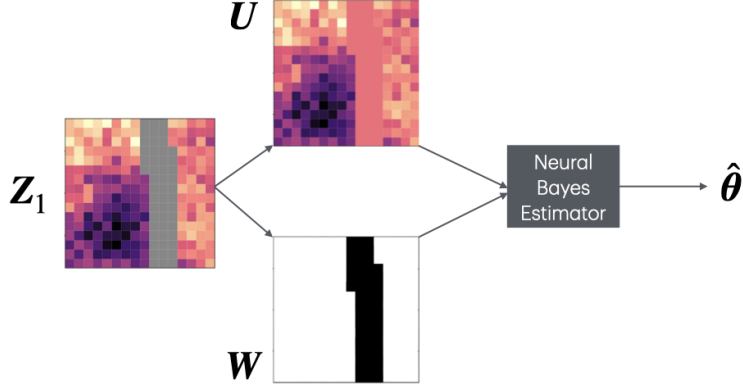


Figure 1: The Estimation stage of Algorithm 1. Observed data  $\mathbf{Z}_1$ , and the associated indices  $\mathcal{I}_1$  (here, implicit) that identify which elements of  $\mathbf{Z}$  are observed, are used to construct  $\mathbf{U}$ , a masked version of the complete data  $\mathbf{Z}$  with missing entries replaced by a constant  $c \in \mathbb{R}$ , and  $\mathbf{W}$ , a vector of indicator variables that encode the missingness pattern. The encoded data  $\mathbf{U}$  and  $\mathbf{W}$  are then input to an NBE to obtain point estimates  $\hat{\theta}$  of a model parameter  $\theta$ .

Algorithm 1 has a number of strengths. It only requires simulation from  $p(\mathcal{I}_1 | \theta)$  and  $p(\mathbf{Z} | \theta)$ , and no information on  $\theta$  is lost by using  $\mathbf{U}$  and  $\mathbf{W}$  instead of  $\mathbf{Z}_1$  and  $\mathcal{I}_1$ , since there is a one-to-one mapping between these quantities (see Theorem 1 in Section S1 of the Supplementary Material). However, the approach has two drawbacks. First, the neural network must learn a mapping from  $\mathcal{U} \times \mathcal{W}$  to  $\Theta$ . This learning task can be more challenging than learning a mapping from  $\mathcal{Z}$  to  $\Theta$ , since an element in  $\mathcal{U} \times \mathcal{W}$  is semi-discrete and of dimension  $2n$ . Second, the quality of the fit is subject to a judicious choice of the missingness model. To see this, rewrite the Bayes risk (1) in terms of an estimator  $\hat{\theta}(\cdot, \cdot)$  treating  $\mathbf{U}$  and  $\mathbf{W}$  as the data:

$$r(\hat{\theta}(\cdot, \cdot)) \equiv \sum_{\mathbf{w} \in \mathcal{W}} \int_{\Theta} \int_{\mathcal{U}} L(\theta, \hat{\theta}(\mathbf{u}, \mathbf{w})) p_{\mathbf{U}, \mathbf{W} | \theta}(\mathbf{u}, \mathbf{w} | \theta) \pi(\theta) d\mathbf{u} d\theta. \quad (8)$$

It is a straightforward corollary of Theorem 1 in Section S1 of the Supplementary Material and Bayesian sufficiency (e.g., Cox and Hinkley, 1974, Ch. 2) that a Bayes estimator that minimizes (8) also minimizes the Bayes risk defined in terms of  $\mathbf{Z}_1$  and  $\mathcal{I}_1$ . Further, under the assumption that  $\mathcal{I}_1$  is independent of  $\theta$ , which is often reasonable in practice, a Bayes estimator that minimizes (8) is invariant to distributions on  $\mathcal{I}_1$  that are positive on the power set of  $\{1, \dots, n\}$  (see Theorem 2 in Section S1 of the Supplementary Material). However, in practice, the empirical analogue of (8), given by the sum on the right-hand-side of (7), is subject to Monte Carlo error that depends on the chosen distribution for  $\mathcal{I}_1$ . Therefore, the choice of distribution has practical implications on the approximation of the Bayes estimator obtained by substituting (7) into (6), particularly in high-dimensional settings where the total number of possible missingness patterns ( $2^n$ ) is large and the missingness mechanism is difficult to specify. In Section 3, we show through simulation that selecting a distribution for  $\mathcal{I}_1$  that assigns low probability to the observed missingness pattern can lead to statistically inefficient and biased estimators.

To address these limitations, in this paper we propose an alternative statistical approach to neural Bayes estimation with incomplete data. Our approach does not require the missingness pattern to be an input to the neural network, or the specification of a missingness mechanism. We do this by embedding neural networks in a classical data-augmentation approach to solving incomplete-data problems, namely an MCEM algorithm.

## 2.3 The EM approach for missing data

In Section 2.3.1, we provide an overview of the classical EM algorithm and its Monte Carlo version. In Section 2.3.2, we outline the general structure of our proposed EM approach to neural Bayes estimation with incomplete data. In Section 2.3.3, we detail the construction of a neural approximation to the MAP estimator, which is needed for our EM approach.

### 2.3.1 The classical EM algorithm and its Monte Carlo version

Recall that we use  $\mathbf{Z}_1$  and  $\mathbf{Z}_2$  to denote the subvectors of  $\mathbf{Z}$  that are treated as observed and missing, respectively, and that we use  $\mathbf{Z}$  to denote the complete data. We also have available an ordered set of indices,  $\mathcal{I}_1$ , associated with  $\mathbf{Z}_1$ . However, since one does not need to construct a mask from these indices in our approach described below, we omit the explicit notation of these indices in this subsection.

In the classical statistics literature, many algorithms have been developed based on the “data augmentation principle”, which is applied when inference based on  $\mathbf{Z}$  is easier than inference based only on  $\mathbf{Z}_1$  (see, e.g., [Tanner and Wong, 1987](#); [van Dyk and Meng, 2001](#)). A popular approach to point estimation that follows from this principle is the EM algorithm ([Dempster et al., 1977](#); [Wu, 1983](#); [McLachlan and Krishnan, 2008](#)), an iterative algorithm for estimating  $\boldsymbol{\theta}$  with the  $l$ th iteration given by

$$\hat{\boldsymbol{\theta}}^{(l)} = M(\hat{\boldsymbol{\theta}}^{(l-1)}) \equiv \arg \max_{\boldsymbol{\theta} \in \Theta} \left\{ \log \pi(\boldsymbol{\theta}) + \mathbb{E}_{\mathbf{Z}_2 | \mathbf{Z}_1, \hat{\boldsymbol{\theta}}^{(l-1)}} \ell(\boldsymbol{\theta}; \mathbf{Z}_1, \mathbf{Z}_2) \right\}; \quad l = 1, 2, \dots, \quad (9)$$

where  $\pi(\boldsymbol{\theta})$  denotes a prior density (sometimes referred to as a penalty function) and  $\ell(\boldsymbol{\theta}; \mathbf{Z}_1, \mathbf{Z}_2) \equiv \log p(\mathbf{Z} | \boldsymbol{\theta})$  denotes the complete-data log-likelihood. The EM algorithm satisfies the ascent property, which means that the incomplete-data posterior density  $p(\boldsymbol{\theta} | \mathbf{Z}_1)$  is non-decreasing at each iteration. Thus, under mild conditions ([Boyles, 1983](#); [Wu, 1983](#); [McLachlan and Krishnan, 2008](#), Ch. 3), it yields a local maximizer of  $p(\boldsymbol{\theta} | \mathbf{Z}_1)$ . For the special case of  $\pi(\boldsymbol{\theta}) \propto 1$ , the EM algorithm increases the incomplete-data likelihood  $p(\mathbf{Z}_1 | \boldsymbol{\theta})$  at each iteration and, therefore, yields a local maximizer of  $p(\mathbf{Z}_1 | \boldsymbol{\theta})$ .

When the conditional expectation in (9) is intractable but conditional simulation is feasible, one often adopts a Monte Carlo version of the EM algorithm, MCEM ([Wei and Tanner, 1990](#); [Ruth, 2024](#)), which has as the  $l$ th iteration,

$$\hat{\boldsymbol{\theta}}^{(l)} = M_m(\boldsymbol{\theta}^{(l-1)}) \equiv \arg \max_{\boldsymbol{\theta} \in \Theta} \left\{ \log \pi(\boldsymbol{\theta}) + \frac{1}{m} \sum_{j=1}^m \ell(\boldsymbol{\theta}; \mathbf{Z}_1, \mathbf{Z}_2^{(l,j)}) \right\}, \quad (10)$$

where  $\{\mathbf{Z}_2^{(l,j)}\}_{j=1}^m$  are simulated from the conditional distribution of  $\mathbf{Z}_2 | \mathbf{Z}_1, \hat{\boldsymbol{\theta}}^{(l-1)}$ . The

frequentist MCEM algorithm is recovered as a special case of (10) by taking  $\pi(\boldsymbol{\theta}) \propto 1$ .

A practical challenge in implementing the MCEM algorithm is choosing the Monte Carlo sample size  $m$ . One way to tackle this challenge is through averaging (Fort and Moulines, 2003; Cappé et al., 2005, Sec. 11.1.2.2), where convergence assessment and final estimates are based on the averaged subsequence,

$$\bar{\boldsymbol{\theta}}_b^{(l)} \equiv \frac{1}{l-b} \sum_{t=b+1}^l \hat{\boldsymbol{\theta}}^{(t)}, \quad (11)$$

where  $b < l$  denotes a burn-in chosen such that  $\{\hat{\boldsymbol{\theta}}^{(t)} : t = b+1, \dots, l\}$  is approximately stationary. This averaging greatly reduces sensitivity to the choice of  $m$ , as Monte Carlo variability is effectively “averaged out” over multiple iterations. It is also formally motivated by the result of Chan and Ledolter (1995), that for large  $m$ , an MCEM sequence starting in a small neighborhood of a local maximizer of  $p(\boldsymbol{\theta} | \mathbf{Z}_1)$  can be approximated by a stationary first-order autoregressive (AR(1)) process centered at that maximizer. When employing averaging, the main consideration in choosing  $m$  is ensuring that the iterates become stable, in the sense that they eventually remain centered around a single point. Since the Monte Carlo variability is driven by the conditional variance  $\mathbb{V}_{\mathbf{Z}_2 | \mathbf{Z}_1, \boldsymbol{\theta}} \{\ell(\boldsymbol{\theta}; \mathbf{Z}_1, \mathbf{Z}_2)\}$ , which typically increases with both the tail-heaviness of the model and the proportion of missing data,  $m$  should be increased with both of these quantities whenever stability is a concern.

A drawback of the (MC)EM algorithm is that it can be slow since it is “doubly iterative” in the typical case where each maximization step requires numerical optimization. Although a substantial amount of work has been devoted to trying to speed up the algorithm, primarily by accelerating its rate of convergence (e.g., Louis, 1982; Meng and Rubin, 1993; Liu and Rubin, 1994; Jamshidian and Jennrich, 1997; Liu et al., 1998; Neal and Hinton, 1998; Varadhan and Roland, 2008; Lewandowski et al., 2010), computational speed remains a practical limitation in many settings. Further, although the MCEM algorithm bypasses the conditional expectation in (9), it still requires evaluation of the complete-data log-likelihood function, which is not always possible. Next, we describe how the MCEM algorithm can incorporate NBEs with incomplete data in a manner that is not subject to these limitations.

### 2.3.2 NBEs and approximate MCEM algorithms

Our EM approach to using NBEs with incomplete data is predicated on the fact that (10) is equivalent to,

$$\hat{\boldsymbol{\theta}}^{(l)} = M_m(\hat{\boldsymbol{\theta}}^{(l-1)}) = \arg \max_{\boldsymbol{\theta} \in \Theta} \left\{ \log \pi_m(\boldsymbol{\theta}) + \sum_{j=1}^m \ell(\boldsymbol{\theta}; \mathbf{Z}_1, \mathbf{Z}_2^{(l,j)}) \right\}, \quad (12)$$

where the probability density  $\pi_m(\boldsymbol{\theta}) \propto \{\pi(\boldsymbol{\theta})\}^m$ . The reformulation of (10) as (12) shows that the conventional MCEM update  $M_m(\boldsymbol{\theta})$  is a MAP estimate under a modified prior distribution, which can be approximated by an NBE (denoted by  $\mathbf{h}(\cdot)$  in (16) and fitted according to (17) in Section 2.3.3). This leads to our proposed EM approach (Algorithm 2), a fast version of the MCEM algorithm that does not require the evaluation of any likelihood

---

**Algorithm 2** The EM approach to neural Bayes estimation with missing data.

---

**Training stage** (slow, to be done only once offline)

**Require:** Prior  $\pi(\boldsymbol{\theta})$ , number of training samples  $K$ , number of Monte Carlo samples  $m$  used in the Estimation stage, probability model  $p(\mathbf{Z} \mid \boldsymbol{\theta})$ , neural network  $\mathbf{h} : \mathcal{Z}^m \rightarrow \Theta$  parameterized by  $\boldsymbol{\gamma}$ .

- 1: **for**  $k = 1, \dots, K$  **do**
- 2:     Sample parameters  $\boldsymbol{\theta}^{(k)} \sim \pi(\boldsymbol{\theta})$ .
- 3:     Simulate data  $\mathbf{Z}^{(k,j)} \sim p(\mathbf{Z} \mid \boldsymbol{\theta}^{(k)})$  for  $j = 1, \dots, m$ .
- 4: **end for**
- 5: Solve  $\boldsymbol{\gamma}^* \equiv \operatorname{argmin}_{\boldsymbol{\gamma}} \sum_{k=1}^K \{\pi(\boldsymbol{\theta}^{(k)})\}^{m-1} L\{\boldsymbol{\theta}^{(k)}, \mathbf{h}(\{\mathbf{Z}^{(k,j)}\}_{j=1}^m; \boldsymbol{\gamma})\}$  (see (17)) with  $L(\cdot, \cdot)$  a continuous and almost-everywhere differentiable approximation of the 0–1 loss function (e.g., (15)), to obtain the NBE,  $\mathbf{h}(\cdot; \boldsymbol{\gamma}^*)$ , that approximates the MAP estimator.

**Estimation stage** (fast, repeatable for arbitrarily many observed data sets)

**Require:** Observed data  $\mathbf{Z}_1$ , number of Monte Carlo samples  $m$ , initial estimates  $\hat{\boldsymbol{\theta}}^{(0)}$ , convergence criterion, burn-in  $b$ , maximum number of iterations, algorithm to simulate from the conditional distribution  $p(\mathbf{Z}_2 \mid \mathbf{Z}_1, \boldsymbol{\theta})$ .

- 1: Set  $l = 0$ .
  - 2: **repeat**
  - 3:     Set  $l = l + 1$ .
  - 4:     Simulate missing data  $\mathbf{Z}_2^{(l,j)} \sim p(\mathbf{Z}_2 \mid \mathbf{Z}_1, \hat{\boldsymbol{\theta}}^{(l-1)})$ ,  $j = 1, \dots, m$ , resulting in  $m$  conditionally independent replicates of the completed data,  $\{\mathbf{Z}^{(l,j)}\}_{j=1}^m$ .
  - 5:     Update  $\hat{\boldsymbol{\theta}}^{(l)} = \mathbf{h}(\{\mathbf{Z}^{(l,j)}\}_{j=1}^m; \boldsymbol{\gamma}^*)$ .
  - 6:     **if**  $l > b$  **then**
  - 7:         Compute the post–burn-in mean  $\bar{\boldsymbol{\theta}}_b^{(l)} = \frac{1}{l-b} \sum_{t=b+1}^l \hat{\boldsymbol{\theta}}^{(t)}$ .
  - 8:         Check convergence of  $\bar{\boldsymbol{\theta}}_b^{(l)}$  according to the specified criterion.
  - 9:     **end if**
  - 10: **until** converged or maximum number of iterations reached.
  - 11: Return  $\bar{\boldsymbol{\theta}}_b^{(l)}$ .
- 

functions. Figure 2 illustrates the Estimation stage of the algorithm. After conditional simulation, the update (12) is obtained in a fraction of a second. Importantly, since the incomplete data are completed by conditional simulation, the NBE is applied to complete-data vectors only. Therefore, our proposed algorithm does not require a model for the missingness mechanism.

Algorithm 2 is ideally suited when simulations can be carried out from the distributions of  $\mathbf{Z} \mid \boldsymbol{\theta}$  and  $\mathbf{Z}_2 \mid \mathbf{Z}_1, \boldsymbol{\theta}$ , and when the incomplete-data and complete-data likelihoods are unavailable or computationally intractable. Statistical models that have these properties include (hidden) Markov random fields (e.g., Besag, 1974; Rue and Held, 2005), such as the (hidden) Potts (1952) model considered in Section 3.3, the autologistic model (Besag, 1972), and other auto-models proposed by Besag (1974). These models have intractable likelihoods due to the computational complexity of the required normalizing constants. However,

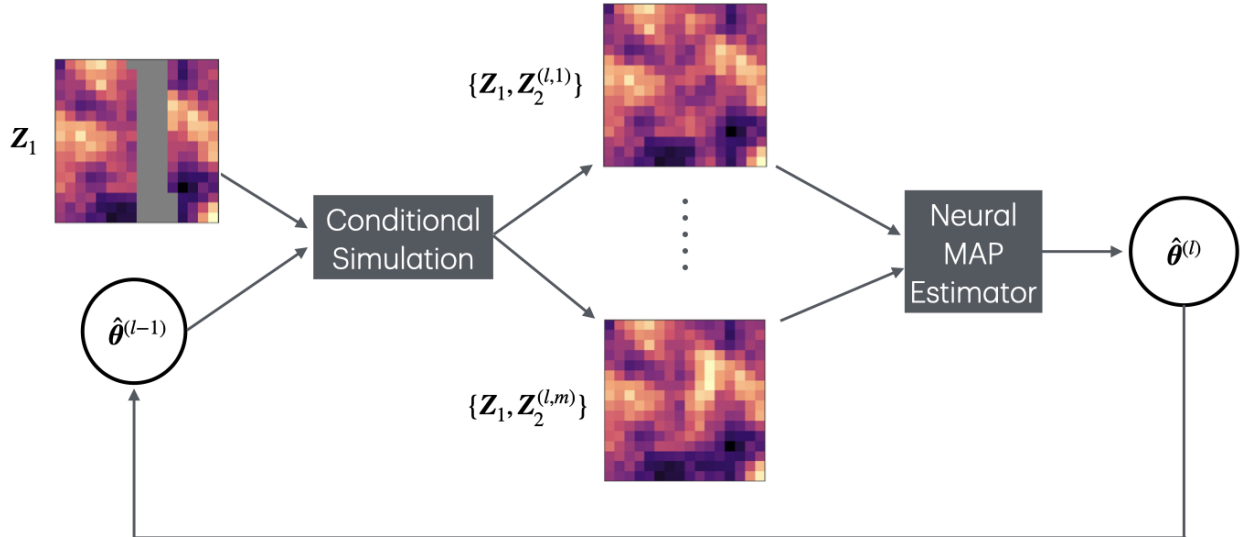


Figure 2: The Estimation stage of Algorithm 2. Incomplete data  $\mathbf{Z}_1$  with missing entries are completed by conditional simulation using the previous parameter estimate  $\hat{\theta}^{(l-1)}$  of model parameter  $\theta$ . The  $m$  conditionally-independent replicates are then input to an NBE trained to approximate the MAP estimator. The parameter estimate  $\hat{\theta}^{(l)}$  is then used for conditional simulation in the next iteration of the algorithm.

marginal and conditional simulation is feasible through Gibbs sampling.

Algorithm 2 is equivalent to the conventional MCEM algorithm, up to the error introduced by using an NBE to approximate the conventional update  $M_m(\cdot)$ . Indeed, it is one member of a broader family of approximate MCEM algorithms that may be expressed in the following general form:

$$\hat{\theta}^{(l)} = M_m(\hat{\theta}^{(l-1)}) + \delta_m(\hat{\theta}^{(l-1)}), \quad l = 1, 2, \dots, \quad (13)$$

where  $\delta_m(\cdot)$  denotes (random) approximation error. In Section S2 of the Supplementary Material, we derive the asymptotic behavior of the sequence (13). For instance, for large  $m$  and with mean-zero approximation error, the sequence (13) behaves approximately as an inhomogeneous nonlinear AR(1) process centered on the EM update (9). Further, if  $\theta^*$  is an isolated (local) maximizer of the incomplete data posterior density  $p(\theta | \mathbf{Z}_1)$ , then a sequence (13) starting in the vicinity of  $\theta^*$  behaves approximately as a stationary AR(1) process with mean  $\theta^*$ . These results provide a justification for Algorithm 2 and motivate its use with the averaging procedure in (11).

Finally, most of the considerations regarding the choice of Monte Carlo sample size  $m$  and the convergence criterion carry over directly from the conventional MCEM algorithm to Algorithm 2. In particular, we employ the averaging procedure (11) to improve robustness to the choice of  $m$ ; and we adopt the convergence criterion of Booth and Hobert (1999) that terminates the algorithm when the relative change in the averaged estimates falls below a specified tolerance for a number of successive iterations. Details on our specific choices for  $m$ , burn-in  $b$ , and convergence threshold are provided in Section 3.1.

### 2.3.3 Neural MAP estimation

Algorithm 2 hinges on the capacity to approximate the MAP estimator using an NBE. Here, we outline how this can be done, and address additional practical considerations.

**Approximating the MAP estimator.** For continuous parameter spaces, the MAP estimator is, under mild conditions (Bassett and Deride, 2019), the limit as  $\epsilon \rightarrow 0$  of the Bayes estimators associated with the 0–1 loss function

$$L(\boldsymbol{\theta}, \hat{\boldsymbol{\theta}}) = \mathbb{I}(\|\boldsymbol{\theta} - \hat{\boldsymbol{\theta}}\| > \epsilon), \quad (14)$$

where  $\|\cdot\|$  denotes any norm in  $\mathbb{R}^d$  (Robert, 2007, pg. 166), which in our work we choose to be the Euclidean norm. However, (14) is not amenable to gradient-based methods for solving (3), and therefore it cannot be used to construct an NBE that approximates the MAP estimator. This challenge may be circumvented by noting that, under suitable regularity conditions, for large  $m$  and uniform prior  $\pi(\boldsymbol{\theta})$ , the objective in (12) tends to the logarithm of an unnormalized Gaussian density (Bernstein–von Mises theorem; see, e.g., van der Vaart, 1998, pg. 140–141). Since the mean of a Gaussian random variable is also its mode, one could therefore choose a quadratic loss function instead of (14) under a uniform prior. For robustness reasons, we prefer to adopt a mathematically convenient surrogate for (14) with derivatives that are continuous almost everywhere; for example,

$$L(\boldsymbol{\theta}, \hat{\boldsymbol{\theta}}; \kappa) \equiv \tanh(\|\hat{\boldsymbol{\theta}} - \boldsymbol{\theta}\|/\kappa), \quad \kappa > 0, \quad (15)$$

where  $\tanh(\cdot)$  denotes the hyperbolic tangent function, yields the 0–1 loss function in the limit as  $\kappa \rightarrow 0$  (see Section S3 of the Supplementary Material, where we also discuss alternative loss functions). Therefore, instead of (14) for some  $\epsilon$  close to 0, we use (15) for some  $\kappa$  close to 0.

#### Neural-network architecture for handling $m$ conditionally independent replicates.

In Algorithm 2, the update (12) involves neural Bayes estimation based on a set of  $m$  completed data vectors. A suitable neural-network architecture for these data that ensures scalability with respect to  $m$  is DeepSets (Zaheer et al., 2017):

$$\mathbf{h}(\{\mathbf{Z}^{(j)}\}_{j=1}^m; \boldsymbol{\gamma}) = \boldsymbol{\phi}\left\{\frac{1}{m} \sum_{j=1}^m \boldsymbol{\psi}(\mathbf{Z}^{(j)}; \boldsymbol{\gamma}_\psi); \boldsymbol{\gamma}_\phi\right\}, \quad (16)$$

where  $\mathbf{Z}^{(j)} \in \mathcal{Z}$  for  $j = 1, \dots, m$ ,  $\boldsymbol{\psi}(\cdot; \boldsymbol{\gamma}_\psi)$  is a neural network whose architecture depends on the structure of the data,  $\boldsymbol{\phi}(\cdot; \boldsymbol{\gamma}_\phi)$  is an MLP, and the neural-network parameters are  $\boldsymbol{\gamma} = (\boldsymbol{\gamma}_\psi^\top, \boldsymbol{\gamma}_\phi^\top)^\top$ . The representation (16) has several motivations. First, when the data are exchangeable, the MAP estimator is invariant to permutations of the data, and estimators constructed from (16) are guaranteed to exhibit this property. Second, under certain conditions, (16) is a universal approximator for continuously differentiable permutation-invariant functions; therefore, any MAP estimator that is a continuously differentiable function of the data can be approximated arbitrarily well by an estimator of the form (16). Third, (16)

may be used with any value of  $m$ . Sainsbury-Dale et al. (2024) give further details on the motivation and use of (16) in the general setting of neural Bayes estimation.

**Accounting for the concentrated probability density**  $\pi_m(\boldsymbol{\theta}) \propto \{\pi(\boldsymbol{\theta})\}^m$ . The update (12) involves  $\pi_m(\boldsymbol{\theta}) \propto \{\pi(\boldsymbol{\theta})\}^m$ , the prior raised to the power of  $m$ . Note that the prior remains  $\pi(\boldsymbol{\theta})$ , since (10) and (12) are equivalent. There are at least two ways in which this distribution can be accounted for. In the first way, one may sample directly from  $\pi_m(\boldsymbol{\theta})$  when constructing the set  $\{\boldsymbol{\theta}^{(k)}\}_{k=1}^K$ , and then train the network as usual. In the second way, one may sample from  $\pi(\boldsymbol{\theta})$  and adjust the objective function through an importance sampling scheme in which samples drawn from  $\pi(\boldsymbol{\theta})$  are reweighted to approximate expectations under  $\pi_m(\boldsymbol{\theta})$ . When constructing an NBE under the loss function (15), the optimization task becomes

$$\boldsymbol{\gamma}^* \equiv \arg \min_{\boldsymbol{\gamma} \in \Gamma} \frac{1}{K} \sum_{k=1}^K \{\pi(\boldsymbol{\theta}^{(k)})\}^{m-1} L\{\boldsymbol{\theta}^{(k)}, \mathbf{h}(\{\mathbf{Z}^{(k,j)}\}_{j=1}^m; \boldsymbol{\gamma}); \boldsymbol{\kappa}\}, \quad (17)$$

where, independently for each  $k$ ,  $\boldsymbol{\theta}^{(k)} \sim \pi(\boldsymbol{\theta})$  and  $\{\mathbf{Z}^{(k,j)}\}_{j=1}^m$  are simulated from  $p(\mathbf{Z} | \boldsymbol{\theta}^{(k)})$ . The choice of how to account for  $\pi_m(\boldsymbol{\theta})$  depends on whether it is easier to sample from  $\pi_m(\boldsymbol{\theta})$  or to evaluate  $\pi(\boldsymbol{\theta})$ . Since it is usually straightforward to evaluate  $\pi(\boldsymbol{\theta})$ , we present Algorithm 2 in terms of (17). Finally, when  $\pi(\boldsymbol{\theta}) \propto 1$ , the posterior is identical under  $\pi_m(\boldsymbol{\theta})$  and  $\pi(\boldsymbol{\theta})$ , and no change to the workflow is required.

### 3 Simulation studies

We now conduct simulation studies to investigate the strengths and weaknesses of the masking approach (Algorithm 1) compared to our EM approach (Algorithm 2), both developed for estimation in the presence of missing data. We refer to an NBE employing the masking approach as a “Masking NBE”, and an NBE employing our EM approach as an “EM NBE”. In Section 3.1, we outline the general setting. In Section 3.2, we consider a spatial Gaussian-process model and estimate its parameters. In Section 3.3, we examine the hidden Potts (1952) model.

#### 3.1 General setting

We conduct our experiments using functionality we have added to the package **NeuralEstimators** (Sainsbury-Dale, 2024), which is available in Julia and R. We use a workstation with an AMD EPYC 7402 3.00GHz CPU with 128 GB of CPU RAM, and a Nvidia Quadro RTX 6000 GPU with 24 GB of GPU RAM. All subsequent results can be generated using reproducible code at <https://github.com/msainsburydale/NeuralIncompleteData>.

To elucidate the differences between the masking approach (Algorithm 1) and our proposed EM approach (Algorithm 2), which are greater with data that are high-dimensional, our simulation studies consider spatial models where the data are observed incompletely over a regular grid of size  $n = 64^2 = 4096$ , and we therefore use a CNN-based architecture for (6) and (16) detailed in Section S5 of the Supplementary Material. There, we also illustrate the

benefits of using an ensemble (Hansen and Salamon, 1990) of neural networks in the context of neural Bayes estimation; throughout our experiments we use an ensemble of five NBEs for both the masking approach and the EM approach.

We train our NBEs under the pre-limiting 0–1 loss function (15), with  $\kappa = 0.1$  and  $K = 25000$  in both (7) (Masking) and (17) (EM). To avoid vanishing gradients early in training, we first pretrain each NBE using the mean-absolute-error loss function before switching to (15). During training, we use the default values of **NeuralEstimators**; specifically, we utilize the Adam optimizer (Kingma and Ba, 2014) with an initial learning rate of 0.0005 and a cosine-annealing learning-rate schedule (Loshchilov and Hutter, 2016). We cease training when the objective function in (7) or (17) has not decreased in five consecutive epochs, where an epoch is defined to be one complete pass through the entire training data set when doing stochastic gradient descent to decrease the objective functions. When training the Masking NBEs, we use a missing-completely-at-random (MCAR) model for the missingness mechanism, with the percentage of missing data varying uniformly between 10% and 50% across data sets. Figure S5 of the Supplementary Material shows the value of the objective function in (7) or (17) evaluated at the end of each epoch.

Post training, the estimators’ statistical efficiencies are compared on unseen test data under both MCAR missingness and a model for the missingness where data are missing in a contiguous block (MICB). This is done to assess the Masking NBEs under the correct and an incorrect specification of the missingness mechanism. We compute empirical root-mean-squared errors (RMSEs) based on simulated data using a new set of 1000 parameter vectors sampled from the prior. For the parameter vectors  $\{\boldsymbol{\theta}^{(1)}, \dots, \boldsymbol{\theta}^{(1000)}\}$ ,

$$\text{RMSE}(\hat{\boldsymbol{\theta}}(\cdot)) = \left\{ \frac{1}{1000} \sum_{j=1}^{1000} \|\hat{\boldsymbol{\theta}}^{(j)} - \boldsymbol{\theta}^{(j)}\|^2 \right\}^{1/2}, \quad (18)$$

where, for  $j = 1, \dots, 1000$ ,  $\hat{\boldsymbol{\theta}}^{(j)}$  is the corresponding estimate using the estimator  $\hat{\boldsymbol{\theta}}(\cdot)$  from incomplete data  $\mathbf{Z}_1^{(j)} \sim p(\mathbf{Z}_1 | \boldsymbol{\theta}^{(j)})$ , and recall that  $\|\cdot\|$  denotes the Euclidean norm. We use  $\text{RMSE}_{\text{MCAR}}$  and  $\text{RMSE}_{\text{MICB}}$  to denote the RMSE of an estimator based on incomplete data simulated under the MCAR and MICB mechanisms, respectively. For the EM NBEs, we set  $m = 30$  in (12); we use the mean of the prior distribution for the initial estimates,  $\hat{\boldsymbol{\theta}}^{(0)}$ ; we use a fixed burn-in of  $b = 5$  in (11); and we stop the algorithm after 50 iterations or if the maximum elementwise relative change in  $\bar{\boldsymbol{\theta}}_b^{(l)}$ , as defined in (11), is less than 0.001 for three consecutive values of  $l$ .

### 3.2 Gaussian process model

In this simulation study, we consider a spatial Gaussian process model, where  $\mathbf{Z} \equiv (Z_1, \dots, Z_n)^\top$  are data at locations  $\{\mathbf{s}_1, \dots, \mathbf{s}_n\}$  in a spatial domain  $\mathcal{D} \subseteq \mathbb{R}^2$ . The data are modeled as spatially-correlated mean-zero Gaussian random variables with Matérn covariance function given by

$$\text{cov}(Z_i, Z_j) = \sigma^2 \frac{2^{1-\nu}}{\Gamma(\nu)} \left( \frac{\|\mathbf{s}_i - \mathbf{s}_j\|}{\rho} \right)^\nu K_\nu \left( \frac{\|\mathbf{s}_i - \mathbf{s}_j\|}{\rho} \right) + \tau^2 \mathbb{I}(i = j); \quad i, j = 1, \dots, n, \quad (19)$$

Table 1: The training time, estimation time for a single test data set, and empirical RMSE under two missingness models for three estimators of the parameters of the Gaussian process model (Section 3.2).

Estimator	Training time (mins)	Estimation time (s)	RMSE <sub>MCAR</sub>	RMSE <sub>MICB</sub>
MAP	–	1.12	<b>0.015</b>	<b>0.014</b>
EM NBE	<b>21.6</b>	0.39	<b>0.015</b>	0.015
Masking NBE	25.3	<b>0.01</b>	0.016	0.202

where  $\sigma^2$  is a variance parameter;  $\Gamma(\cdot)$  is the gamma function;  $K_\nu(\cdot)$  is the modified Bessel function of the second kind of order  $\nu$ ;  $\rho > 0$  and  $\nu > 0$  are range and smoothness parameters, respectively; and  $\tau^2$  is a fine-scale variance parameter.

In this example, we take the spatial domain to be  $\mathcal{D} \equiv [0, 1] \times [0, 1]$ , and we simulate complete data on a regular square grid of size  $n = 64^2 = 4096$ . For computational tractability, we use the package **GpGp** to simulate training data via the Vecchia (1988) approximation. We implement the Vecchia approximation using a “maxmin” ordering of the locations, with a maximum of 30 neighbors assigned to each location; see Guinness (2018) for further details. The parameters to be estimated are  $\boldsymbol{\theta} \equiv (\tau, \rho)^\top$ , and we fix  $\nu = 1$  and  $\sigma^2 = 1$ . We assume that  $\tau$  and  $\rho$  are independent *a priori*, and we use the priors  $\tau \sim \text{Unif}(0.01, 1)$  and  $\rho \sim \text{Unif}(0.03, 0.35)$ .

We compare the estimators using the time taken for their training and for estimation for a single data set post-training (computational efficiency); and their empirical RMSEs (statistical efficiency). Since the likelihood function is available for this model, we compare the two competing NBEs to the MAP estimator that numerically maximizes the incomplete-data posterior density. Our results, summarized in Table 1 and Figure 3, highlight several important properties of the estimators.

First, the EM NBE is agnostic to the missingness pattern and it performs well under both MCAR and MICB data, as illustrated by the similarity of its sampling distribution (Figure 3) and RMSE (Table 1) to those of the MAP estimator. By contrast, the Masking NBE has substantial bias and inflated RMSE on MICB test data (recall that the Masking NBE was trained with MCAR data). The almost-as-good RMSE performance of the EM NBE relative to the MAP estimator indicates that Algorithm 2 in the Estimation stage converges to a suitable point estimate across most, if not all, data sets; convergence for a single data set is illustrated in Figure S6 of the Supplementary Material.

Second, the NBEs represent a trade-off between computational efficiency and statistical efficiency. The speed of the Masking NBE is due to it not requiring likelihood computation or conditional simulation, and because it is not an iterative algorithm. For the spatial Gaussian process model, the MAP estimate is obtained straightforwardly by numerically maximizing the unnormalized posterior density, which is available in closed form. Hence, for this model, the EM NBE provides only a moderate reduction in estimation time compared to the MAP estimator (Table 1).

These results provide empirical evidence that NBEs can come close to the statistical efficiency of a gold-standard likelihood-based estimator. It will be seen in the next section that NBEs are even more beneficial when the incomplete data likelihood function is unavailable in closed form or is computationally intractable.

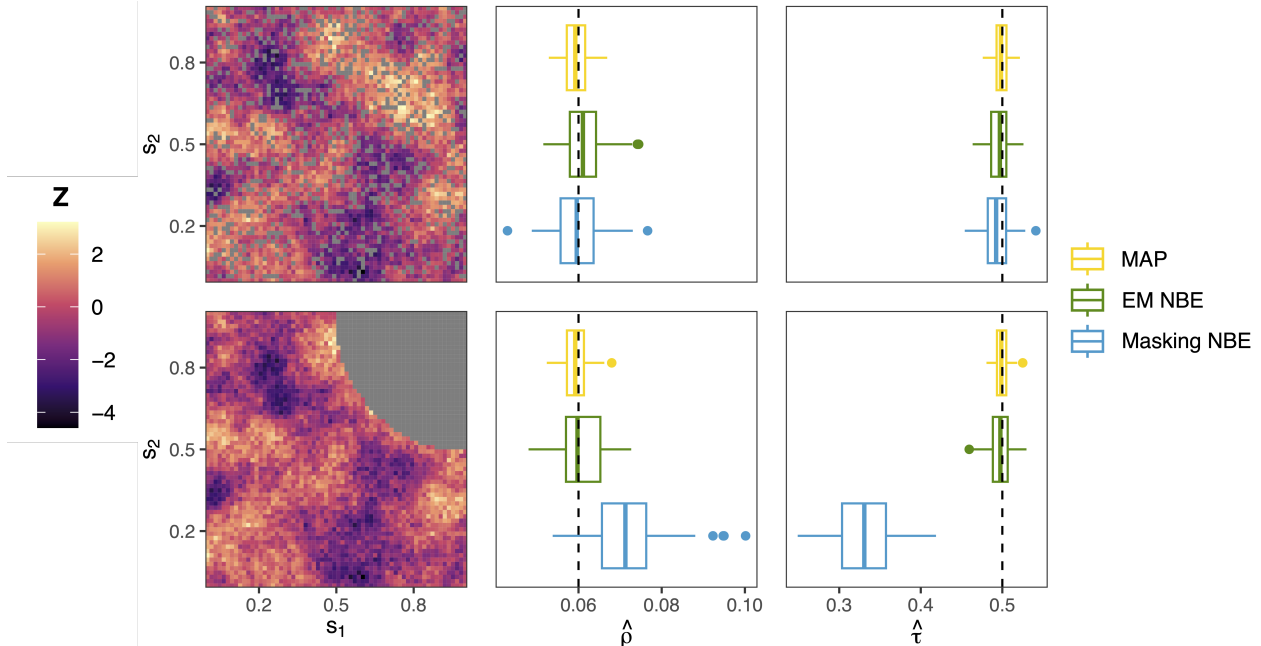


Figure 3: Spatial data (first column) where the missingness is of type MCAR (first row) or MICB (second row) with missingness shown in gray, and corresponding empirical distributions (second and third columns) for three estimators of the parameters of the Gaussian process model (Section 3.2). True parameter values are shown as a dashed vertical line.

### 3.3 Hidden Potts model

We now consider a hidden Markov random field (e.g., Besag, 1974; Cressie, 1993, Ch. 6; Rue and Held, 2005) based on the so-called Potts (1952) model. Consider a regular grid of pixels indexed by  $i = 1, \dots, n$ , where each pixel takes on a label  $Y_i$  from a finite set of discrete states  $\mathcal{Q} \equiv \{1, \dots, Q\}$ . Then, the Potts model is specified through the conditional distributions,

$$\Pr(Y_i = y \mid \mathbf{Y}_{\setminus i}, \beta) \propto \exp \left\{ \beta \sum_{j \in \mathcal{N}_i} \mathbb{I}(Y_j = y) \right\}, \text{ for } y \in \mathcal{Q}, \quad (20)$$

where  $\mathbf{Y}_{\setminus i}$  denotes all pixel labels excluding the  $i$ th pixel;  $\beta > 0$  is a parameter controlling the strength of spatial dependence; and  $\mathcal{N}_i$  contains the indices of the “neighbors” of pixel  $i$ . Here, we consider a Potts model modified to account for edge effects. Specifically, we let the neighbors  $\mathcal{N}_i$  be the adjacent pixels of pixel  $i$ , with four neighbors for interior pixels, three for edge pixels, and two for corner pixels. The Potts model exhibits a phase transition at the critical parameter value  $\beta_c = \log(1 + \sqrt{Q})$  (Moores et al., 2021), transitioning from disorder when  $\beta < \beta_c$  (where most neighboring pixels do not have the same label) to order when  $\beta > \beta_c$  (most neighboring pixels have the same label). Its likelihood function, obtained from (20), involves a normalizing constant that is computationally intractable for moderate-to-large  $n$ . In what follows in this section, we focus on a hierarchical extension of the Potts model, the hidden Potts model.

The hidden Potts model extends the Potts model to settings where the labels are not directly observed. The observed data  $\mathbf{Z} \equiv (Z_1, \dots, Z_n)^\top$  are assumed conditionally indepen-

Table 2: The training time, estimation time for a single test data set, and empirical RMSE for two estimators of the parameters of the hidden Potts model (Section 3.3).

Estimator	Training time (mins)	Estimation time (s)	RMSE <sub>M<sub>CAR</sub></sub>	RMSE <sub>M<sub>ICB</sub></sub>
EM NBE	<b>20.4</b>	0.23	<b>0.037</b>	<b>0.042</b>
Masking NBE	28.1	<b>0.01</b>	<b>0.037</b>	0.166

dent given the latent labels  $\mathbf{Y} \equiv (Y_1, \dots, Y_n)^\top$ , with a label-specific observation distribution:

$$p(Z_i | Y_i = y, \boldsymbol{\lambda}_y); \quad i = 1, \dots, n, \quad (21)$$

where each label  $y \in \mathcal{Q}$  is associated with observation-distribution parameters  $\boldsymbol{\lambda}_y$  that we collect in  $\boldsymbol{\lambda} \equiv (\boldsymbol{\lambda}_1^\top, \dots, \boldsymbol{\lambda}_Q^\top)^\top$ . The parameters of the hidden Potts model are  $\boldsymbol{\theta} \equiv (\beta, \boldsymbol{\lambda}^\top)^\top$ . As with the standard Potts model, likelihood-based inference in the hidden Potts model is computationally prohibitive except for grids with a small number of grid cells.

The general hidden Potts model given by (20) and (21) is often made concrete by specifying Gaussian data distributions in (21). We focus on this common case in the current simulation study, while in Section 4, we consider a more complex hidden Potts model in which the observations follow either point-mass or Beta distributions. Specifically, in the current simulation study, we assume a hidden Potts model with  $Q = 3$  states and observation distributions

$$p(Z_i | Y_i = y, \boldsymbol{\lambda}_y) = \text{Gau}(\mu_y, \sigma_y^2); \quad i = 1, \dots, n, \quad (22)$$

where each label  $y \in \mathcal{Q}$  is associated with its own mean  $\mu_y \in \mathbb{R}$  and variance  $\sigma_y^2 > 0$ . With three hidden states, the phase transition occurs at  $\beta_c = 1.005$ . We adopt the priors  $\beta \sim \text{Unif}(0, 1.5)$ ,  $\mu_1 \sim \text{Gau}(-1, 0.3^2)$ ,  $\mu_2 \sim \text{Gau}(0, 0.3^2)$ ,  $\mu_3 \sim \text{Gau}(1, 0.3^2)$ , and  $\sigma_y \sim \text{Unif}(0, 1/3)$  for  $y \in \{1, 2, 3\}$ , and we impose the identifiability constraint  $\mu_1 < \mu_2 < \mu_3$ . We estimate the seven unknown parameters  $\boldsymbol{\theta} \equiv (\beta, \mu_1, \mu_2, \mu_3, \sigma_1, \sigma_2, \sigma_3)^\top$  based on incomplete data on a square grid of size  $n = 64^2 = 4096$ . To simulate realizations  $\mathbf{Y}$ , we use the Swendsen and Wang (1987) algorithm implemented in **bayesImageS** (Moore et al., 2021). During the Estimation stage of Algorithm 2, we simulate conditionally on a partially observed, noisy field using Gibbs sampling (see Section S6 of the Supplementary Material).

Table 2 and Figure 4 report our results (in Figure 4 we focus on the parameter  $\beta$ ). As with the Gaussian process model, the EM NBE is agnostic to the missingness pattern, and performs well under both missingness models considered in this experiment. By contrast, the Masking NBE is biased for most values of  $\beta$  when the missingness model is misspecified. The performance of the EM NBE indicates that Algorithm 2 in the Estimation stage converges to a suitable point estimate across most, if not all, data sets; convergence for a single data set is illustrated in Figure S7 of the Supplementary Material.

Finally, this example highlights the advantages of NBEs (and related neural inferential methods) over another popular simulation-based method of inference, approximate Bayesian computation (ABC; Lintusaari et al., 2017; Sisson et al., 2018). ABC typically relies on user-defined summary statistics, which are difficult to construct for latent variable models such as the hidden Potts model. In contrast, NBEs do not require user-defined summary statistics and can be applied directly to high-dimensional data. To provide a comparison in a setting where informative summary statistics are available, in Section S4 of the Supplementary

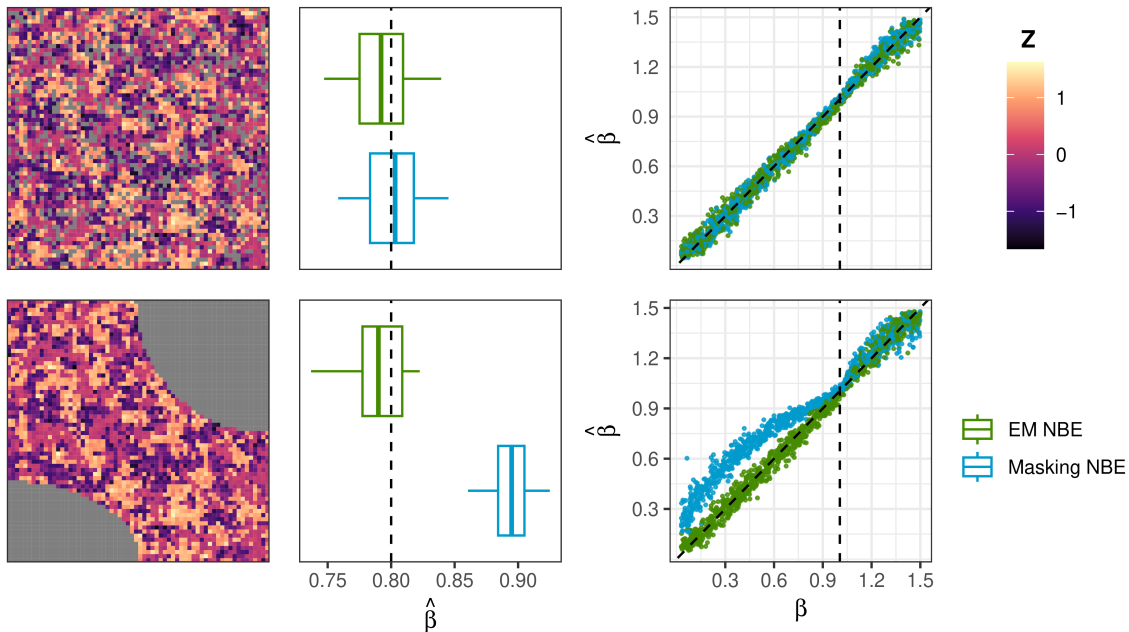


Figure 4: Spatial data (first column) simulated from the hidden Potts model of Section 3.3, where the missingness is of type MCAR (first row) or MICB (second row); empirical distributions (second column) for two estimators of the parameter  $\beta$ , with  $\beta = 0.8$  fixed (dashed vertical line); and estimates versus true values (third column) for many different values of  $\beta$ , with the critical parameter value  $\beta_c = 1.005$  demarcated by a dashed vertical line.

Material we present an additional simulation study using a spatial version of the generalized hyperbolic distribution. Even in this case where informative summary statistics are available, we find that ABC leads to less statistically efficient estimates than the EM NBE.

## 4 Application

Here, we consider a remote-sensing application with Arctic sea-ice data. These data are high-dimensional with a missingness mechanism that is difficult to model, but these challenges can be overcome using the EM NBE (Algorithm 2).

Arctic sea ice plays an important role in regulating our climate: it acts as a reflective surface that reduces the amount of solar energy absorbed by Earth. Melting sea ice exposes darker ocean water, thereby further accelerating the melting process due to an albedo-ice feedback effect. Changes in Arctic sea-ice area and thickness also affect atmospheric circulation and ocean currents, which can influence weather patterns worldwide (Cvijanovic et al., 2017). Further, Arctic sea ice provides vital habitats for species such as polar bears and seals, and its loss can disrupt fragile ecosystems, thereby affecting biodiversity, food webs, and fisheries (Meier et al., 2014). Understanding the temporal evolution of Arctic sea ice is therefore crucial for informing policies aimed at mitigating the impacts of climate change, managing resources sustainably, and protecting vulnerable ecosystems (United Nations, 2024).

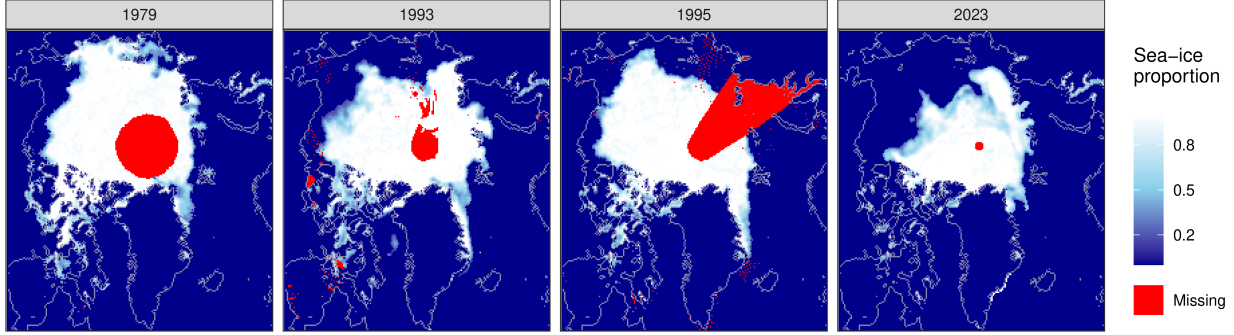


Figure 5: Arctic sea-ice data from the first day of September for the years 1979, 1993, 1995, and 2023. Faint gray lines denote coastlines, with Greenland appearing at the bottom. The data are subject to both random sources of missingness (e.g., cloud cover) and more systematic sources of missingness due to remote-sensing limitations (e.g., the Arctic Pole Hole).

In this application, we consider spatial data of Arctic sea-ice proportion, that is, the proportion of sea ice in grid cells at given spatial locations (also commonly referred to as sea-ice concentration), produced by the National Oceanic and Atmospheric Administration (NOAA) as part of their National Snow and Ice Data Center’s (NSIDC) Climate Data Record (CRD; Meier et al., 2021). The data are derived from passive microwave remote sensing retrievals from the Nimbus 7 satellite and the F8, F11, F13, and F17 satellites of the Defence Meteorological Satellite Program, projected onto  $25\text{km} \times 25\text{km}$  grid cells within a region of the Northern Hemisphere spanning longitudes  $180^\circ\text{E}$  to  $180^\circ\text{W}$  and latitudes at or above  $60^\circ\text{N}$  (Zhang and Cressie, 2020; Meier et al., 2021). Arctic-sea-ice cover typically reaches its annual minimum in September (Parkinson, 2014), and we therefore base our analysis on the ice cover on the first day of September in each year. Our data set comprises 45 spatial images (one image for each year between 1979 and 2023), with each image containing  $199 \times 219 = 43581$  grid cells, and we analyze each year separately.

Figure 5 shows that the data are incomplete and that the missingness patterns are relatively complicated. Here, missingness occurs for several reasons, including cloud cover and unpredictable issues with the remote-sensing instrument (Meier et al., 2021). The data are also subject to a more consistent form of missingness around the North Pole: this area, called the Arctic Pole Hole, changes in size over time as it is a function of both the remote-sensing instrument and the prevailing atmospheric conditions (Meier et al., 2021).

Previous studies of Arctic sea-ice (e.g., Parkinson, 2014; Zhang and Cressie, 2020) often apply a fixed threshold (e.g., 15%) to classify each grid cell as either “ice” or “not ice”. This binarization simplifies modeling but it has important limitations: the threshold is arbitrary, it discards valuable information from the underlying data (which gives proportions of sea-ice cover), and it can bias estimates of sea-ice area (the total ice-covered region). Instead, we model the sea-ice proportions directly using a hidden Potts model (see (20)) with  $Q = 4$  states, spatial-dependence parameter  $\beta > 0$ , and the following observation distributions:

$$\begin{aligned}
 p(Z_i | Y_i = 1) &= \delta_0(Z_i), & p(Z_i | Y_i = 2) &= \text{Beta}(Z_i; a_1, b_1), \\
 p(Z_i | Y_i = 3) &= \text{Beta}(Z_i; a_2, b_2), & p(Z_i | Y_i = 4) &= \delta_1(Z_i),
 \end{aligned}$$

where  $\delta_x(\cdot)$  denotes the Dirac delta function that models point mass at  $x \in \mathbb{R}$ ,  $\text{Beta}(z; a, b)$ ,  $z \in (0, 1)$ , denotes the Beta density function with shape parameters  $a > 0$  and  $b > 0$ , and for identifiability we impose ordering of the means:  $a_1(a_1 + b_1)^{-1} < a_2(a_2 + b_2)^{-1}$ . This hidden Potts model captures the multimodal structure evident in the empirical histogram of sea-ice proportions (see Figure S9 of the Supplementary Material). The inclusion of two Beta components allows flexible modeling of the continuous observations in  $(0, 1)$ , which exhibit strong spatial dependence (see, e.g., Figure S12 of the Supplementary Material). Conditional simulation, which is required by our EM NBE (Algorithm 2) and for prediction at grid cells with missing pixels, can be done using MCMC, as described in Section S6 of the Supplementary Material.

In our hidden Potts model, the unknown parameters are  $\boldsymbol{\theta} \equiv (\beta, a_1, a_2, b_1, b_2)^\top$ . We use a relatively uninformative prior for the spatial-dependence parameter  $\beta > 0$ , namely,  $\beta \sim \text{Unif}(0, 1.5)$ . For the Beta shape parameters, we adopt the informative priors  $a_1 \sim \text{Unif}(2, 5)$ ,  $b_1 \sim \text{Unif}(2, 5)$ ,  $a_2 \sim \text{Unif}(2, 5)$ , and  $b_2 \sim \text{Unif}(0, 1)$ . Given the large data size, the computationally intractable model, and the complicated missingness mechanisms, our EM NBE (Algorithm 2) is well suited for inference in this application. We trained the NBE using the same settings given in Sections 3.1 and 3.3, with a total training time (including data simulation) of 32 minutes. We then applied the EM NBE to each of the 45 images. The total time for estimating the 45 parameter vectors  $\{\boldsymbol{\theta}_t : t = 1, \dots, 45\}$ , for each of the 45 years, was 44 seconds.

Figure 6, left panel, shows estimates  $\{\hat{\beta}_t : t = 1, \dots, 45\}$ , as well as 95% pointwise confidence intervals (Figure S10 of the Supplementary Material presents the corresponding plots for all parameters). To obtain these intervals, we used a separate parametric bootstrap for each year. Specifically, for each year, we simulated 100 data sets from the fitted model, removed data from the same grid cells that were missing in the observed data set, and then applied the EM NBE again to each of the 100 simulated (incomplete) data sets. All estimates of  $\beta$  are larger than the critical value  $\beta_c = \log(1 + \sqrt{Q}) = 1.099$ , confirming a strong tendency for neighboring grid cells to share the same label.

Figure 6, center-left panel, shows predictions of sea-ice area as a function of year. To make these predictions, we imputed missing values by simulating 100 times from the fitted model (of the corresponding year) conditionally on the observed data, and we treated the mean of these conditional simulations as the prediction. In line with the general scientific consensus, our analysis indicates that sea-ice area is decreasing dramatically over time, nearly halving over the study period. The center-right and right panels of Figure 6 show the incomplete data from September 1, 1995, and the resulting predictions of sea-ice proportion in a box containing a subset of the incomplete data (see Figures S11 and S12 of the Supplementary Material for individual conditional simulations and predictions of both the data and the hidden labels). Due to the strong spatial dependence, the predicted proportions in the interior of the ice sheet and in regions far from ice are close to 1 and 0, respectively; however, there is greater variability within the region corresponding to the sea-ice boundary. Post-training, inference (including bootstrap) for all 45 years of data took a total of 1.7 hours clock time. This can be compared to Zhang and Cressie’s (2020) fully Bayesian inference who, with a binary model and with a smaller data set, needed more than a day of clock time on a comparable high-performance computer.

Finally, we note evidence of spatial nonstationarity in these Arctic sea-ice data: see

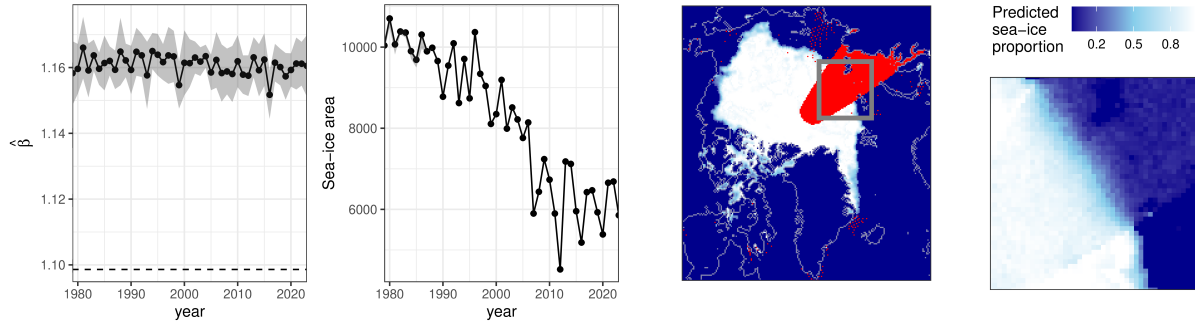


Figure 6: Analysis of Arctic sea-ice data. (Left) EM NBE estimates of the spatial dependence parameter  $\beta$  in (20) versus year. Shaded areas display 95% pointwise confidence intervals obtained using parametric bootstrap sampling, while the dashed horizontal line indicates the critical value  $\beta_c = \log(1 + \sqrt{Q}) = 1.099$ . (Center-left) Predictions of sea-ice area versus year. Note that 95% prediction intervals are plotted, but these are not visible due to the low uncertainty in the predictions. (Center-right) Arctic sea-ice data for September 1, 1995. Faint gray lines denote coastlines, with Greenland appearing at the bottom. (Right) Predicted sea-ice proportion for all grid cells within the gray box of the center-right panel.

Figure S13 of the Supplementary Material, which summarizes our analysis over a subdomain of interest, namely, the Canadian Arctic Archipelago. Future work in this application might hence consider spatially-varying versions of  $a_1$ ,  $a_2$ ,  $b_1$ , and  $b_2$ . The advantage of the proposed EM NBE is that more complicated (nonstationary) models will not alter the workflow, and that more complicated models can be fitted and assessed with relative ease.

## 5 Conclusion

Incomplete data are ubiquitous in applications of AI, arising from various sources such as cloud cover, equipment malfunctions, and data corruption. In this article, we focus on the problem of missing data in the context of neural Bayes estimation, which uses neural networks to map data to point estimates of parameters. We first discuss and give new insights on the masking approach of Wang et al. (2024) (Algorithm 1), where inference is performed on an extended data set containing the observed data and auxiliary variables that encode the missingness pattern. The masking approach has advantages: It can be used to quickly generate Bayes estimates under general loss functions; it only requires marginal (i.e., unconditional) simulation from the data model; and it is theoretically well motivated (see Theorems 1 and 2 in Section S1 of the Supplementary Material). However, its major disadvantage is that it requires a stochastic model for the missingness mechanism, which can lead to bias and statistical inefficiency when the model is wrong and the data are high-dimensional. We therefore propose an alternative approach that is based on the MCEM algorithm, where the E- and M-steps are approximated using conditional simulation and an NBE that returns the (approximate) MAP estimate from the conditionally-simulated complete data. Our EM approach (Algorithm 2) is likelihood-free, in the sense that it does not require evaluation or knowledge of the likelihood function; it is fast, since it does not require numerical optimization at each iteration; and, in contrast to the masking approach,

it is agnostic to the missingness pattern of the observed data. Moreover, our research can be viewed as a prototype problem that indicates how improvements could be made in AI by introducing statistical inferential tools.

Our EM approach to neural Bayes estimation with incomplete data relies on conditional simulation, which can be a computational bottleneck for certain models. Future research will explore the use of approximate conditional simulation (e.g., Wu et al., 2023; Simkus et al., 2023; Simkus and Gutmann, 2025) to extend the applicability of our EM approach to models for which conditional simulation is intractable or computationally prohibitive. While we focus on point estimation, our insights on the masking approach extend to methods that use it to approximate the full posterior distribution of the parameters and more general inference frameworks (e.g., Gloeckler et al., 2024). In these contexts, the data-augmentation algorithm of Tanner and Wong (1987) offers advantages analogous to those of our EM approach in the point-estimation setting. Finally, neural Bayes estimation requires specifying a potentially large set of hyperparameters related to the neural network’s architecture and its training. Although automated search methods (see, e.g., Elsken et al., 2019) can be useful, and Rödder et al. (2025) provide important initial theoretical results, further developments are needed to establish practical guidelines for hyperparameter selection.

## Acknowledgements

The authors thank Matthew Moores for discussion on, and code relating to, the Potts model.

## Funding

MSD’s research was supported by an Australian Government Research Training Program Scholarship. MSD, AZM, and RH were supported by the KAUST Opportunity Fund Program ORFS-2023-OF-5550.2. AZM’s research was supported by Australian Research Council (ARC) Discovery Early Career Research Award, DE180100203. AZM and NC were supported by ARC Discovery Project (DP), DP190100180. RH was also partially supported by KAUST Office of Sponsored Research (OSR) under Award No. OSR-CRG2020-4394. This material is based upon work supported by the Air Force Office of Scientific Research under award number FA2386-23-1-4100 (AZM and NC).

## References

- Banesh, D., Panda, N., Biswas, A., Roekel, L. V., Oyen, D., Urban, N., Grosskopf, M., Wolfe, J., and Lawrence, E. (2021). Fast Gaussian process estimation for large-scale in situ inference using convolutional neural networks. In Chen, Y., Ludwig, H., Tu, Y., Fayyad, U., Zhu, X., Hu, X., Byna, S., Liu, X., Zhang, J., Pan, S., Papalexakis, V., Wang, J., Cuzzocrea, A., and Ordonez, C., editors, *IEEE International Conference on Big Data (2021)*, pages 3731–3739. <https://doi.org/10.1109/BigData52589.2021.9671929>.
- Bassett, R. and Deride, J. (2019). Maximum a posteriori estimators as a limit of Bayes estimators. *Mathematical Programming*, 174:129–144.

- Besag, J. (1972). Nearest-neighbour systems and the auto-logistic model for binary data. *Journal of the Royal Statistical Society B*, 34:75–83.
- Besag, J. (1974). Spatial interaction and the statistical analysis of lattice systems. *Journal of the Royal Statistical Society B*, 36:192–225.
- Booth, J. G. and Hobert, J. P. (1999). Maximizing generalized linear mixed model likelihoods with an automated Monte Carlo EM algorithm. *Journal of the Royal Statistical Society B*, 61:265–285.
- Boyles, R. A. (1983). On the convergence of the EM algorithm. *Journal of the Royal Statistical Society B*, 45:47–50.
- Cappé, O., Moulines, E., and Rydén, T. (2005). *Inference in Hidden Markov Models*. Springer, New York, NY.
- Chan, K.-S. and Ledolter, J. (1995). Monte Carlo EM estimation for time series models involving counts. *Journal of the American Statistical Association*, 90:242–252.
- Coloma, N. and Kleiber, W. (2025). Fast likelihood-free parameter estimation for Lévy processes. <https://doi.org/10.48550/arXiv.2505.01639>.
- Cox, D. R. and Hinkley, D. V. (1974). *Theoretical Statistics*. Chapman and Hall, New York, NY.
- Cranmer, K., Brehmer, J., and Louppe, G. (2020). The frontier of simulation-based inference. *Proceedings of the National Academy of Sciences*, 117:30055–30062.
- Cressie, N. (1993). *Statistics for Spatial Data*, revised edition. Wiley, Hoboken, NJ.
- Cvijanovic, I., Santer, B. D., Bonfils, C., Lucas, D. D., JCH, C., and Zimmerman, S. (2017). Future loss of Arctic sea-ice cover could drive a substantial decrease in California’s rainfall. *Nature Communications*, 8:1947.
- Dell’Oro, L. and Gaetan, C. (2025). Flexible space-time models for extreme data. *Spatial Statistics*, 68:100916.
- Dempster, A. P., Laird, N. M., and Rubin, D. B. (1977). Maximum likelihood from incomplete data via the EM algorithm. *Journal of the Royal Statistical Society B*, 39:1–38.
- Diggle, P. J. and Gratton, R. J. (1984). Monte Carlo methods of inference for implicit statistical models. *Journal of the Royal Statistical Society B*, 46:193–227.
- Elsken, T., Metzen, J. H., and Hutter, F. (2019). Neural architecture search: A survey. *Journal of Machine Learning Research*, 20(55):1–21.
- Flagel, L., Brandvain, Y., and Schrider, D. R. (2018). The unreasonable effectiveness of convolutional neural networks in population genetic inference. *Molecular Biology and Evolution*, 36:220–238.
- Fort, G. and Moulines, E. (2003). Convergence of the Monte Carlo expectation maximization for curved exponential families. *Annals of Statistics*, 31:1220–1259.
- Gerber, F. and Nychka, D. W. (2021). Fast covariance parameter estimation of spatial Gaussian process models using neural networks. *Stat*, 10:e382.
- Gloeckler, M., Deistler, M., Weilbach, C., Wood, F., and Macke, J. H. (2024). All-in-one simulation-based inference. In Salakhutdinov, R., Kolter, Z., Heller, K., Weller, A., Oliver, N., Scarlett, J., and Berkenkamp, F., editors, *Proceedings of the 41st Conference on Machine Learning*, volume 235, pages 15735–15766.
- Gonçalves, P. J., Lueckmann, J.-M., Deistler, M., Nonnenmacher, M., Öcal, K., Bassetto, G., Chintaluri, C., Podlaski, W. F., Haddad, S. A., Vogels, T. P., Greenberg, D. S., and Macke, J. H. (2020). Training deep neural density estimators to identify mechanistic models of neural dynamics. *eLife*, 9:e56261.
- Goodfellow, I., Bengio, Y., and Courville, A. (2016). *Deep Learning*. MIT Press, Cambridge, MA. <http://www.deeplearningbook.org>.

- Greenberg, D., Nonnenmacher, M., and Macke, J. (2019). Automatic posterior transformation for likelihood-free inference. In Chaudhuri, K. and Salakhutdinov, R., editors, *Proceedings of the 36th International Conference on Machine Learning*, volume 97 of *Proceedings of Machine Learning Research*, pages 2404–2414.
- Guinness, J. (2018). Permutation and grouping methods for sharpening Gaussian process approximations. *Technometrics*, 60:415–429.
- Hansen, L. K. and Salamon, P. (1990). Neural network ensembles. *IEEE Transactions on Pattern Analysis and Machine Intelligence*, 12:993–1001.
- Hardie, R., Eismann, M., and Wilson, G. (2004). MAP estimation for hyperspectral image resolution enhancement using an auxiliary sensor. *IEEE Transactions on Image Processing*, 13:1174–1184.
- Hermans, J., Begy, V., and Louppe, G. (2020). Likelihood-free MCMC with amortized approximate ratio estimators. In Daumé III, H. and Singh, A., editors, *Proceedings of the 37th International Conference on Machine Learning*, volume 119 of *Proceedings of Machine Learning Research*, pages 4239–4248.
- Hernandez, A. (2017). Model calibration with neural networks. *Risk*. <http://dx.doi.org/10.2139/ssrn.2812140>.
- Hornik, K., Stinchcombe, M., and White, H. (1989). Multilayer feedforward networks are universal approximators. *Neural Networks*, 2:359–366.
- Horvath, B., Muguruza, A., and Tomas, M. (2021). Deep learning volatility: a deep neural network perspective on pricing and calibration in (rough) volatility models. *Quantitative Finance*, 21:11–27.
- Jamshidian, F. and Jennrich, R. I. (1997). Acceleration of the EM algorithm by using quasi-Newton methods. *Journal of the Royal Statistical Society B*, 59:569–587.
- Kingma, D. P. and Ba, J. (2014). Adam: A method for stochastic optimization. <https://doi.org/10.48550/arXiv.1412.6980>.
- Lambe, J. J., Chen, F., Stindl, T., and Kwan, T.-K. J. (2025). Neural networks for parameter estimation of the discretely observed Hawkes process. <https://doi.org/10.48550/arXiv.2506.01258>.
- Lehmann, E. L. and Casella, G. (1998). *Theory of Point Estimation*, 2nd edition. Springer, New York, NY.
- Lenzi, A., Bessac, J., Rudi, J., and Stein, M. L. (2023). Neural networks for parameter estimation in intractable models. *Computational Statistics & Data Analysis*, 185:107762.
- Lewandowski, A., Liu, C., and Wiel, S. V. (2010). Parameter expansion and efficient inference. *Statistical Science*, 25:533–544.
- Lintusaari, J., Gutmann, M., Dutta, R., Kaski, S., and Corander, J. (2017). Fundamentals and recent developments in approximate Bayesian computation. *Systematic Biology*, 66:66–82.
- Liu, C., Rubin, D. B., and Wu, Y. N. (1998). Parameter expansion to accelerate EM: The PX-EM algorithm. *Biometrika*, 85:755–770.
- Liu, J. S. and Rubin, D. B. (1994). The ECME algorithm: A simple extension of EM and ECM with faster monotone convergence. *Biometrika*, 81:633–648.
- Loshchilov, I. and Hutter, F. (2016). SGDR: Stochastic gradient descent with warm restarts. <https://doi.org/10.48550/arXiv.1608.03983>.
- Louis, T. A. (1982). Finding the observed information matrix when using the EM algorithm. *Journal of the Royal Statistical Society B*, 44:226–233.
- McLachlan, G. J. and Krishnan, T. (2008). *The EM Algorithm and Extensions*, 2nd edition. Wiley, Hoboken, NJ.

- Meier, W. N., Fetterer, F., Windnagel, A. K., and Stewart, J. S. (2021). *NOAA/NSIDC Climate Data Record of Passive Microwave Sea Ice Concentration, Version 4. Northern Hemisphere*. NSIDC: National Snow and Ice Data Center, Boulder, Colorado USA. <https://doi.org/10.7265/efmz-2t65>.
- Meier, W. N., Hovelsrud, G. K., Oort, B. E., Key, J. R., Kovacs, K. M., Michel, C., Haas, C., Granskog, M. A., Gerland, S., Perovich, D. K., et al. (2014). Arctic sea ice in transformation: A review of recent observed changes and impacts on biology and human activity. *Reviews of Geophysics*, 52:185–217.
- Meng, X.-L. and Rubin, D. B. (1993). Maximum likelihood estimation via the ECM algorithm: A general framework. *Biometrika*, 80:267–278.
- Montesinos-López, A., Gutierrez-Pulido, H., Montesinos-López, O. A., and Crossa, J. (2020). Maximum a posteriori threshold genomic prediction model for ordinal traits. *G3*, 10:4083–4102.
- Moore, M. T., Feng, D., and Mengersen, K. (2021). *bayesImageS: Bayesian Methods for Image Segmentation using a Potts Model*. R package version 0.6.1, <https://CRAN.R-project.org/package=bayesImageS>.
- Neal, R. M. and Hinton, G. E. (1998). A view of the EM algorithm that justifies incremental, sparse, and other variants. In Jordan, M. I., editor, *Learning in Graphical Models*, pages 355–368. Springer, New York, NY.
- OpenAI (2025). ChatGPT. <https://openai.com/chatgpt>.
- Pan, T.-F., Li, J.-J., Thompson, B., and Collins, A. G. (2025). Latent variable sequence identification for cognitive models with neural network estimators. *Behavior Research Methods*, 57(10):272.
- Papamakarios, G., Sterratt, D., and Murray, I. (2019). Sequential neural likelihood: Fast likelihood-free inference with autoregressive flows. In Chaudhuri, K. and Sugiyama, M., editors, *Proceedings of the Twenty-Second International Conference on Artificial Intelligence and Statistics*, volume 89 of *Proceedings of Machine Learning Research*, pages 837–848.
- Parkinson, C. L. (2014). Global sea ice coverage from satellite data: Annual cycle and 35-yr trends. *Journal of Climate*, 27:9377–9382.
- Potts, R. B. (1952). Some generalized order-disorder transformations. *Mathematical Proceedings of the Cambridge Philosophical Society*, 48:106–109.
- Radev, S. T., Mertens, U. K., Voss, A., Ardizzone, L., and Köthe, U. (2022). BayesFlow: Learning complex stochastic models with invertible neural networks. *IEEE Transactions on Neural Networks and Learning Systems*, 33:1452–1466.
- Richards, J., Sainsbury-Dale, M., Huser, R., and Zammit-Mangion, A. (2024). Neural Bayes estimators for censored inference with peaks-over-threshold models. *Journal of Machine Learning Research*, 25(390):1–49.
- Robert, C. P. (2007). *The Bayesian Choice*, 2nd edition. Springer, New York, NY.
- Rue, H. and Held, L. (2005). *Gaussian Markov Random Fields: Theory and Applications*. CRC Press, Boca Raton, FL.
- Ruth, W. (2024). A review of Monte Carlo-based versions of the EM algorithm. <https://doi.org/10.48550/arXiv.2401.00945>.
- Rödter, A., Hentschel, M., and Engelke, S. (2025). Theoretical guarantees for neural estimators in parametric statistics. <https://doi.org/10.48550/arXiv.2506.18508>.
- Sainsbury-Dale, M. (2024). *NeuralEstimators: Likelihood-Free Parameter Estimation using Neural Networks*. R package version 0.1.2, <https://CRAN.R-project.org/package=NeuralEstimators>.

- Sainsbury-Dale, M., Zammit-Mangion, A., and Huser, R. (2024). Likelihood-free parameter estimation with neural Bayes estimators. *The American Statistician*, 78:1–14.
- Sainsbury-Dale, M., Zammit-Mangion, A., Richards, J., and Huser, R. (2025). Neural Bayes estimators for irregular spatial data using graph neural networks. *Journal of Computational and Graphical Statistics*, 34:1153–1168.
- Simkus, V. and Gutmann, M. U. (2025). CFMI: Flow matching for missing data imputation. <https://doi.org/10.48550/arXiv.2506.09258>.
- Simkus, V., Rhodes, B., and Gutmann, M. U. (2023). Variational Gibbs inference for statistical model estimation from incomplete data. *Journal of Machine Learning Research*, 24(196):1–72.
- Sisson, S. A., Fan, Y., and Beaumont, M. (2018). *Handbook of Approximate Bayesian Computation*. Chapman & Hall/CRC Press, Boca Raton, FL.
- Swendsen, R. H. and Wang, J.-S. (1987). Nonuniversal critical dynamics in Monte Carlo simulations. *Physical Review Letters*, 58:86–88.
- Tanner, M. A. and Wong, W. H. (1987). The calculation of posterior distributions by data augmentation. *Journal of the American Statistical Association*, 82:528–540.
- Tavaré, S., Balding, D. J., Griffiths, R. C., and Donnelly, P. (1997). Inferring coalescence times from DNA sequence data. *Genetics*, 145:505–518.
- Thomas, O., Dutta, R., Corander, J., Kaski, S., and Gutmann, M. U. (2022). Likelihood-free inference by ratio estimation. *Bayesian Analysis*, 17:1–31.
- Tsyrlunikov, M. and Sotskiy, A. (2024). Regularization of the ensemble Kalman filter using a non-parametric, non-stationary spatial model. *Spatial Statistics*, 64:100870.
- United Nations (2024). Sustainable Development Goals. <https://sdgs.un.org/goals>.
- van der Vaart, A. W. (1998). *Asymptotic Statistics*. Cambridge University Press, Cambridge, UK.
- van Dyk, D. A. and Meng, X.-L. (2001). The art of data augmentation. *Journal of Computational and Graphical Statistics*, 10:1–50.
- Varadhan, R. and Roland, C. (2008). Simple and globally convergent methods for accelerating the convergence of any EM algorithm. *Scandinavian Journal of Statistics*, 35:335–353.
- Vecchia, A. V. (1988). Estimation and model identification for continuous spatial processes. *Journal of the Royal Statistical Society B*, 50:297–312.
- Villazón, A., Alegría, A., and Emery, X. (2025). Neural networks for parameter estimation in geostatistical models with geometric anisotropies. *Machine Learning: Science and Technology*, 6:025025.
- Walchessen, J., Lenzi, A., and Kuusela, M. (2024). Neural likelihood surfaces for spatial processes with computationally intensive or intractable likelihoods. *Spatial Statistics*, 62:100848.
- Wang, K. and Genton, M. G. (2024). A generalized unified skew-normal process with neural Bayes inference. <https://doi.org/10.48550/arXiv.2411.17400>.
- Wang, Z., Hasenauer, J., and Schälte, Y. (2024). Missing data in amortized simulation-based neural posterior estimation. *PLOS Computational Biology*, 20:e1012184.
- Wei, G. C. G. and Tanner, M. A. (1990). A Monte Carlo implementation of the EM algorithm and the poor man’s data augmentation algorithms. *Journal of the American Statistical Association*, 85:699–704.
- Wu, C. F. J. (1983). On the convergence properties of the EM algorithm. *The Annals of Statistics*, 11:95–103.
- Wu, L., Trippe, B. L., Naesseth, C. A., Blei, D. M., and Cunningham, J. P. (2023). Practical and asymptotically exact conditional sampling in diffusion models. In Oh, A., Naumann, T., Globerson, A., Saenko, K., Hardt, M., and Levine, S., editors, *Proceedings of the 36th Conference on Neural Information Processing Systems*, pages 31372–31403, Red Hook, NY.

- Zaheer, M., Kottur, S., Ravanbakhsh, S., Poczos, B., Salakhutdinov, R. R., and Smola, A. J. (2017). Deep sets. In Guyon, I., Luxburg, U. V., Bengio, S., Wallach, H., Fergus, R., Vishwanathan, S., and Garnett, R., editors, *Proceedings of the 30th Conference on Neural Information Processing Systems*, pages 3392–3402, Red Hook, NY.
- Zammit-Mangion, A., Sainsbury-Dale, M., and Huser, R. (2025). Neural methods for amortized inference. *Annual Review of Statistics and Its Application*, 12:311–335.
- Zhang, B. and Cressie, N. (2020). Bayesian inference of spatio-temporal changes of Arctic sea ice. *Bayesian Analysis*, 15:605–631.
- Zhou, D. (2020). Universality of deep convolutional neural networks. *Applied and Computational Harmonic Analysis*, 48:787–794.

# Supplementary Material for “Neural Parameter Estimation with Incomplete Data”

In Section S1, we provide a theoretical rationale for the masking approach of Wang et al. (2024). In Section S2, we discuss the asymptotic behavior of the Monte Carlo EM (MCEM) algorithm when the conventional update is approximate. In Section S3, we consider several continuous approximations of the 0–1 loss function that may be used when training an NBE to approximate the MAP estimator. In Section S4, we conduct an additional simulation experiment using a spatial version of the generalized hyperbolic (GH) distribution. In Section S5, we propose and illustrate the benefits of using an ensemble of deep neural networks in the context of neural Bayes estimation. In Section S6, we discuss Markov chain Monte Carlo (MCMC) sampling in hidden Potts models. Finally, in Section S7, we provide additional figures supporting our methodology.

## S1 Rationale for the masking approach

Here, we use a sufficiency argument to show that the masking approach of Wang et al. (2024) does not lead to any loss of information on  $\theta$ .

**Theorem 1.** *Let the complete data  $\mathbf{Z} \in \mathbb{R}^n$  be distributed according to a family of probability distributions indexed by  $\theta$ . Partition  $\mathbf{Z}$  into the components  $\mathbf{Z}_1$  and  $\mathbf{Z}_2$  containing the observed and missing elements, respectively, where it is assumed that there is at least one observation. Define the ordered set  $\mathcal{I}_1 \equiv \{i : Z_i \text{ is observed}\}$  such that  $\mathbf{Z}_1 = (Z_i : i \in \mathcal{I}_1)^\top$ , and let  $\mathbf{U}$  and  $\mathbf{W}$  be defined as in Equations (4) and (5) of the main text. Then,*

$$\mathbf{T}(\mathbf{Z}_1, \mathcal{I}_1) \equiv (\mathbf{U}, \mathbf{W}),$$

*is a sufficient statistic for  $\theta$ .*

*Proof.* Given that there is at least one observation,  $\mathcal{I}_1$  is non-empty and  $\mathbf{Z}_1$  is well defined. Now,  $\mathbf{Z}_1$  and  $\mathcal{I}_1$  represent all of the available information from which to make inference on  $\theta$ , that is, together they are sufficient for  $\theta$ , and hence we need only show that  $\mathbf{T}(\cdot, \cdot)$  defines a one-to-one mapping from the space of  $(\mathbf{Z}_1, \mathcal{I}_1)$  to that of  $(\mathbf{U}, \mathbf{W})$ , since any one-to-one transformation of a sufficient statistic is itself sufficient (Casella and Berger, 2001, pg. 280). First, note that the construction of  $\mathbf{U}$  using Equation (4) of the main text can be equivalently written as  $\mathbf{U} = \mathbf{Z} \odot \mathbf{W} + c(\mathbf{1} - \mathbf{W})$ , where  $\odot$  denotes elementwise multiplication, and  $\mathbf{1}$  denotes the vector of 1s of appropriate dimension. Now, for any  $\mathbf{Z}_1^a$  and  $\mathcal{I}_1^a$ , any  $\mathbf{Z}_1^b$  and  $\mathcal{I}_1^b$ ,

and any  $c \in \mathbb{R}$ ,

$$\begin{aligned}
\mathbf{T}(\mathbf{Z}_1^a, \mathcal{I}_1^a) = \mathbf{T}(\mathbf{Z}_1^b, \mathcal{I}_1^b) &\implies (\mathbf{U}^a, \mathbf{W}^a) = (\mathbf{U}^b, \mathbf{W}^b) \\
&\implies \mathbf{U}^a = \mathbf{U}^b \text{ and } \mathbf{W}^a = \mathbf{W}^b \neq \mathbf{0} \\
&\implies \mathbf{Z}^a \odot \mathbf{W}^a + c(\mathbf{1} - \mathbf{W}^a) = \mathbf{Z}^b \odot \mathbf{W}^a + c(\mathbf{1} - \mathbf{W}^a) \text{ and } \mathcal{I}_1^a = \mathcal{I}_1^b \\
&\implies \mathbf{Z}^a \odot \mathbf{W}^a = \mathbf{Z}^b \odot \mathbf{W}^a \text{ and } \mathcal{I}_1^a = \mathcal{I}_1^b \\
&\implies \mathbf{Z}_1^a = \mathbf{Z}_1^b \text{ and } \mathcal{I}_1^a = \mathcal{I}_1^b,
\end{aligned}$$

since  $\mathbf{W}^a \neq \mathbf{0}$ . Therefore,  $\mathbf{T}(\cdot, \cdot)$  defines a one-to-one mapping from the space of  $(\mathbf{Z}_1, \mathcal{I}_1)$  to that of  $(\mathbf{U}, \mathbf{W})$  and, hence,  $\mathbf{T}(\mathbf{Z}_1, \mathcal{I}_1)$  is sufficient for  $\boldsymbol{\theta}$ .  $\square$

Theorem 1 is important in establishing that the masking approach makes full use of the information contained in the data. However, using  $\mathbf{U}$  and  $\mathbf{W}$  in place of  $\mathbf{Z}_1$  and  $\mathcal{I}_1$  in a neural Bayes estimation setting requires assigning a distribution to  $\mathcal{I}_1$  (or equivalently, to  $\mathbf{W}$ ). Using an argument that closely follows that of Richards et al. (2024, Theorem 1) and Sainsbury-Dale et al. (2025, Theorem 1), we now show that, under mild conditions, the Bayes estimator is invariant to this distribution.

**Theorem 2.** *Let the complete data  $\mathbf{Z} \in \mathbb{R}^n$  be distributed according to a family of probability distributions indexed by  $\boldsymbol{\theta}$ . Partition  $\mathbf{Z}$  into the components  $\mathbf{Z}_1$  and  $\mathbf{Z}_2$  containing the observed and missing elements, respectively. Let  $\mathbf{U} \in \mathcal{U} \subseteq \mathbb{R}^n$  and  $\mathbf{W} \in \mathcal{W} = \{0, 1\}^n$  be defined as in Equations (4) and (5) of the main text. Let  $L : \Theta \times \Theta \rightarrow [0, \infty)$  denote a loss function, and assume that the Bayes estimate  $\hat{\boldsymbol{\theta}}^*$  under this loss function exists, is unique, and has finite posterior expected loss for all  $\mathbf{U} \in \mathcal{U}$  and  $\mathbf{W} \in \mathcal{W}$ . Then the Bayes estimator  $\hat{\boldsymbol{\theta}}^*(\mathbf{U}, \mathbf{W})$  that returns  $\hat{\boldsymbol{\theta}}^*$  for any  $\mathbf{U} \in \mathcal{U}$  and  $\mathbf{W} \in \mathcal{W}$  is invariant to the distribution  $p_{\mathbf{W}}(\cdot)$  of  $\mathbf{W}$ , provided*

- (i)  $p_{\mathbf{W}}(\mathbf{w}) > 0$  for all  $\mathbf{w} \in \mathcal{W}$ ,
- (ii)  $\mathbf{W}$  and  $\boldsymbol{\theta}$  are independent.

*Proof.* For all fixed  $\mathbf{U} \in \mathcal{U}$  and  $\mathbf{W} \in \mathcal{W}$ , the Bayes estimate  $\hat{\boldsymbol{\theta}}^*$  minimizes the posterior expected loss; that is,

$$\hat{\boldsymbol{\theta}}^* = \arg \min_{\hat{\boldsymbol{\theta}}} \int_{\Theta} L(\boldsymbol{\theta}, \hat{\boldsymbol{\theta}}) p_{\boldsymbol{\theta}|\mathbf{U}, \mathbf{W}}(\boldsymbol{\theta} | \mathbf{U}, \mathbf{W}) d\boldsymbol{\theta}. \quad (\text{S1})$$

Consider now the Bayes estimator  $\hat{\boldsymbol{\theta}}^*(\mathbf{U}, \mathbf{W})$  that returns the Bayes estimate for any fixed  $\mathbf{U} \in \mathcal{U}$  and  $\mathbf{W} \in \mathcal{W}$  (see Brown and Purves, 1973, for a proof of the existence of a Borel measurable Bayes estimator under mild conditions). Since the posterior expected loss is, by assumption, bounded and nonnegative for all  $\mathbf{U} \in \mathcal{U}$  and  $\mathbf{W} \in \mathcal{W}$ , we have that

$$\hat{\boldsymbol{\theta}}^*(\cdot, \cdot) = \arg \min_{\hat{\boldsymbol{\theta}}(\cdot, \cdot)} \sum_{\mathbf{w} \in \mathcal{W}} \tilde{p}_{\mathbf{W}}(\mathbf{w}) \int_{\mathcal{U}} \int_{\Theta} L(\boldsymbol{\theta}, \hat{\boldsymbol{\theta}}(\mathbf{u}, \mathbf{w})) p_{\boldsymbol{\theta}|\mathbf{U}, \mathbf{W}}(\boldsymbol{\theta} | \mathbf{u}, \mathbf{w}) d\boldsymbol{\theta} dF(\mathbf{u} | \mathbf{w}), \quad (\text{S2})$$

for any strictly positive conditional (on  $\mathbf{W}$ ) probability measure  $F(\mathbf{u} | \mathbf{w})$  and any strictly positive probability mass function  $\tilde{p}_{\mathbf{W}}(\cdot)$  on  $\mathcal{W}$ . Choosing  $dF(\mathbf{u} | \mathbf{w}) = p_{\mathbf{U}|\mathbf{W}}(\mathbf{u} | \mathbf{w}) d\mathbf{u}$  for

the conditional measure in (S2), we have that

$$\hat{\boldsymbol{\theta}}^*(\cdot, \cdot) = \arg \min_{\boldsymbol{\theta}(\cdot, \cdot)} \sum_{\mathbf{w} \in \mathcal{W}} \tilde{p}_{\mathbf{W}}(\mathbf{w}) \int_{\mathcal{U}} \int_{\Theta} L(\boldsymbol{\theta}, \hat{\boldsymbol{\theta}}(\mathbf{u}, \mathbf{w})) p_{\boldsymbol{\theta}|\mathbf{U}, \mathbf{W}}(\boldsymbol{\theta} | \mathbf{u}, \mathbf{w}) d\boldsymbol{\theta} p_{\mathbf{U}|\mathbf{W}}(\mathbf{u} | \mathbf{w}) d\mathbf{u}.$$

Applying Bayes rule to  $p_{\boldsymbol{\theta}|\mathbf{U}, \mathbf{W}}(\boldsymbol{\theta} | \mathbf{u}, \mathbf{w})$  yields

$$\hat{\boldsymbol{\theta}}^*(\cdot, \cdot) = \arg \min_{\boldsymbol{\theta}(\cdot, \cdot)} \sum_{\mathbf{w} \in \mathcal{W}} \int_{\mathcal{U}} \int_{\Theta} L(\boldsymbol{\theta}, \hat{\boldsymbol{\theta}}(\mathbf{u}, \mathbf{w})) \frac{p_{\mathbf{U}|\mathbf{W}, \boldsymbol{\theta}}(\mathbf{u} | \mathbf{w}, \boldsymbol{\theta}) p_{\mathbf{W}|\boldsymbol{\theta}}(\mathbf{w} | \boldsymbol{\theta}) p_{\boldsymbol{\theta}}(\boldsymbol{\theta})}{p_{\mathbf{W}}(\mathbf{w})} \tilde{p}_{\mathbf{W}}(\mathbf{w}) d\boldsymbol{\theta} d\mathbf{u}. \quad (\text{S3})$$

From (S3) we see that if  $p_{\mathbf{W}|\boldsymbol{\theta}}(\mathbf{w} | \boldsymbol{\theta}) = p_{\mathbf{W}}(\mathbf{w})$ , then

$$\hat{\boldsymbol{\theta}}^*(\cdot, \cdot) = \arg \min_{\boldsymbol{\theta}(\cdot, \cdot)} \sum_{\mathbf{w} \in \mathcal{W}} \int_{\mathcal{U}} \int_{\Theta} L(\boldsymbol{\theta}, \hat{\boldsymbol{\theta}}(\mathbf{u}, \mathbf{w})) p_{\mathbf{U}|\mathbf{W}, \boldsymbol{\theta}}(\mathbf{u} | \mathbf{w}, \boldsymbol{\theta}) p_{\boldsymbol{\theta}}(\boldsymbol{\theta}) \tilde{p}_{\mathbf{W}}(\mathbf{w}) d\boldsymbol{\theta} d\mathbf{u},$$

for any positive  $\tilde{p}_{\mathbf{W}}(\cdot)$  on  $\mathcal{W}$ , thus completing the proof.  $\square$

Theorem 2 establishes that, apart from the requirement of strict positivity, the choice of distribution for  $\mathcal{I}_1$  (equivalently,  $\mathbf{W}$ ) is immaterial for the Bayes estimator. However, in practice, NBEs are trained on a finite number of realizations from the statistical model, and the empirical Bayes risk is therefore affected by Monte Carlo error that does depend on this distribution, particularly in high-dimensional settings where the number of possible missingness patterns ( $2^n$ ) is very large. This pitfall is demonstrated in Section 3 of the main text, where we show that choosing a distribution for  $\mathcal{I}_1$  that assigns low probability to the observed missingness pattern can yield a statistically inefficient estimator. For further discussion, see Section 2.2 of the main text.

## S2 Asymptotic behavior of approximate MCEM sequences

Chan and Ledolter (1995) showed formally that, for large Monte Carlo sample size  $m$ , a sequence generated by the MCEM algorithm behaves approximately as a first-order autoregressive (AR(1)) process centered on the conventional EM update. They also showed that, in the vicinity of an isolated local maximizer  $\boldsymbol{\theta}^*$  of the incomplete-data posterior density, a sequence generated by the MCEM algorithm behaves approximately as a stationary AR(1) process with mean  $\boldsymbol{\theta}^*$ . Here, we extend these results to the more general setting where each MCEM update is only approximate, for example, when each update is performed using an NBE, like in our proposed Algorithm 2 of the main text.

We first recall the EM and MCEM algorithms that were reviewed in Section 2.3.1 of the main text, and the family of approximate MCEM algorithms introduced in Section 2.3.2 of the main text. There we use  $\mathbf{Z}_1$  and  $\mathbf{Z}_2$  to denote the subvectors of  $\mathbf{Z}$  that are treated as observed and missing, respectively, and we use  $\mathbf{Z}$  to denote the complete data. In what follows, we take a Bayesian perspective, based on maximization of the posterior density; the frequentist version of the subsequent algorithms are recovered by taking the prior, which can

be viewed as a penalty function, to be  $\pi(\boldsymbol{\theta}) \propto 1$ . The expected complete-data log-posterior, central to EM-based algorithms, is given by

$$Q(\boldsymbol{\theta}' | \boldsymbol{\theta}) = \log \pi(\boldsymbol{\theta}') + \mathbb{E}_{\mathbf{Z}_2 | \mathbf{Z}_1, \boldsymbol{\theta}} \log p(\boldsymbol{\theta}' | \mathbf{Z}_1, \mathbf{Z}_2)$$

where the ‘prime’ notation  $\boldsymbol{\theta}'$  is used to denote an alternative parameter vector (and not the transpose of  $\boldsymbol{\theta}$ ). The EM algorithm (Dempster et al., 1977; Wu, 1983; McLachlan and Krishnan, 2008) iteratively finds  $\boldsymbol{\theta}^{(l)}$  such that

$$\boldsymbol{\theta}^{(l)} = M(\boldsymbol{\theta}^{(l-1)}) \equiv \arg \max_{\boldsymbol{\theta}' \in \Theta} Q(\boldsymbol{\theta}' | \boldsymbol{\theta}^{(l-1)}); \quad l = 1, 2, \dots, \quad (\text{S4})$$

where  $M(\cdot)$  is deterministic and  $\Theta$  denotes the parameter space. In the MCEM algorithm (Wei and Tanner, 1990), one replaces  $Q(\boldsymbol{\theta}' | \boldsymbol{\theta})$  with a Monte Carlo approximation,

$$Q_m(\boldsymbol{\theta}' | \boldsymbol{\theta}) = \log \pi(\boldsymbol{\theta}') + \frac{1}{m} \sum_{j=1}^m \log p(\boldsymbol{\theta}' | \mathbf{Z}_1, \mathbf{Z}_2^{(j)}), \quad (\text{S5})$$

where  $m$  is the Monte Carlo sample size and  $\mathbf{Z}_2^{(j)} \sim p(\mathbf{Z}_2 | \mathbf{Z}_1, \boldsymbol{\theta})$ , independently for  $j = 1, \dots, m$ . Hence, the MCEM algorithm iteratively finds  $\boldsymbol{\theta}_m^{(l)}$  such that

$$\boldsymbol{\theta}_m^{(l)} = M_m(\boldsymbol{\theta}_m^{(l-1)}) \equiv \arg \max_{\boldsymbol{\theta}' \in \Theta} Q_m(\boldsymbol{\theta}' | \boldsymbol{\theta}_m^{(l-1)}); \quad l = 1, 2, \dots$$

In this work, we consider an approximate version of the MCEM algorithm that we write as:

$$\tilde{\boldsymbol{\theta}}_m^{(l)} = \tilde{M}_m(\tilde{\boldsymbol{\theta}}_m^{(l-1)}) \equiv M_m(\tilde{\boldsymbol{\theta}}_m^{(l-1)}) + \boldsymbol{\delta}_m(\tilde{\boldsymbol{\theta}}_m^{(l-1)}); \quad l = 1, 2, \dots, \quad (\text{S6})$$

where  $\boldsymbol{\delta}_m(\cdot)$  denotes (random) approximation error that may or may not have mean zero. In our setting, the additional approximation error  $\boldsymbol{\delta}_m(\cdot)$  is due to our use of an NBE to approximate the random map  $M_m(\cdot)$ .

We now extend the formal analysis of Chan and Ledolter (1995) to algorithms of the form (S6), under the assumptions that, for  $\boldsymbol{\theta} \in \Theta$ ,  $\mathbb{E}\{\boldsymbol{\delta}_m(\boldsymbol{\theta})\} \rightarrow \boldsymbol{\mu}(\boldsymbol{\theta})$  and  $\mathbb{V}\{\boldsymbol{\delta}_m(\boldsymbol{\theta})\} \rightarrow \boldsymbol{\Sigma}(\boldsymbol{\theta})$ , as  $m \rightarrow \infty$ . The starting point is the expansion of the gradient of (S5) around  $M(\boldsymbol{\theta})$ :

$$\nabla_{\boldsymbol{\theta}'} Q_m(\boldsymbol{\theta}' | \boldsymbol{\theta}) \approx \nabla_{\tilde{\boldsymbol{\theta}}} Q_m(\tilde{\boldsymbol{\theta}} | \boldsymbol{\theta}) \Big|_{\tilde{\boldsymbol{\theta}}=M(\boldsymbol{\theta})} + \nabla_{\tilde{\boldsymbol{\theta}}}^2 Q_m(\tilde{\boldsymbol{\theta}} | \boldsymbol{\theta}) \Big|_{\tilde{\boldsymbol{\theta}}=M(\boldsymbol{\theta})} \{\boldsymbol{\theta}' - M(\boldsymbol{\theta})\}, \quad (\text{S7})$$

where we neglect higher-order terms. Evaluating (S7) at  $\boldsymbol{\theta}' = \tilde{M}_m(\boldsymbol{\theta})$ , we obtain:

$$\tilde{M}_m(\boldsymbol{\theta}) \approx M(\boldsymbol{\theta}) - \left\{ \nabla_{\tilde{\boldsymbol{\theta}}}^2 Q_m(\tilde{\boldsymbol{\theta}} | \boldsymbol{\theta}) \Big|_{\tilde{\boldsymbol{\theta}}=M(\boldsymbol{\theta})} \right\}^{-1} \left\{ \nabla_{\tilde{\boldsymbol{\theta}}} Q_m(\tilde{\boldsymbol{\theta}} | \boldsymbol{\theta}) \Big|_{\tilde{\boldsymbol{\theta}}=M(\boldsymbol{\theta})} - \boldsymbol{\xi}(\boldsymbol{\theta}) \right\}, \quad (\text{S8})$$

where

$$\boldsymbol{\xi}(\boldsymbol{\theta}) \equiv \nabla_{\tilde{\boldsymbol{\theta}}} Q_m(\tilde{\boldsymbol{\theta}} | \boldsymbol{\theta}) \Big|_{\tilde{\boldsymbol{\theta}}=\tilde{M}_m(\boldsymbol{\theta})}. \quad (\text{S9})$$

Evaluating (S8) at  $\boldsymbol{\theta} = \tilde{\boldsymbol{\theta}}_m^{(l-1)}$  and substituting the resulting expression for  $\tilde{M}_m(\tilde{\boldsymbol{\theta}}_m^{(l-1)})$

into (S6), we obtain the following first-order autoregressive model:

$$\tilde{\boldsymbol{\theta}}_m^{(l)} \approx M(\tilde{\boldsymbol{\theta}}_m^{(l-1)}) + \boldsymbol{\epsilon}_m(\tilde{\boldsymbol{\theta}}_m^{(l-1)}), \quad (\text{S10})$$

where

$$\boldsymbol{\epsilon}_m(\boldsymbol{\theta}) \equiv - \left\{ \nabla_{\tilde{\boldsymbol{\theta}}}^2 Q_m(\tilde{\boldsymbol{\theta}} | \boldsymbol{\theta}) \Big|_{\tilde{\boldsymbol{\theta}}=M(\boldsymbol{\theta})} \right\}^{-1} \left\{ \nabla_{\tilde{\boldsymbol{\theta}}} Q_m(\tilde{\boldsymbol{\theta}} | \boldsymbol{\theta}) \Big|_{\tilde{\boldsymbol{\theta}}=M(\boldsymbol{\theta})} - \boldsymbol{\xi}(\boldsymbol{\theta}) \right\}. \quad (\text{S11})$$

To derive the asymptotic properties of the innovations defined in (S11), we first derive expressions for the asymptotic expectation and asymptotic variance of  $\boldsymbol{\xi}(\boldsymbol{\theta})$ , defined in (S9). To proceed, we consider a second expansion of the gradient of (S5), this time around  $M_m(\boldsymbol{\theta})$ . Neglecting higher-order terms,

$$\begin{aligned} \nabla_{\boldsymbol{\theta}'} Q_m(\boldsymbol{\theta}' | \boldsymbol{\theta}) &\approx \nabla_{\tilde{\boldsymbol{\theta}}} Q_m(\tilde{\boldsymbol{\theta}} | \boldsymbol{\theta}) \Big|_{\tilde{\boldsymbol{\theta}}=M_m(\boldsymbol{\theta})} + \nabla_{\tilde{\boldsymbol{\theta}}}^2 Q_m(\tilde{\boldsymbol{\theta}} | \boldsymbol{\theta}) \Big|_{\tilde{\boldsymbol{\theta}}=M_m(\boldsymbol{\theta})} \{ \boldsymbol{\theta}' - M_m(\boldsymbol{\theta}) \} \\ &= \nabla_{\tilde{\boldsymbol{\theta}}}^2 Q_m(\tilde{\boldsymbol{\theta}} | \boldsymbol{\theta}) \Big|_{\tilde{\boldsymbol{\theta}}=M_m(\boldsymbol{\theta})} \{ \boldsymbol{\theta}' - M_m(\boldsymbol{\theta}) \}, \end{aligned} \quad (\text{S12})$$

since  $\nabla_{\tilde{\boldsymbol{\theta}}} Q_m(\tilde{\boldsymbol{\theta}} | \boldsymbol{\theta}) \Big|_{\tilde{\boldsymbol{\theta}}=M_m(\boldsymbol{\theta})} = \mathbf{0}$  by definition. Evaluating (S12) at  $\boldsymbol{\theta}' = \tilde{M}_m(\boldsymbol{\theta})$  and substituting the resulting expression into (S9), we have

$$\begin{aligned} \boldsymbol{\xi}(\boldsymbol{\theta}) &\approx \nabla_{\tilde{\boldsymbol{\theta}}}^2 Q_m(\tilde{\boldsymbol{\theta}} | \boldsymbol{\theta}) \Big|_{\tilde{\boldsymbol{\theta}}=M_m(\boldsymbol{\theta})} \left\{ \tilde{M}_m(\boldsymbol{\theta}) - M_m(\boldsymbol{\theta}) \right\} \\ &= \nabla_{\tilde{\boldsymbol{\theta}}}^2 Q_m(\tilde{\boldsymbol{\theta}} | \boldsymbol{\theta}) \Big|_{\tilde{\boldsymbol{\theta}}=M_m(\boldsymbol{\theta})} \boldsymbol{\delta}_m(\boldsymbol{\theta}), \end{aligned}$$

where  $\boldsymbol{\delta}_m(\boldsymbol{\theta}) \equiv \tilde{M}_m(\boldsymbol{\theta}) - M_m(\boldsymbol{\theta})$  is the approximation error that appears in (S6). Now, as  $m \rightarrow \infty$ , assuming the law of large numbers holds, and suitable regularity conditions on  $\log p(\boldsymbol{\theta} | \mathbf{Z}_1, \mathbf{Z}_2)$ , we have that  $M_m(\boldsymbol{\theta}) \rightarrow M(\boldsymbol{\theta})$ , and

$$-\nabla_{\tilde{\boldsymbol{\theta}}}^2 Q_m(\tilde{\boldsymbol{\theta}} | \boldsymbol{\theta}) \Big|_{\tilde{\boldsymbol{\theta}}=M_m(\boldsymbol{\theta})} \longrightarrow -\mathbb{E}_{\mathbf{Z}_2 | \mathbf{Z}_1, \boldsymbol{\theta}} \left[ \nabla_{\tilde{\boldsymbol{\theta}}}^2 \log p(\tilde{\boldsymbol{\theta}} | \mathbf{Z}_1, \mathbf{Z}_2) \Big|_{\tilde{\boldsymbol{\theta}}=M(\boldsymbol{\theta})} \right] \equiv \mathbf{V}(\boldsymbol{\theta}). \quad (\text{S13})$$

Therefore, for large  $m$ , we have

$$\mathbb{E}\{\boldsymbol{\xi}(\boldsymbol{\theta})\} \approx \mathbb{E}\{\mathbf{V}(\boldsymbol{\theta})\boldsymbol{\delta}_m(\boldsymbol{\theta})\} \approx -\mathbf{V}(\boldsymbol{\theta})\boldsymbol{\mu}(\boldsymbol{\theta}), \quad (\text{S14})$$

$$\mathbb{V}\{\boldsymbol{\xi}(\boldsymbol{\theta})\} \approx \mathbb{V}\{\mathbf{V}(\boldsymbol{\theta})\boldsymbol{\delta}_m(\boldsymbol{\theta})\} \approx \mathbf{V}(\boldsymbol{\theta})\boldsymbol{\Sigma}(\boldsymbol{\theta})\mathbf{V}(\boldsymbol{\theta}). \quad (\text{S15})$$

We now derive the asymptotic expectation and asymptotic variance of the innovations  $\boldsymbol{\epsilon}_m(\boldsymbol{\theta})$  defined in (S11). Suppose it holds that

$$\mathbb{E}_{\{\mathbf{Z}_2^{(j)} | \mathbf{Z}_1, \boldsymbol{\theta}\}_{j=1}^m} \left[ \nabla_{\tilde{\boldsymbol{\theta}}} Q_m(\tilde{\boldsymbol{\theta}} | \boldsymbol{\theta}) \Big|_{\tilde{\boldsymbol{\theta}}=M(\boldsymbol{\theta})} \right] = \nabla_{\tilde{\boldsymbol{\theta}}} \mathbb{E}_{\{\mathbf{Z}_2^{(j)} | \mathbf{Z}_1, \boldsymbol{\theta}\}_{j=1}^m} \left[ Q_m(\tilde{\boldsymbol{\theta}} | \boldsymbol{\theta}) \Big|_{\tilde{\boldsymbol{\theta}}=M(\boldsymbol{\theta})} \right].$$

Then,

$$\mathbb{E}_{\{\mathbf{Z}_2^{(j)} | \mathbf{Z}_1, \boldsymbol{\theta}\}_{j=1}^m} \left[ \nabla_{\tilde{\boldsymbol{\theta}}} Q_m(\tilde{\boldsymbol{\theta}} | \boldsymbol{\theta}) \Big|_{\tilde{\boldsymbol{\theta}}=M(\boldsymbol{\theta})} \right] = \nabla_{\tilde{\boldsymbol{\theta}}} Q(\tilde{\boldsymbol{\theta}} | \boldsymbol{\theta}) \Big|_{\tilde{\boldsymbol{\theta}}=M(\boldsymbol{\theta})} = \mathbf{0}, \quad (\text{S16})$$

since the gradient at the true maximizer is zero by definition. Therefore, for large  $m$ ,  $\boldsymbol{\epsilon}_m(\boldsymbol{\theta}) \approx -\mathbf{V}^{-1}(\boldsymbol{\theta})\boldsymbol{\xi}(\boldsymbol{\theta})$ , so that from (S14) we have  $\mathbb{E}\{\boldsymbol{\epsilon}_m(\boldsymbol{\theta})\} \approx \boldsymbol{\mu}(\boldsymbol{\theta})$ . Further, for an

independent Monte Carlo sample, which we assume throughout, we have that

$$\begin{aligned} \mathbb{V}_{\{\mathbf{Z}_2^{(j)} | \mathbf{Z}_1, \boldsymbol{\theta}\}_{j=1}^m} \left[ \nabla_{\tilde{\boldsymbol{\theta}}} Q_m(\tilde{\boldsymbol{\theta}} | \boldsymbol{\theta}) \Big|_{\tilde{\boldsymbol{\theta}}=M(\boldsymbol{\theta})} \right] &= \mathbb{V}_{\{\mathbf{Z}_2^{(j)} | \mathbf{Z}_1, \boldsymbol{\theta}\}_{j=1}^m} \left[ \frac{1}{m} \sum_{j=1}^m \nabla_{\tilde{\boldsymbol{\theta}}} \log p(\tilde{\boldsymbol{\theta}} | \mathbf{Z}_1, \mathbf{Z}_2^{(j)}) \Big|_{\tilde{\boldsymbol{\theta}}=M(\boldsymbol{\theta})} \right] \\ &= \frac{1}{m} \boldsymbol{\Gamma}(\boldsymbol{\theta}), \end{aligned}$$

where

$$\boldsymbol{\Gamma}(\boldsymbol{\theta}) \equiv \frac{1}{m} \sum_{j=1}^m \mathbb{V}_{\{\mathbf{Z}_2^{(j)} | \mathbf{Z}_1, \boldsymbol{\theta}\}_{j=1}^m} \left[ \nabla_{\tilde{\boldsymbol{\theta}}} \log p(\tilde{\boldsymbol{\theta}} | \mathbf{Z}_1, \mathbf{Z}_2^{(j)}) \Big|_{\tilde{\boldsymbol{\theta}}=M(\boldsymbol{\theta})} \right].$$

Now, as  $m \rightarrow \infty$ ,  $\boldsymbol{\Gamma}(\boldsymbol{\theta}) \rightarrow \mathbf{V}(\boldsymbol{\theta})$ , given by (S13). Then, using (S15), for large  $m$  we have:

$$\begin{aligned} \mathbb{V}\{\boldsymbol{\epsilon}_m(\boldsymbol{\theta})\} &\approx \mathbf{V}(\boldsymbol{\theta})^{-1} \mathbb{V}\{\boldsymbol{\xi}(\boldsymbol{\theta})\} \mathbf{V}(\boldsymbol{\theta})^{-1} + \frac{1}{m} \mathbf{V}(\boldsymbol{\theta})^{-1} \boldsymbol{\Gamma}(\boldsymbol{\theta}) \mathbf{V}(\boldsymbol{\theta})^{-1} \\ &\approx \boldsymbol{\Sigma}(\boldsymbol{\theta}) + \frac{1}{m} \mathbf{V}(\boldsymbol{\theta})^{-1}. \end{aligned}$$

Having obtained the first-order autoregressive formulation (S10) and a formal derivation of its asymptotic properties, we now consider the behavior near an isolated local maximizer  $\boldsymbol{\theta}^*$  of the incomplete-data posterior density  $p(\boldsymbol{\theta} | \mathbf{Z}_1)$ . Since  $\boldsymbol{\theta}^*$  is an isolated local maximizer of  $p(\boldsymbol{\theta} | \mathbf{Z}_1)$ , it is also an asymptotically stable fixed point of  $M(\cdot)$  (Chan and Ledolter, 1995, Lemma 1). In particular,  $M(\boldsymbol{\theta}^*) = \boldsymbol{\theta}^*$ , and hence a first-order Taylor expansion of  $M(\boldsymbol{\theta})$  around  $\boldsymbol{\theta}^*$  yields:

$$\begin{aligned} M(\boldsymbol{\theta}) &\approx M(\boldsymbol{\theta}^*) + \mathbf{A}(\boldsymbol{\theta}^*) (\boldsymbol{\theta} - \boldsymbol{\theta}^*) \\ &= \boldsymbol{\theta}^* + \mathbf{A}(\boldsymbol{\theta}^*) (\boldsymbol{\theta} - \boldsymbol{\theta}^*), \end{aligned} \tag{S17}$$

where  $\mathbf{A}(\boldsymbol{\theta}^*) \equiv \nabla_{\boldsymbol{\theta}} M(\boldsymbol{\theta}) \Big|_{\boldsymbol{\theta}=\boldsymbol{\theta}^*}$ . Substituting the approximation (S17) into (S10) yields

$$\tilde{\boldsymbol{\theta}}_m^{(l)} \approx \boldsymbol{\theta}^* + \mathbf{A}(\boldsymbol{\theta}^*) \left\{ \tilde{\boldsymbol{\theta}}_m^{(l-1)} - \boldsymbol{\theta}^* \right\} + \boldsymbol{\epsilon}_m(\tilde{\boldsymbol{\theta}}_m^{(l-1)}), \tag{S18}$$

and therefore  $\{\tilde{\boldsymbol{\theta}}_m^{(l)}\}$  is approximately an AR(1) process with autoregressive parameter  $\mathbf{A}(\boldsymbol{\theta}^*)$ . Further, substituting the approximation (S17) into (S4) yields the linearized system (i.e., linear approximation to (S4)),

$$\boldsymbol{\theta}^{(l)} \approx \boldsymbol{\theta}^* + \mathbf{A}(\boldsymbol{\theta}^*) \left\{ \boldsymbol{\theta}^{(l-1)} - \boldsymbol{\theta}^* \right\}. \tag{S19}$$

Under the assumption that the local maximizer  $\boldsymbol{\theta}^*$  is also an asymptotically stable fixed point of (S19), the spectral radius of  $\mathbf{A}(\boldsymbol{\theta}^*)$  is strictly less than one (Elaydi, 2005, Thm. 4.13). Therefore, the AR(1) process (S18) that approximates  $\{\tilde{\boldsymbol{\theta}}_m^{(l)}\}$  is stationary, and the innovations can be treated as independent and identically distributed with mean and variance

evaluated at  $\boldsymbol{\theta}^*$ . This gives the following stationary AR(1) representation:

$$\tilde{\boldsymbol{\theta}}_m^{(l)} \approx \boldsymbol{\theta}^* + \mathbf{A}(\boldsymbol{\theta}^*) \left\{ \tilde{\boldsymbol{\theta}}_m^{(l-1)} - \boldsymbol{\theta}^* \right\} + \boldsymbol{\epsilon}_m(\boldsymbol{\theta}^*), \quad (\text{S20})$$

where  $\mathbb{E}\{\boldsymbol{\epsilon}_m(\boldsymbol{\theta}^*)\} \approx \boldsymbol{\mu}(\boldsymbol{\theta}^*)$  and  $\mathbb{V}\{\boldsymbol{\epsilon}_m(\boldsymbol{\theta}^*)\} \approx \boldsymbol{\Sigma}(\boldsymbol{\theta}^*) + \frac{1}{m} \mathbf{V}(\boldsymbol{\theta}^*)^{-1}$ . The process (S20) has mean

$$\mathbb{E}\{\tilde{\boldsymbol{\theta}}_m^{(l)}\} \approx \boldsymbol{\theta}^* + \{\mathbf{I} - \mathbf{A}(\boldsymbol{\theta}^*)\}^{-1} \boldsymbol{\mu}(\boldsymbol{\theta}^*), \quad (\text{S21})$$

where  $\mathbf{I}$  denotes the identity matrix; and variance  $\mathbb{V}\{\tilde{\boldsymbol{\theta}}_m^{(l)}\} \approx \mathbf{C}(\boldsymbol{\theta}^*)$ , where  $\mathbf{C}(\boldsymbol{\theta}^*)$  is the solution to  $\mathbf{C}(\boldsymbol{\theta}^*) = \mathbf{A}(\boldsymbol{\theta}^*) \mathbf{C}(\boldsymbol{\theta}^*) \mathbf{A}(\boldsymbol{\theta}^*)^\top + \boldsymbol{\Sigma}(\boldsymbol{\theta}^*) + \frac{1}{m} \mathbf{V}(\boldsymbol{\theta}^*)^{-1}$ .

Importantly, in the ideal special case of mean-zero approximation error,  $\boldsymbol{\mu}(\boldsymbol{\theta}) = \mathbf{0}$ , and the mean (S21) reduces to  $\boldsymbol{\theta}^*$ , allowing one to recover  $\boldsymbol{\theta}^*$  through the averaging procedure described in Section 2.3.1 of the main text.

### S3 Continuous approximations of the 0–1 loss function

In Section 2.3.3 of the main text, we describe how an NBE can be constructed to approximate the MAP estimator. The approach hinges on the use of a continuous approximation of the 0–1 loss function. In this section, we consider several candidate loss functions.

In the main text, we adopt the loss function,

$$L_{\text{TANH}}(\boldsymbol{\theta}, \hat{\boldsymbol{\theta}}; \kappa) = \tanh(\|\hat{\boldsymbol{\theta}} - \boldsymbol{\theta}\|/\kappa), \quad \kappa > 0. \quad (\text{S22})$$

where  $\|\cdot\|$  denotes the Euclidean norm (although any norm in  $\mathbb{R}^d$  could be used) and  $d$  denotes the dimension of  $\boldsymbol{\theta}$ . For  $d = 1$ , Figure S1, panel A, shows (S22) and its gradient for  $\kappa \in \{1, 0.5, 0.1, 0.05\}$ . For fixed  $\kappa$ , the gradient of (S22) is bounded as  $\|\hat{\boldsymbol{\theta}} - \boldsymbol{\theta}\| \rightarrow 0$ , and it yields the 0–1 loss function in the limit as  $\kappa \rightarrow 0$ , which we now prove.

*Proof.* From the definition of the hyperbolic tangent function, it follows that

$$\begin{aligned} L_{\text{TANH}}(\boldsymbol{\theta}, \hat{\boldsymbol{\theta}}; \kappa) &= \tanh(\|\hat{\boldsymbol{\theta}} - \boldsymbol{\theta}\|/\kappa) \\ &= \frac{\exp(\|\hat{\boldsymbol{\theta}} - \boldsymbol{\theta}\|/\kappa) - \exp(-\|\hat{\boldsymbol{\theta}} - \boldsymbol{\theta}\|/\kappa)}{\exp(\|\hat{\boldsymbol{\theta}} - \boldsymbol{\theta}\|/\kappa) + \exp(-\|\hat{\boldsymbol{\theta}} - \boldsymbol{\theta}\|/\kappa)}, \\ &= \frac{1 - \exp(-2\|\hat{\boldsymbol{\theta}} - \boldsymbol{\theta}\|/\kappa)}{1 + \exp(-2\|\hat{\boldsymbol{\theta}} - \boldsymbol{\theta}\|/\kappa)}. \end{aligned}$$

First, suppose that  $\hat{\boldsymbol{\theta}} = \boldsymbol{\theta}$ , so that  $\|\hat{\boldsymbol{\theta}} - \boldsymbol{\theta}\| = 0$ . In this case, we have that

$$L_{\text{TANH}}(\boldsymbol{\theta}, \hat{\boldsymbol{\theta}}; \kappa)|_{\hat{\boldsymbol{\theta}}=\boldsymbol{\theta}} = \frac{1 - \exp(0)}{1 + \exp(0)} = 0.$$

Second, suppose that  $\hat{\boldsymbol{\theta}} \neq \boldsymbol{\theta}$ , so that  $\|\hat{\boldsymbol{\theta}} - \boldsymbol{\theta}\| > 0$ . In this case, we have that

$$\lim_{\kappa \rightarrow 0} L_{\text{TANH}}(\boldsymbol{\theta}, \hat{\boldsymbol{\theta}}; \kappa) = \lim_{\kappa \rightarrow 0} \frac{1 - \exp(-2\|\hat{\boldsymbol{\theta}} - \boldsymbol{\theta}\|/\kappa)}{1 + \exp(-2\|\hat{\boldsymbol{\theta}} - \boldsymbol{\theta}\|/\kappa)} = 1,$$

since  $\lim_{x \rightarrow \infty} e^{-ax} = 0$  for all  $a > 0$ . Therefore, we obtain

$$\lim_{\kappa \rightarrow 0} L_{\text{TANH}}(\boldsymbol{\theta}, \hat{\boldsymbol{\theta}}; \kappa) = \begin{cases} 0 & \text{if } \hat{\boldsymbol{\theta}} = \boldsymbol{\theta}, \\ 1 & \text{otherwise,} \end{cases}$$

which is the 0–1 loss function. □

Other continuous approximations are available. For example, the loss function

$$L(\boldsymbol{\theta}, \hat{\boldsymbol{\theta}}; \beta) = (\|\hat{\boldsymbol{\theta}} - \boldsymbol{\theta}\|)^\beta, \quad \beta > 0, \tag{S23}$$

generalizes the loss function given in [Cressie \(2022, Eqn. 6\)](#) to the multiparameter setting, and it also yields the 0–1 loss in the limit as  $\beta \rightarrow 0$ . A possible surrogate for the 0–1 loss function is therefore given by (S23) with  $\beta$  close to zero. However, with  $\beta < 1$ , the gradient of (S23) diverges as  $\|\hat{\boldsymbol{\theta}} - \boldsymbol{\theta}\| \rightarrow 0$ , which can cause numerical instability during training. There are several ways to alleviate this issue. For instance, one may add a small positive constant  $\delta$  to  $\|\hat{\boldsymbol{\theta}} - \boldsymbol{\theta}\|$  in (S23), yielding the loss function,

$$L_{\text{POW}}(\boldsymbol{\theta}, \hat{\boldsymbol{\theta}}; \beta, \delta) = (\|\hat{\boldsymbol{\theta}} - \boldsymbol{\theta}\| + \delta)^\beta - \delta^\beta, \quad \beta > 0, \delta > 0, \tag{S24}$$

Figure S1, panel B, shows (S24) and its gradient for  $\beta \in \{1, 0.5, 0.1, 0.05\}$  and  $\delta \in \{0, 0.1\}$ .

Another possible surrogate loss function is given by

$$L_{\text{CORR}}(\boldsymbol{\theta}, \hat{\boldsymbol{\theta}}; \rho, \alpha) = 1 - \{1 + (\|\hat{\boldsymbol{\theta}} - \boldsymbol{\theta}\|/\rho)^\alpha\}^{-1}, \quad \rho > 0, \alpha \geq 1, \tag{S25}$$

which yields the 0–1 loss in the limit as  $\rho \rightarrow 0$ , where the right-hand side of (S25) is a variogram constructed from the Cauchy correlation function ([Gneiting and Schlather, 2004](#)). Similar to (S24) and (S22), the gradient of (S25) is bounded. In general, similarly constructed variogram models provide a broad family of functions that may serve as continuous approximations of the 0–1 loss function, with various degrees of differentiability at the origin that may be controlled by the practitioner. These classes are mentioned here for completeness; in this paper we use the loss function (S22), which we find to work well in practice.

Finally, we make practical remarks relating to the training of NBEs under continuous approximations of the 0–1 loss function. First, for most conventional norms,  $\|\hat{\boldsymbol{\theta}} - \boldsymbol{\theta}\|$  tends to increase as the dimension  $d$  of  $\boldsymbol{\theta}$  increases. This represents a potential pitfall since, for most approximations of the 0–1 loss function, like (S22), the gradient vanishes as  $\|\hat{\boldsymbol{\theta}} - \boldsymbol{\theta}\|$  becomes large. A simple remedy for this is to replace the Euclidean norm with a scaled norm, for instance,  $\|\cdot\|_p/d^{1/p}$ , where  $\|\cdot\|_p$  denotes the  $L_p$  norm, to reduce the growth of distances with increasing dimension. Second, to prevent the NBE from becoming “stuck” in regions of the parameter space where gradients are extremely small at the start of training, it can be beneficial to pretrain the network using conventional, well behaved loss functions,

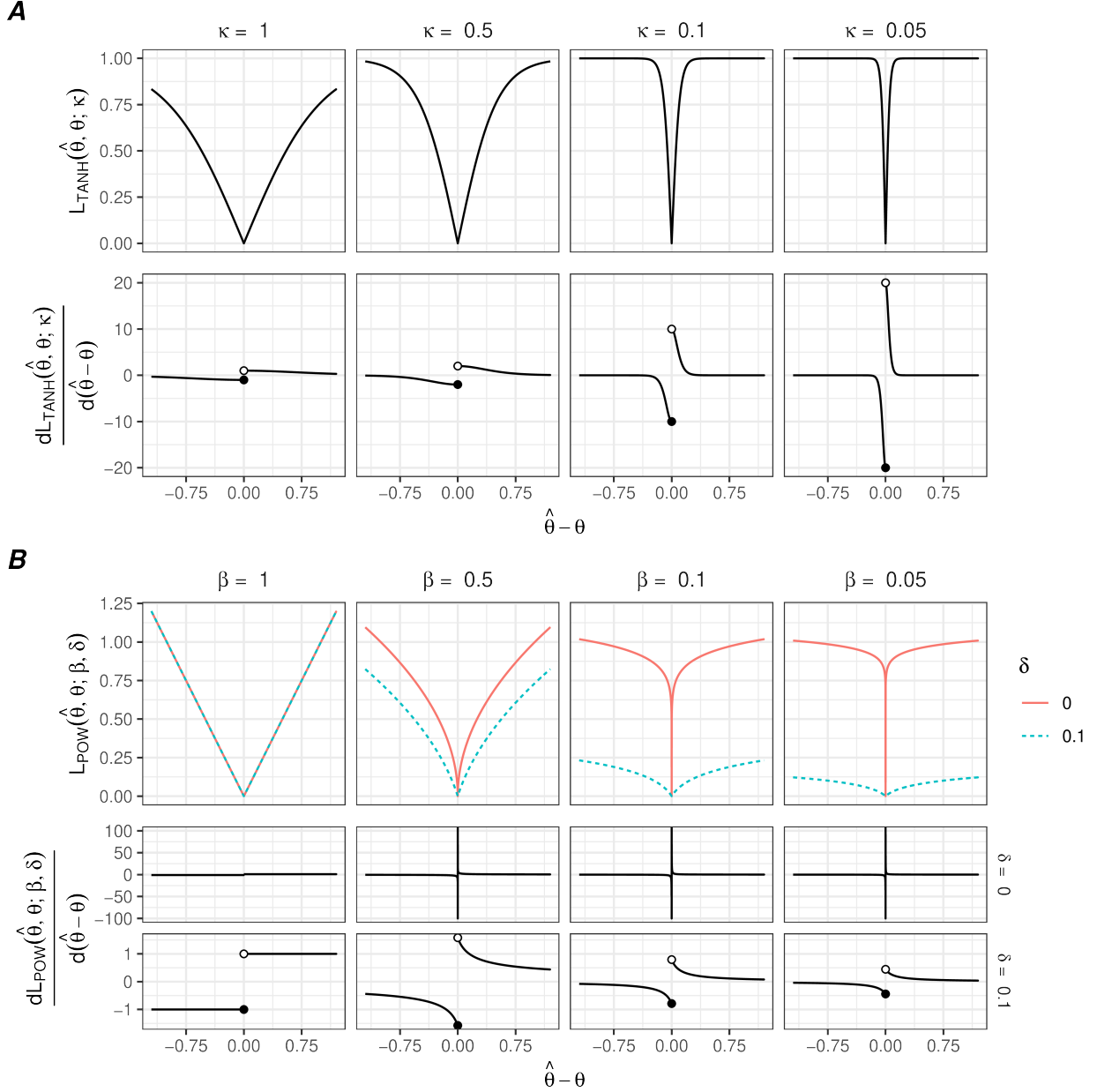


Figure S1: (A) The loss function (S22) and its gradient for  $\kappa \in \{1, 0.5, 0.1, 0.05\}$ . (B) The loss function (S24) and its gradient for  $\beta \in \{1, 0.5, 0.1, 0.05\}$  and  $\delta \in \{0, 0.1\}$ . For  $\delta = 0$  and  $\beta < 1$ , the gradient diverges at the origin; for  $\delta = 0.1$ , the gradient at the origin is finite and decreases as  $\beta$  decreases.

such as the mean-absolute-error or the mean-squared-error loss functions. Importantly, once the NBE has been pretrained, it can be trained under an approximation of the 0–1 loss function at almost no additional computational cost. This is achieved by fixing the initial portion of the network (often referred to as the “summary network”, when the architecture is viewed in a modular fashion), which typically contains relatively expensive operations, such as convolution. Then updating occurs only in the latter portion of the network (often

referred to as the “inference network”), which typically consists of a simple, fast-to-evaluate multilayer perceptron. In our experiments, the pretraining stage using the mean-absolute-error loss function, ranges from several minutes to a few hours, whereas training under the approximate 0–1 loss function requires only a matter of seconds.

## S4 Additional simulation study

In Section 3 of the main text, we conducted simulation studies involving spatial versions of the Gaussian process model and the hidden Potts model. Here, we conduct an additional simulation experiment, using a spatial version of a popular normal mean-variance mixture known as the generalized hyperbolic (GH) distribution. The likelihood is available for this case, permitting comparison with a gold-standard likelihood-based estimator, namely the MAP estimator obtained by directly maximizing the posterior density. Here, we also consider a conventional simulation-based approach, approximate Bayesian computation (ABC; Tavaré et al., 1997; Pritchard et al., 1999; Lintusaari et al., 2017; Sisson et al., 2018). Before proceeding with the analysis, we first review the GH distribution, including its density function and the formulas required for conditional simulation.

The  $n$ -dimensional random vector  $\mathbf{Z}$  is called a NMVM if it can be represented as,

$$\mathbf{Z} = \boldsymbol{\mu} + M\boldsymbol{\alpha} + \sqrt{M}\mathbf{V}, \quad (\text{S26})$$

where  $\boldsymbol{\mu} \in \mathbb{R}^n$ ,  $\boldsymbol{\alpha} \in \mathbb{R}^n$ ,  $M$  is a positive latent random variable that is independent of the small-scale variation  $\mathbf{V} \sim \text{Gau}(\mathbf{0}, \boldsymbol{\Sigma})$ , and where  $\boldsymbol{\Sigma}$  is a covariance matrix. This family of distributions is closed under conditioning: for any partitioning of  $\mathbf{Z}$  into components  $\mathbf{Z}_1$  and  $\mathbf{Z}_2$ , and with  $\boldsymbol{\mu}$ ,  $\boldsymbol{\alpha}$ , and  $\boldsymbol{\Sigma}$  partitioned accordingly,  $\mathbf{Z}_2 \mid \mathbf{Z}_1$  is also a NMVM, with parameters

$$\begin{aligned} \boldsymbol{\mu}_{2|1} &= \boldsymbol{\mu}_2 + \boldsymbol{\Sigma}_{21}\boldsymbol{\Sigma}_{11}^{-1}(\mathbf{Z}_1 - \boldsymbol{\mu}_1), \\ \boldsymbol{\alpha}_{2|1} &= \boldsymbol{\alpha}_2 - \boldsymbol{\Sigma}_{21}\boldsymbol{\Sigma}_{11}^{-1}\boldsymbol{\alpha}_1, \\ \boldsymbol{\Sigma}_{22|1} &= \boldsymbol{\Sigma}_{22} - \boldsymbol{\Sigma}_{21}\boldsymbol{\Sigma}_{11}^{-1}\boldsymbol{\Sigma}_{12}, \end{aligned}$$

and with latent variable  $M_{2|1}$  that is distributed according to  $M \mid \mathbf{Z}_1$  (Jamalizadeh and Balakrishnan, 2019, Theorem 1).

The generalized hyperbolic (GH) distribution is obtained when  $M$  in (S26) follows a generalized inverse Gaussian (GIG) distribution. The GH distribution is prominent in financial modeling due to its flexible marginal distributions and infinite divisibility (Barndorff-Nielsen, 1997; Prause, 1999). We consider the parameterization of the GIG density employed by Browne and McNicholas (2015),

$$f_{\text{GIG}}(m; \omega, \phi, \lambda) = \frac{(m/\phi)^{\lambda-1}}{2\phi K_\lambda(\omega)} \exp \left\{ -\frac{\omega}{2} \left( \frac{\phi}{m} + \frac{m}{\phi} \right) \right\}, \quad m > 0, \quad (\text{S27})$$

with concentration parameter  $\omega > 0$ , shape parameter  $\lambda \in \mathbb{R}$ , scale parameter  $\phi > 0$ , and where  $K_\lambda(\cdot)$  denotes the modified Bessel function of the second kind of order  $\lambda$ . Then,  $M_{2|1}$

also follows a GIG distribution with parameters

$$\begin{aligned}\omega_{2|1} &= \sqrt{\{\omega\phi + (\mathbf{Z}_1 - \boldsymbol{\mu}_1)' \boldsymbol{\Sigma}_{11}^{-1} (\mathbf{Z}_1 - \boldsymbol{\mu}_1)\} \{\omega\phi^{-1} + \boldsymbol{\alpha}'_1 \boldsymbol{\Sigma}_{11}^{-1} \boldsymbol{\alpha}_1\}}, \\ \phi_{2|1} &= \sqrt{\{\omega\phi + (\mathbf{Z}_1 - \boldsymbol{\mu}_1)' \boldsymbol{\Sigma}_{11}^{-1} (\mathbf{Z}_1 - \boldsymbol{\mu}_1)\} / \{\omega\phi^{-1} + \boldsymbol{\alpha}'_1 \boldsymbol{\Sigma}_{11}^{-1} \boldsymbol{\alpha}_1\}}, \\ \lambda_{2|1} &= \lambda - n_1/2,\end{aligned}$$

where  $n_1$  is the dimension of  $\mathbf{Z}_1$  (Jamalizadeh and Balakrishnan, 2019, Cor. 2). Throughout, we fix  $\phi = 1$  for identifiability reasons. We then write  $\mathbf{Z} \sim \text{GH}(\boldsymbol{\mu}, \boldsymbol{\alpha}, \boldsymbol{\Sigma}, \omega, \phi, \lambda)$ , which has density function,

$$f_{\text{GH}}(\mathbf{z}; \boldsymbol{\mu}, \boldsymbol{\alpha}, \boldsymbol{\Sigma}, \omega, \phi, \lambda) \propto \frac{K_{\lambda-d/2} \left( \sqrt{\{\omega\eta + (\mathbf{z} - \boldsymbol{\mu})' \boldsymbol{\Sigma}^{-1} (\mathbf{z} - \boldsymbol{\mu})\} (\omega/\eta + \boldsymbol{\gamma}' \boldsymbol{\Sigma}^{-1} \boldsymbol{\gamma})} \right) e^{(\mathbf{z} - \boldsymbol{\mu})' \boldsymbol{\Sigma}^{-1} \boldsymbol{\alpha}}}{\left[ \sqrt{\{\omega\eta + (\mathbf{z} - \boldsymbol{\mu})' \boldsymbol{\Sigma}^{-1} (\mathbf{z} - \boldsymbol{\mu})\} (\omega/\eta + \boldsymbol{\gamma}' \boldsymbol{\Sigma}^{-1} \boldsymbol{\gamma})} \right]^{n/2-\lambda}},$$

with normalizing constant,  $(\omega\phi^{-1} + \boldsymbol{\alpha}' \boldsymbol{\Sigma}^{-1} \boldsymbol{\alpha})^{n/2-\lambda} (2\pi)^{-n/2} |\boldsymbol{\Sigma}|^{-1/2} \phi^{-\lambda} / K_{\lambda}(\omega)$  (McNeil et al., 2015, Eqn. 6.29; Zhang et al., 2022). In addition to being closed under conditioning, the GH family of distributions is also closed under marginalization (Wei et al., 2019, Prop. 2). That is, if  $\mathbf{Z} \equiv (\mathbf{Z}'_1, \mathbf{Z}'_2)' \sim \text{GH}(\boldsymbol{\mu}, \boldsymbol{\alpha}, \boldsymbol{\Sigma}, \omega, \phi, \lambda)$ , then  $\mathbf{Z}_1 \sim \text{GH}(\boldsymbol{\mu}_1, \boldsymbol{\alpha}_1, \boldsymbol{\Sigma}_{11}, \omega, \phi, \lambda)$ . However, although the likelihood function is available, likelihood-based estimators for the GH distribution require repeated evaluation of the Bessel function, which can be computationally burdensome. Likelihood-free methods may therefore still be useful for improving computational efficiency.

Following Zhang et al. (2022), we consider a spatial version of the GH distribution. In this example, we take the spatial domain to be  $\mathcal{D} \equiv [0, 1] \times [0, 1]$ , we simulate complete data on a regular square grid of size  $n = 16^2 = 256$ , and we consider inference from 150 incompletely observed spatial fields. In (S26), we set  $\boldsymbol{\alpha} = \alpha \mathbf{1}$  for  $\alpha \in \mathbb{R}$ ; we take  $\boldsymbol{\Sigma}$  to be a correlation matrix determined by Equation (19) of the main text with range parameter  $\rho > 0$ , shape parameter  $\nu > 0$ , and  $\tau = 0$ ; and we assume that the mean is modeled separately so that  $\boldsymbol{\mu}$  can be set to zero. The parameters to be estimated are thus  $\boldsymbol{\theta} \equiv (\alpha, \omega, \lambda, \rho, \nu)^\top$ . We assume that the parameters are independent *a priori* with marginal priors  $\alpha \sim \text{Unif}(-0.3, 0.3)$ ,  $\omega \sim \text{Unif}(0.1, 1)$ ,  $\lambda \sim \text{Unif}(-1, 1)$ ,  $\rho \sim \text{Unif}(0.05, 0.35)$ , and  $\nu \sim \text{Unif}(0.5, 2)$ .

We consider inference using NBEs based on either the masking approach (Algorithm 1 of the main text) or the EM approach (Algorithm 2 of the main text) for handling missing data, under the same general settings given in Section 3.1 of the main text. We compare the competing NBEs to the MAP estimator that numerically maximizes the posterior density, and a MAP estimator based on ABC.

To facilitate a comparison with the NBEs, for ABC inference we use the same 25000 simulated parameter–data pairs that were used to train the NBEs (Mestdagh et al., 2019). As the initial set of user-defined summary statistics, we use the empirical variogram, madogram, and rodogram (corresponding to the variogram of order 2, 1, and 0.5, respectively; Matheron, 1987), obtained by binning pairwise distances into 10 intervals with centers equally spaced between 0.05 and 0.5. We also include two measures of extremal dependence, the pairwise tail correlation coefficient (Joe, 1997) and the residual-tail-dependence coefficient (Ledford

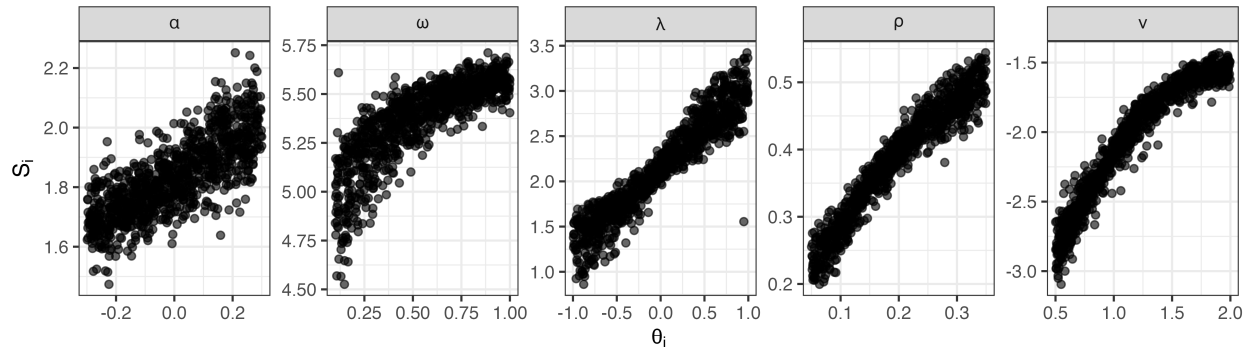


Figure S2: Empirical plot of the semi-automatic summary statistics,  $S_i$ ,  $i = 1, \dots, 5$ , obtained by the method of Fearnhead and Prangle (2012) against the corresponding true parameter values  $\theta_i$ ,  $i = 1, \dots, 5$ , shown separately for each of the five components of  $\boldsymbol{\theta} \equiv (\alpha, \omega, \lambda, \rho, \nu)'$  in the GH distribution (Section S4). Headings above each panel give the model parameter.

and Tawn, 1996), both computed for all site pairs, evaluated at the high-probability threshold  $u = 0.95$ , and averaged using the same distance bins as the variograms. Low-dimensional summary statistics offer numerous advantages for ABC (Blum et al., 2013). To reduce the dimensionality of our user-defined summary statistics, we employ the semi-automatic procedure of Fearnhead and Prangle (2012), implemented via the **abctools** package (Nunes and Prangle, 2016), which yields a  $d$ -dimensional vector of summary statistics, where recall that  $d$  denotes the dimension of  $\boldsymbol{\theta}$  (see Figure S2). ABC sampling is then performed by comparing the Euclidean distance between the summary statistics of the observed data and simulated data, using the package **abc** (Csillery et al., 2012). We retain only the parameter vectors whose corresponding simulated summary statistics fall within the smallest 1% of distances from the observed summary statistics, yielding  $25000 \times 0.01 = 250$  accepted parameter vectors. To refine the ABC posterior, we apply regression-adjustment methods (Blum, 2018) using the default neural-network regression model (Blum and François, 2010) employed by **abc**. We then define the “ABC MAP” by computing the mode of each parameter via kernel density estimation. Although the mode of the joint posterior generally does not coincide with the modes of the marginal posteriors, we adopt this approximation for simplicity of implementation.

We compare the estimators using the time taken for their “set-up” and for estimation for a single data set post set-up (computational efficiency); and the empirical root-mean-squared errors (RMSEs) based on simulated data using 1000 parameter vectors sampled from the prior (statistical efficiency). (Figure S5 of the Supplementary Material shows the value of the objective function in Equation (7) or (17) of the main text evaluated at the end of each epoch during training.) We test the estimators under two missingness mechanisms, MCAR and MICB, as defined in Section 3 of the main text, and we use  $\text{RMSE}_{\text{MCAR}}$  and  $\text{RMSE}_{\text{MICB}}$  to denote the RMSE of an estimator based on incomplete data simulated under the MCAR and MICB mechanisms, respectively. Table S1 summarizes the results, while Figure S3 shows simulated data and corresponding box plots of the empirical distributions of the estimates for one parameter setting.

These results corroborate the findings in the main text. First, NBE approaches can be

Table S1: The “set-up” time, estimation time for a single test data set, and empirical RMSE under two missingness models for four estimators of the parameters of the GH distribution (Section S4). “Set-up” time refers to the total time required to sample 25000 parameter vectors from the prior, simulate data from the model conditional on these parameters, and either train the neural networks (EM NBE and Masking NBE) or compute summary statistics (ABC MAP).

Estimator	Set-up time (hrs)	Estimation time (s)	RMSE <sub>MCAR</sub>	RMSE <sub>MICB</sub>
MAP	–	89.7	<b>0.062</b>	<b>0.064</b>
EM NBE	1.67	0.812	<b>0.062</b>	<b>0.064</b>
Masking NBE	2.01	<b>0.005</b>	0.067	0.191
ABC MAP	<b>1.07</b>	2.03	0.097	0.107

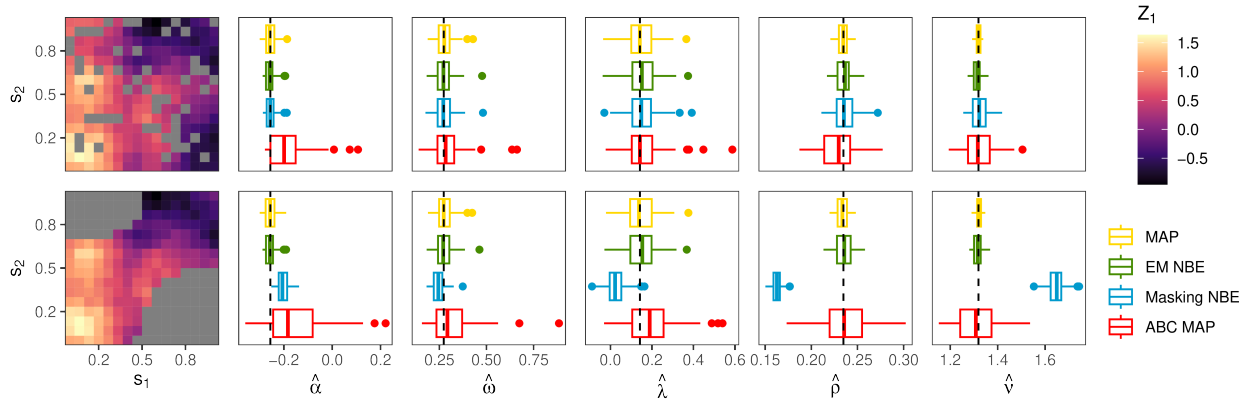


Figure S3: Spatial data (first column) where the missingness is of type MCAR (first row) or MICB (second row) with missingness shown in gray, and corresponding empirical distributions (second and third columns) for four estimators (MAP, EM NBE, Masking NBE, ABC MAP) of the parameters of the GH distribution (Section S4). True parameter values are shown as a dashed vertical line.

almost as statistically efficient as a gold-standard likelihood-based estimator, while being substantially more computationally efficient post-training. Second, the masking and EM approaches to neural Bayes estimation represent a trade-off between computational efficiency and robustness to the missingness mechanism. Third, the almost-as-good performance of the EM NBE relative to the MAP estimator indicates that Algorithm 2 in the Estimation stage converges to a suitable point estimate across most, if not all, data sets; convergence for a single data set is illustrated in Figure S8.

Finally, like the EM NBE, the ABC MAP is agnostic to the missingness pattern, but its reliance on user-defined summary statistics reduces statistical efficiency. This reflects a broader limitation of ABC which is addressed by NBEs: Neural inference methods generally are well suited to settings in which sufficient statistics are unavailable, which is the case for the majority of models used in practice, including the models considered in Sections 3 and 4 of the main text.

## S5 Ensemble of NBEs

An ensemble of neural networks (Hansen and Salamon, 1990; Breiman, 1996) consists of neural networks trained to solve the same task but with variations introduced during the training process. These variations could include different initial values for the neural-network parameters, different architectures, or different learning rates. The inference for an ensemble can be obtained by averaging the outputs of its individual networks, and it is often more accurate than that of any individual network.

In our case, we obtain an ensemble of  $J$  NBEs  $\{\hat{\theta}_{\gamma_j^*}(\cdot) : j = 1, \dots, J\}$  by using  $J$  different initial values for the neural-network parameters. We may posit the following working model to characterize the error of each NBE:

$$\hat{\theta}_{\gamma_j^*}(\mathbf{Z}) = \hat{\theta}_{\text{Bayes}}(\mathbf{Z}) + \epsilon_j(\mathbf{Z}), \quad \mathbf{Z} \in \mathcal{Z}, \quad j = 1, \dots, J, \quad (\text{S28})$$

where  $\hat{\theta}_{\text{Bayes}}(\mathbf{Z})$  is the Bayes estimate of  $\theta$  for the loss function being used, and  $\epsilon_j(\mathbf{Z})$  is a mean-zero error term with variance  $\sigma_\epsilon^2$ . Then, the ensemble estimate is obtained as:

$$\hat{\theta}_{\text{ensemble}}(\mathbf{Z}) \equiv \frac{1}{J} \sum_{j=1}^J \hat{\theta}_{\gamma_j^*}(\mathbf{Z}), \quad \mathbf{Z} \in \mathcal{Z}. \quad (\text{S29})$$

Under our working model, for fixed  $\mathbf{Z} \in \mathcal{Z}$ ,

$$\mathbb{E}\{\hat{\theta}_{\text{ensemble}}(\mathbf{Z})\} = \hat{\theta}_{\text{Bayes}}(\mathbf{Z}), \quad \text{var}\{\hat{\theta}_{\text{ensemble}}(\mathbf{Z})\} = \sigma_\epsilon^2/J,$$

where the expectation and variance are taken over the ensemble estimates for a fixed  $\mathbf{Z}$ . In practice, the errors may not have mean zero, nor be independent; however, provided that they are not perfectly correlated, the ensemble estimate (S29) will still have reduced variance compared with estimates from individual ensemble members.

To illustrate the efficacy of an ensemble of NBEs, we consider a classical spatial Gaussian process model, where  $\mathbf{Z} \equiv (Z_1, \dots, Z_n)'$  are data obtained at locations  $\{\mathbf{s}_1, \dots, \mathbf{s}_n\}$  in a spatial domain  $\mathcal{D}$ . Assume the data are Gaussian random variables with mean zero, variance one, and exponential spatial covariance function,

$$\text{cov}(Z_i, Z_j) = \exp(-\|\mathbf{s}_i - \mathbf{s}_j\|/\theta), \quad i, j = 1, \dots, n,$$

for unknown range parameter  $\theta > 0$ . Here, we take  $\mathcal{D}$  to be the unit square, we simulate data on a grid with  $n = 16^2 = 256$  observation locations, and we adopt the prior  $\theta \sim \text{Unif}(0, 0.5)$ . Note that the data are completely observed in this experiment, where our aim is to show the utility of an ensemble of NBEs.

Since our data are gridded and complete, we construct the NBEs using convolutional neural networks (CNNs; see, e.g., Dumoulin and Visin, 2016; Goodfellow et al., 2016, Ch. 9). To demonstrate that the ensemble approach improves estimation across different neural-network architectures, we consider three architectures, each with a different number of trainable parameters  $\gamma$ . The first architecture (Architecture 1) was used by Zammit-Mangion et al. (2025); it contains two convolutional layers and 150913 trainable parameters. The second

Table S2: Summary of the CNN architecture used in Sections 3 and 4 of the main text, and in Sections S4 and S5, with  $d$  the number of parameters in the given statistical model. The architecture can be used with grids of arbitrary size and shape; however, for simplicity, here we show the input and output dimensions of each layer given a square input grid of dimension  $64 \times 64$ . The table is divided into layers used for the summary network  $\psi(\cdot)$  and inference network  $\phi(\cdot)$  of the DeepSets representation given in Equation (16) of the main text. Each residual block consists of two sequential convolutional layers and batch normalization layers, along with a skip (shortcut) connection that directly connects the input of the block to its output (He et al., 2016). The batch normalization layers compute the mean and variance for each input slice, normalize the input accordingly, and then apply a learnable affine transformation (Ioffe and Szegedy, 2015). A padding of size 1 is used in each convolutional layer, and a stride of 2 is used in layers that reduce the input resolution (a stride of 1 is used otherwise) (Goodfellow et al., 2016, Ch. 9). For all but the final layer, we use rectified linear unit (ReLU) activation functions,  $\text{ReLU}(x) \equiv \max(0, x)$ , while the final layer employs a softplus activation function,  $\text{softplus}(x) \equiv \log(1 + e^x)$ , to ensure positive parameter estimates. When employing the masking approach of Wang et al. (2024), an extra input channel is needed to encode the missingness pattern, which doubles the number of parameters in the first layer.

Network	Layer type	Input dim.	Output dim.	Kernel size	Parameters
$\psi(\cdot)$	Convolutional	[64, 64, 1]	[64, 64, 16]	$3 \times 3$	144
$\psi(\cdot)$	Batch normalization	[64, 64, 16]	[64, 64, 16]	-	32
$\psi(\cdot)$	Residual block	[64, 64, 16]	[64, 64, 16]	$3 \times 3$	4672
$\psi(\cdot)$	Residual block	[64, 64, 16]	[32, 32, 32]	$3 \times 3$	14528
$\psi(\cdot)$	Residual block	[32, 32, 32]	[16, 16, 64]	$3 \times 3$	57728
$\psi(\cdot)$	Residual block	[16, 16, 64]	[8, 8, 128]	$3 \times 3$	230144
$\psi(\cdot)$	Global mean pooling	[8, 8, 128]	[1, 1, 128]	-	0
$\psi(\cdot)$	Flatten	[1, 1, 128]	[128]	-	0
$\phi(\cdot)$	Dense	[128]	[128]	-	16512
$\phi(\cdot)$	Dense	[128]	[512]	-	66048
$\phi(\cdot)$	Dense	[512]	[ $d$ ]	-	513 $d$
Total trainable parameters:					389808 + 513 $d$

architecture (Architecture 2) was proposed by Gerber and Nychka (2021) and subsequently used by Sainsbury-Dale et al. (2024) and Richards et al. (2024); it contains three convolutional layers and 638657 trainable parameters. The third architecture (Architecture 3), summarized in Table S2, is inspired by the well known ResNet architecture (He et al., 2016). It contains a total of nine convolutional layers couched within so-called residual blocks (He et al., 2016), and 390321 trainable parameters. The residual blocks mitigate the issue of vanishing gradients during training, thereby allowing for the construction of deeper networks that often outperform their shallower counterparts. We consider ensembles containing up to 10 NBEs of the range parameter  $\theta$ , where each NBE is initialised with different, randomly generated values for the neural-network parameters  $\gamma$ .

Figure S4 shows box plots of empirical RMSEs for 10 individual NBEs and the corresponding ensemble of  $J = 10$  NBEs, plotted for each architecture (left panel), and empirical RMSEs plotted as a function of the number of NBEs in the ensemble (right panel). The empirical RMSEs are based on a test set of 1000 parameter-data pairs sampled from the

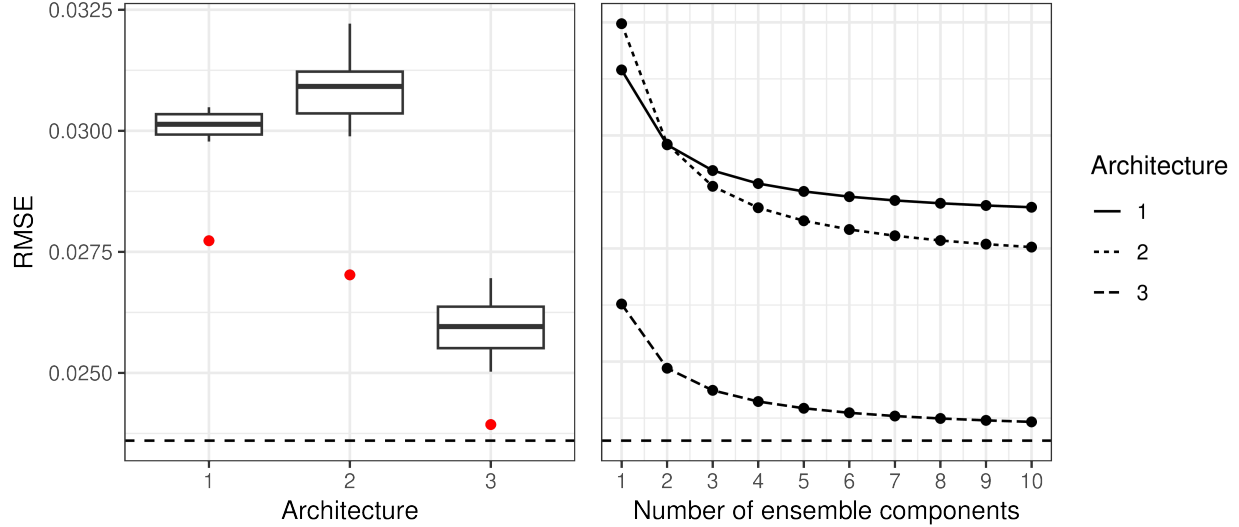


Figure S4: (Left panel) Empirical RMSEs for the three architectures detailed in Section S5, with box plots summarizing the RMSEs for 10 individual NBEs, and red points showing the RMSEs of the corresponding ensemble of  $J = 10$  NBEs. (Right panel) Empirical RMSEs as a function of the number of NBEs in the ensemble, for the three different architectures used in the experiment. For each ensemble size, RMSEs are averaged over all possible combinations of the NBEs, so that performance is not tied to a specific ordering of the components. In both panels, the horizontal dashed line corresponds to the RMSE of the MAP estimator that numerically maximizes the unnormalized analytic posterior density.

joint distribution of the parameters and the data, that is,

$$\text{RMSE}(\hat{\theta}(\cdot)) \equiv \sqrt{\frac{1}{1000} \sum_{k=1}^{1000} \{\hat{\theta}(\mathbf{Z}^{(k)}) - \theta^{(k)}\}^2}, \quad (\text{S30})$$

where  $\theta^{(k)} \sim \text{Unif}(0, 0.5)$ ,  $\mathbf{Z}^{(k)} \sim p(\mathbf{Z} | \theta^{(k)})$ , and the estimator  $\hat{\theta}(\cdot)$  corresponds either to a single NBE or an ensemble of NBEs as defined in (S29). From Figure S4, we see that the use of an ensemble of NBEs substantially reduces the RMSE when compared to a single NBE, irrespective of the architecture.

## S6 MCMC sampling in hidden Potts models

Here we describe two MCMC algorithms for sampling from the joint distribution of the hidden Potts model, which we consider in Sections 3.3 and 4 of the main text, and which consists of a latent Potts (1952) model and a data model. In Section S6.1, we describe a simple Gibbs sampler, while in Section S6.2 we describe a joint Metropolis–Hastings (MH) scheme that allows for point-mass distributions of the observations, given the hidden process, which we proposed for the analysis of the Arctic sea-ice data in Section 4 of the main text.

Throughout, we use the notation for the hidden Potts model introduced in the main text: Let  $\mathbf{Y} \equiv (Y_1, \dots, Y_n)^\top$  and  $\mathbf{Z} \equiv (Z_1, \dots, Z_n)^\top$  denote the hidden labels and observed data, respectively; let  $\mathbf{Y}_{\setminus i}$  and  $\mathbf{Z}_{\setminus i}$  denote all pixel labels and data, respectively, excluding the  $i$ th pixel; let  $\mathcal{N}_i$  denote the indices of the “neighbors” of pixel  $i$ ,  $\beta$  denote the Potts model’s parameter,  $\boldsymbol{\lambda}$  denote the parameters associated with the conditional distributions of the data, and  $\boldsymbol{\theta} \equiv (\beta, \boldsymbol{\lambda}^\top)^\top$ .

### S6.1 Simple Gibbs updates

In the standard Gibbs sampler, for each  $i = 1, \dots, n$ , we alternate between sampling from the following full conditionals:

$$p(Y_i \mid \mathbf{Y}_{\setminus i}, \mathbf{Z}, \boldsymbol{\theta}), \quad (\text{S31})$$

$$p(Z_i \mid \mathbf{Y}, \mathbf{Z}_{\setminus i}, \boldsymbol{\theta}). \quad (\text{S32})$$

By conditional independence, (S32) simplifies to

$$p(Z_i \mid \mathbf{Y}, \mathbf{Z}_{\setminus i}, \boldsymbol{\theta}) = p(Z_i \mid Y_i, \boldsymbol{\lambda}), \quad (\text{S33})$$

which is straightforward to sample from by construction. Next, since  $Y_i$  is discrete, we can sample (S31) by enumerating all possible labels  $y = 1, \dots, Q$  and normalizing their unnormalized probabilities. Specifically,

$$\begin{aligned} p(Y_i = y \mid \mathbf{Y}_{\setminus i}, \mathbf{Z}, \boldsymbol{\theta}) &\propto p(Y_i = y, \mathbf{Y}_{\setminus i}, \mathbf{Z} \mid \boldsymbol{\theta}) \\ &= p(\mathbf{Y} \mid \beta) \prod_{j=1}^n p(Z_j \mid Y_j, \boldsymbol{\lambda}) \Big|_{Y_i=y} \\ &\propto \exp\{\beta T(\mathbf{Y})\} p(Z_i \mid Y_i, \boldsymbol{\lambda}) \Big|_{Y_i=y} \\ &\propto \exp\{\beta S(y, i)\} p(Z_i \mid Y_i = y, \boldsymbol{\lambda}), \end{aligned}$$

where  $T(\mathbf{Y}) \equiv \sum_{\{i', j'\} \in \mathcal{E}} \mathbb{I}(Y_{j'} = Y_{i'})$  is the Potts model’s sufficient statistic,  $\mathcal{E}$  denotes the set of undirected edges between neighbors, and  $S(y, i) \equiv \sum_{j \in \mathcal{N}_i} \mathbb{I}(Y_j = y)$  is the number of

neighbors of site  $i$  with label  $y$ . Normalizing over all possible labels gives

$$p(Y_i = y \mid \mathbf{Y}_{\setminus i}, \mathbf{Z}, \boldsymbol{\theta}) = \frac{\exp\{\beta S(y, i)\} p(Z_i \mid Y_i = y, \boldsymbol{\lambda})}{\sum_{y'=1}^Q \exp\{\beta S(y', i)\} p(Z_i \mid Y_i = y', \boldsymbol{\lambda})}. \quad (\text{S34})$$

When the conditional distribution of the data,  $p(Z_i \mid Y_i = y, \boldsymbol{\lambda})$ , is a point mass for some label  $y$ , the corresponding pair  $\{Y_i, Z_i\}$  becomes an absorbing state in the Markov chain, violating irreducibility (i.e., the chain cannot move between all states with positive probability). Next, we discuss how this problem can be circumvented.

## S6.2 Joint MH updates

To avoid absorbing states when sampling from a hidden Potts model using MCMC, each pair  $\{Y_i, Z_i\}$ ,  $i = 1, \dots, n$ , is treated as a single unit and updated jointly via a MH update step, with carefully chosen proposals that ensure the acceptance probabilities do not depend on the conditional distributions of the data. Specifically, at each iteration and for each pair  $\{Y_i, Z_i\}$ , the target distribution is:

$$\begin{aligned} p(Y_i, Z_i \mid \mathbf{Y}_{\setminus i}, \mathbf{Z}_{\setminus i}, \boldsymbol{\theta}) &= p(Y_i \mid \mathbf{Y}_{\setminus i}, \mathbf{Z}_{\setminus i}, \boldsymbol{\theta}) p(Z_i \mid Y_i, \mathbf{Y}_{\setminus i}, \mathbf{Z}_{\setminus i}, \boldsymbol{\theta}) \\ &= p(Y_i \mid \mathbf{Y}_{\setminus i}, \beta) p(Z_i \mid Y_i, \boldsymbol{\lambda}) \\ &\propto \exp\{\beta S(Y_i, i)\} p(Z_i \mid Y_i, \boldsymbol{\lambda}). \end{aligned}$$

Given that the current value of the pair  $\{Y_i, Z_i\}$  is  $\{y, z\}$ , we propose a new value  $\{y', z'\}$  from a proposal distribution  $q(y', z' \mid y, z)$ , and we accept this proposal with probability

$$\begin{aligned} \alpha &\equiv \min \left\{ 1, \frac{p(Y_i = y', Z_i = z' \mid \mathbf{Y}_{\setminus i}, \mathbf{Z}_{\setminus i}, \boldsymbol{\theta})}{p(Y_i = y, Z_i = z \mid \mathbf{Y}_{\setminus i}, \mathbf{Z}_{\setminus i}, \boldsymbol{\theta})} \cdot \frac{q(y, z \mid y', z')}{q(y', z' \mid y, z)} \right\} \\ &= \min \left\{ 1, \frac{\exp\{\beta S(y', i)\} p(Z_i = z' \mid Y_i = y', \boldsymbol{\lambda})}{\exp\{\beta S(y, i)\} p(Z_i = z \mid Y_i = y, \boldsymbol{\lambda})} \cdot \frac{q(y, z \mid y', z')}{q(y', z' \mid y, z)} \right\}. \end{aligned}$$

Suppose that we take

$$q(y', z' \mid y, z) = g(y' \mid y) r(z' \mid y'),$$

where  $g(y' \mid y)$  is a proposal distribution for the new label given the current label, and  $r(z' \mid y')$  is a proposal distribution for the new observation given the proposed label. Then the MH acceptance probability becomes

$$\alpha = \min \left\{ 1, \frac{\exp\{\beta S(y', i)\} p(Z_i = z' \mid Y_i = y', \boldsymbol{\lambda})}{\exp\{\beta S(y, i)\} p(Z_i = z \mid Y_i = y, \boldsymbol{\lambda})} \cdot \frac{g(y \mid y') r(z \mid y)}{g(y' \mid y) r(z' \mid y')} \right\}.$$

If we choose  $r(z' \mid y') = p(Z_i = z' \mid Y_i = y', \boldsymbol{\lambda})$  (i.e., propose the new observation directly from its conditional distribution given the proposed label), the observation-distribution terms

cancel. If, in addition,  $g(y' | y)$  is symmetric, the label-proposal terms cancel as well, leaving

$$\alpha = \min \left\{ 1, \exp \left[ \beta \{ S(y', i) - S(y, i) \} \right] \right\}.$$

Thus, under these choices, the MH acceptance probability depends only on the parameter  $\beta$  and the difference between the local summary statistics of the proposed and current labels,  $S(y', i) - S(y, i)$ . In particular, it does not depend on the conditional distribution of the data and can therefore be used to sample from a hidden Potts model that has conditional point-mass distributions in the data model.

## S7 Additional figures

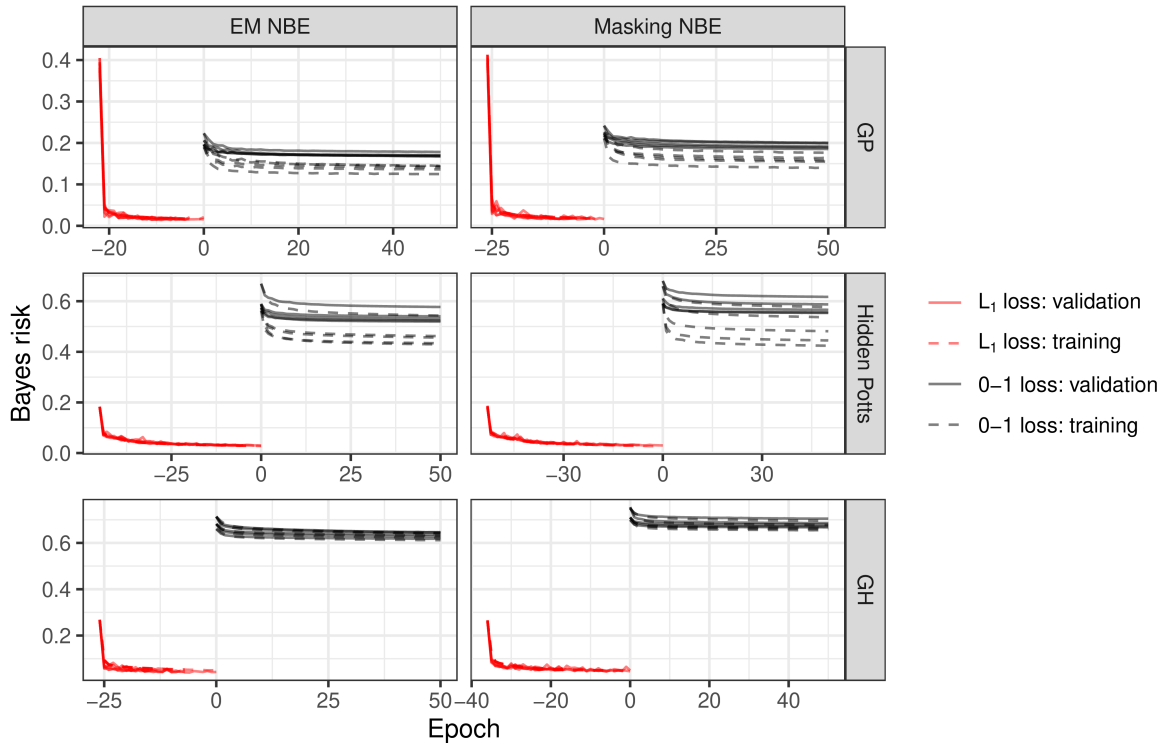


Figure S5: Empirical risk function (objective function in Equation (7) or (17) of the main text) evaluated on the training data (dashed lines) and withheld validation data (solid lines) versus epoch, for an ensemble of five NBEs trained for the EM (first column) and masking (second column) approaches, across all models considered in our simulation experiments: the Gaussian process model (Section 3.2 of the main text), the hidden Potts model (Section 3.3 of the main text), and the spatial GH distribution (Section S4). Red lines correspond to the Bayes risk under the  $L_1$  (mean-absolute-error) loss function, used to pretrain the networks, while gray lines correspond to the Bayes risk under the continuous approximation of the 0–1 loss function in Equation (15) of the main text, with tuning parameter  $\kappa = 0.1$ . Negative epoch values denote the pretraining stage, with epoch 0 corresponding to the transition to the training stage under the continuous approximation of the 0–1 loss function.

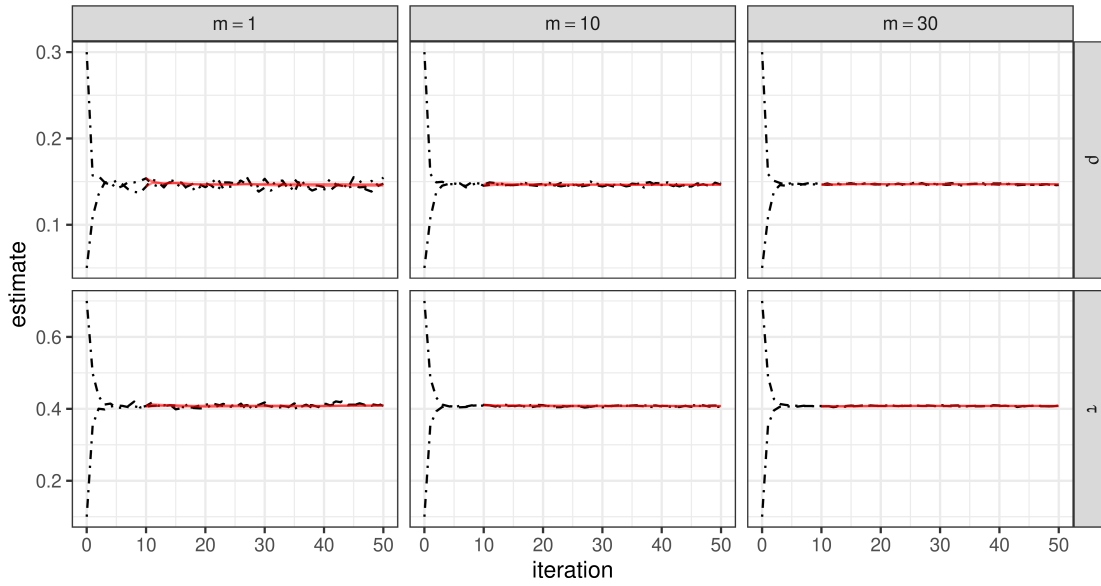


Figure S6: EM NBE sequences (black dot-dash lines) and post-burn-in averaged sequences (red solid lines) for different initial values and different Monte Carlo sample sizes  $m$ , for the Gaussian process model (Section 3.2 of the main text). The data are MCAR with 20% missingness. The true parameter values are  $\rho = 0.15$  and  $\tau = 0.4$ .

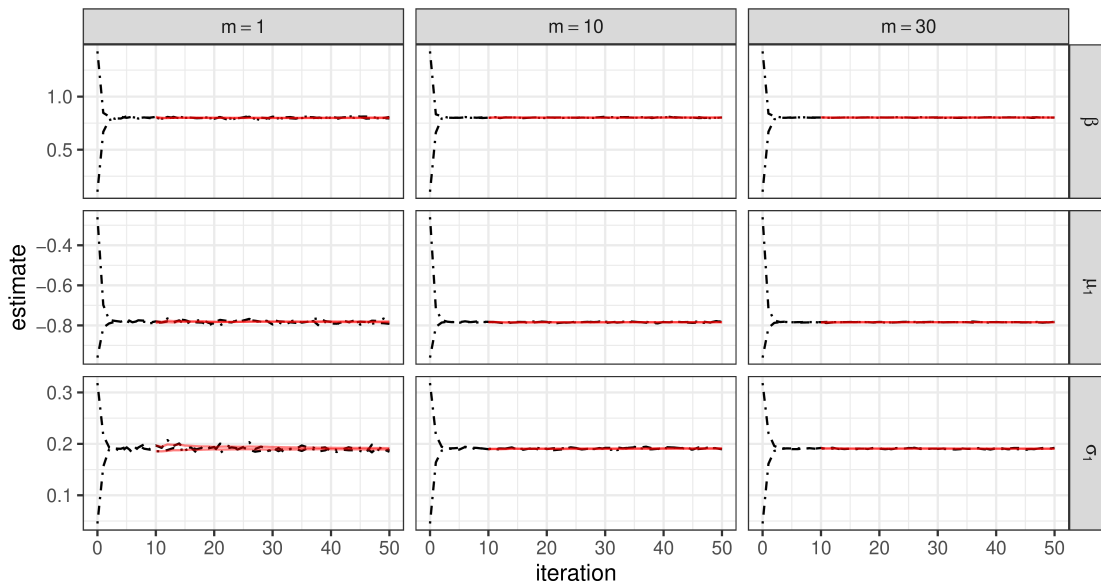


Figure S7: EM NBE sequences (black dot-dash lines) and post-burn-in averaged sequences (red solid lines) for different initial values and different Monte Carlo sample sizes  $m$ , for the hidden Potts model (Section 3.3 of the main text). For simplicity, just three of the seven parameters are shown, where the true parameter values are  $\beta = 0.79$ ,  $\mu_1 = -0.79$ , and  $\sigma_1 = 0.19$ .

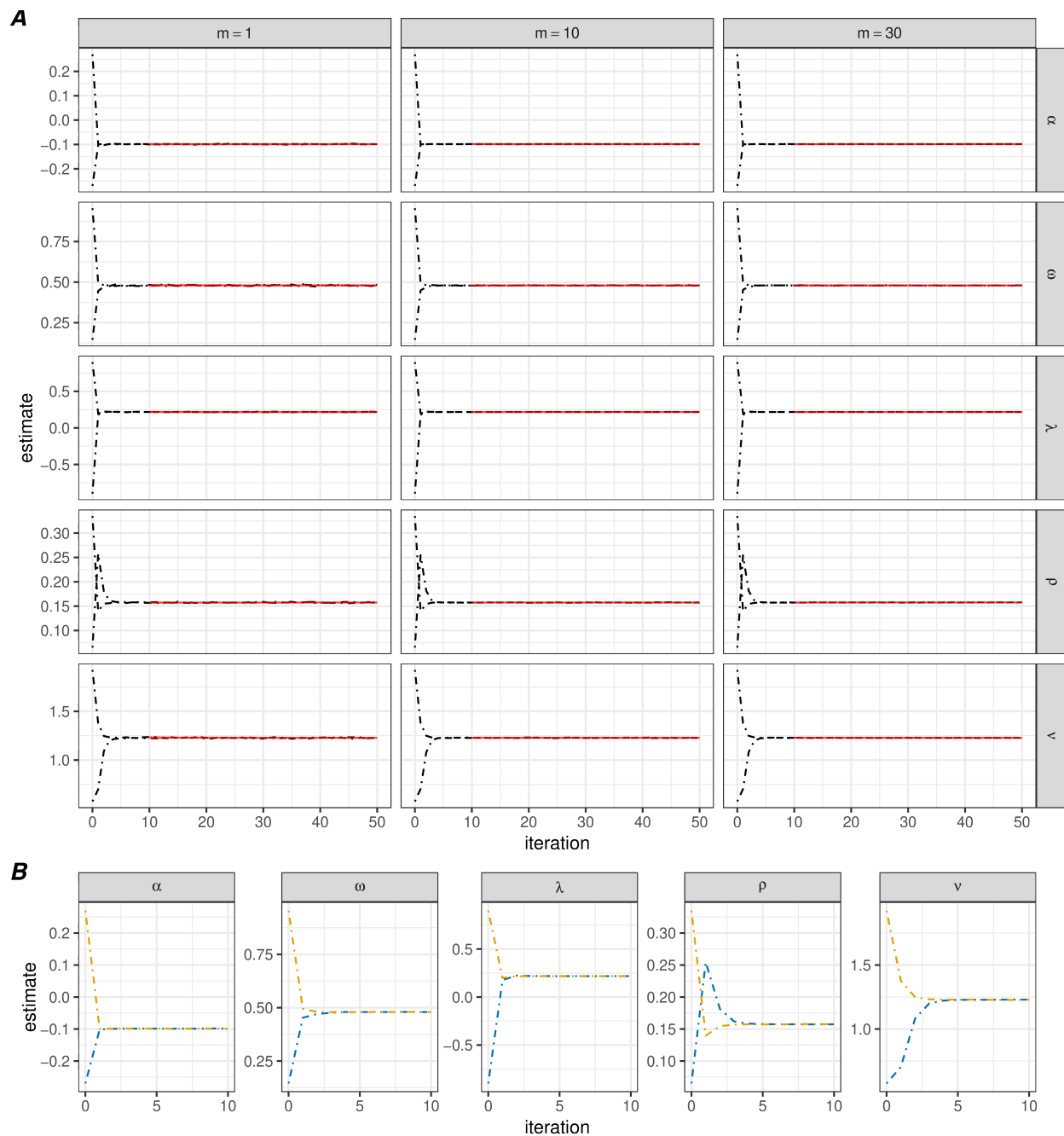


Figure S8: (A) EM NBE sequences (black dot-dash lines) and post-burn-in averaged sequences (red solid lines) for different initial values and different Monte Carlo sample sizes  $m$ , for the GH distribution (Section S4). The data are MCAR with 20% missingness. (B) EM NBE sequences computed with  $m = 30$  and colored by their initial parameter values. The true parameter values are  $\alpha = -0.122$ ,  $\omega = 0.373$ ,  $\lambda = 0.195$ ,  $\rho = 0.160$ , and  $\nu = 1.24$ .

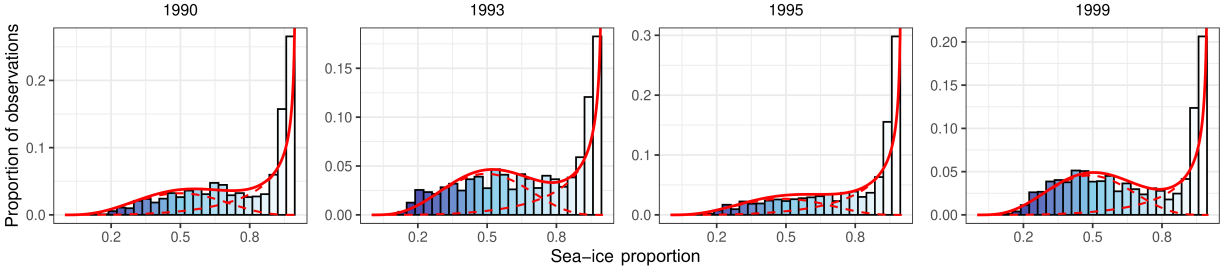


Figure S9: Histograms of observed Arctic sea-ice proportions, restricted to the open interval  $(0, 1)$ , together with fitted marginal Beta mixture densities for selected years. Red solid lines show the fitted marginal mixture densities, and red dashed lines show the individual Beta components.

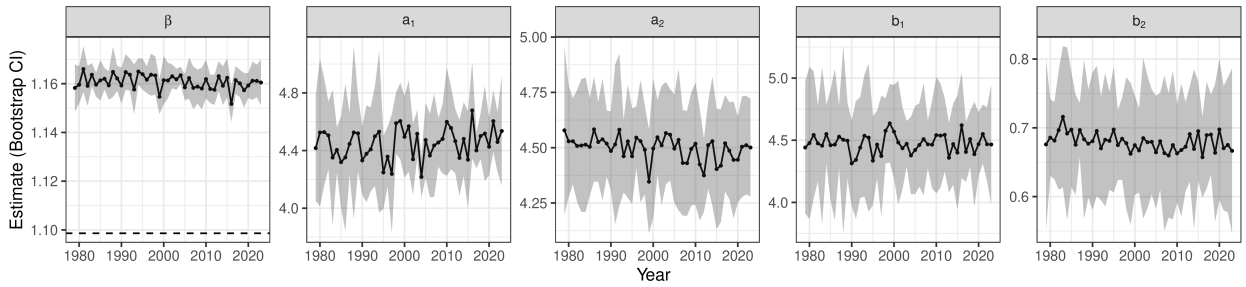


Figure S10: Estimated parameters of the hidden Potts model (described in Section 4 of the main text) for Arctic sea-ice proportion over time. Lines show point estimates with shaded regions indicating bootstrap confidence intervals. Headings above each panel give the model parameter. The dashed horizontal line in the first panel marks the critical value of the spatial-dependence parameter  $\beta$ , separating disordered and ordered spatial regimes.

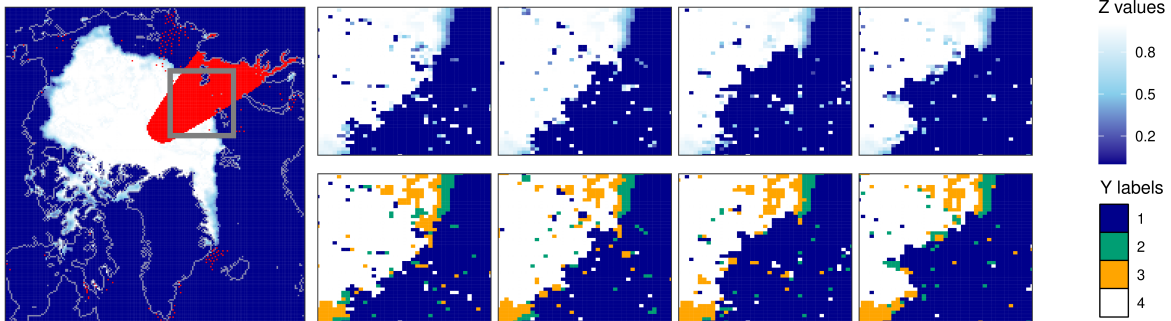


Figure S11: (Left) Arctic sea-ice data from September 1, 1995, with missing pixels colored red and faint gray lines denoting coastlines, with Greenland appearing at the bottom. (Remaining panels) conditional simulations for all grid cells within the gray box of the left panel. The conditional simulations are obtained from the fitted hidden Potts model described in Section 4 of the main text, where the hidden Potts model has  $Q = 4$  labels. Conditional on the label  $Y_i$  (bottom four panels of conditional simulations), the observation  $Z_i$  (top four panels of conditional simulations) follows one of two Beta distributions for proportions in the open interval  $(0, 1)$  ( $Y_i = 2, 3$ ), or a point mass at 0 or 1 corresponding to no sea ice ( $Y_i = 1$ ) and full sea ice ( $Y_i = 4$ ), respectively.

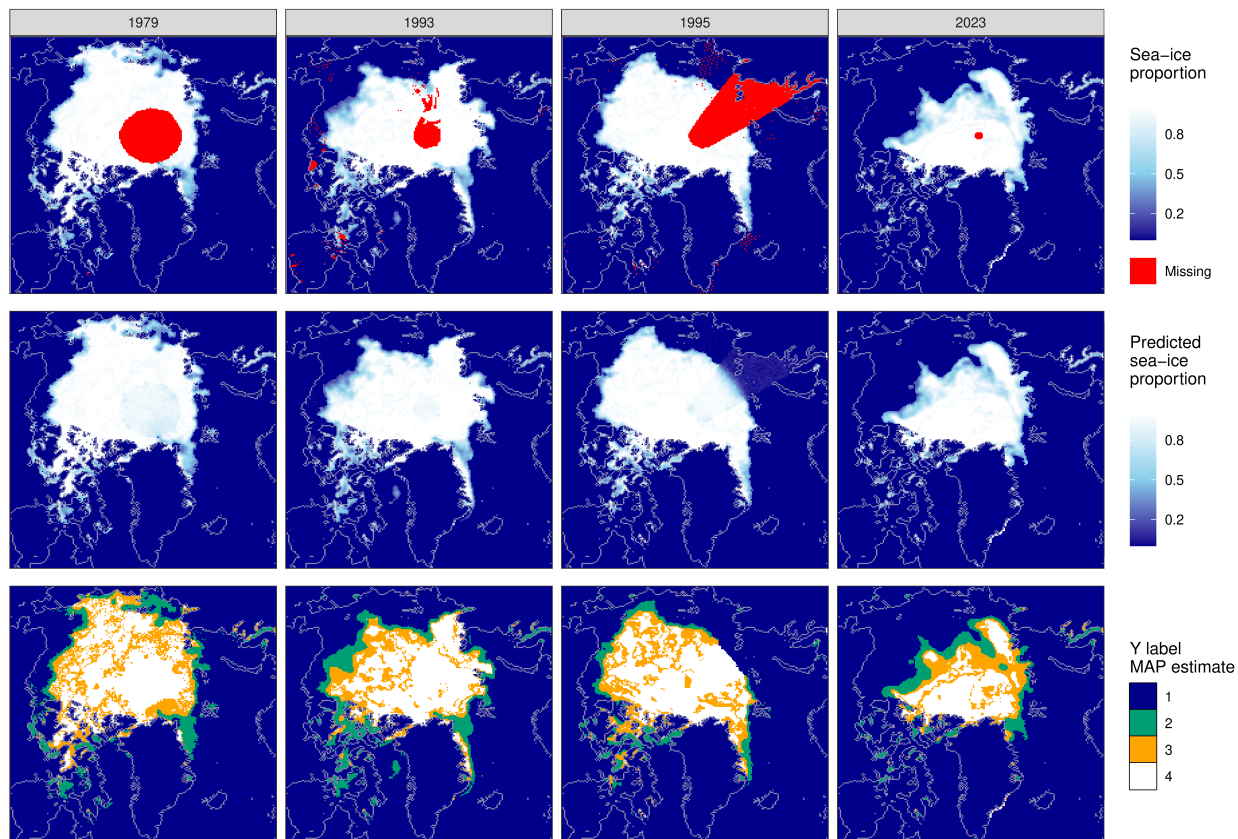
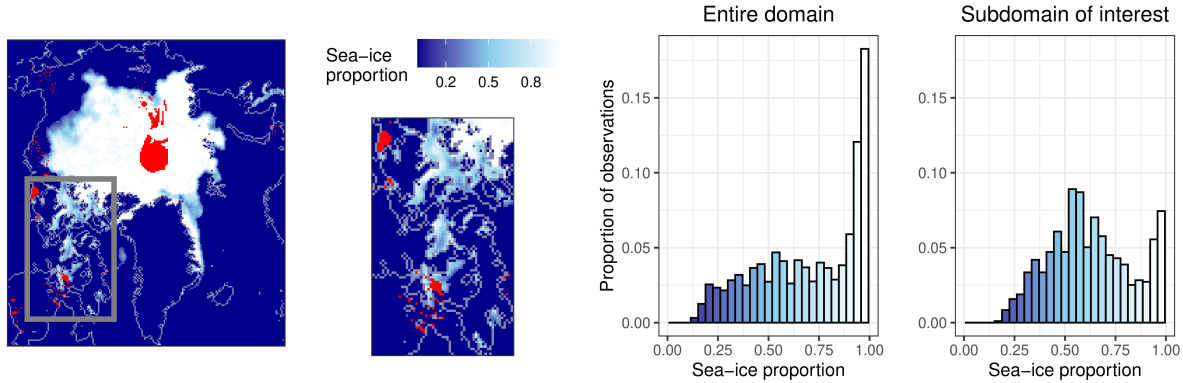
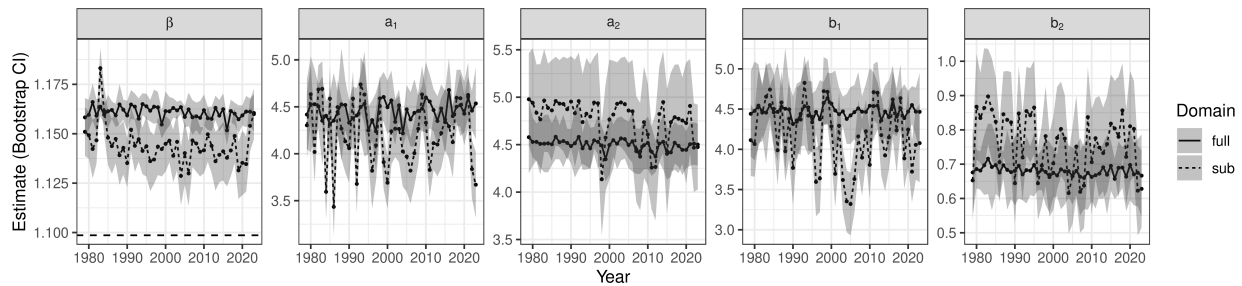


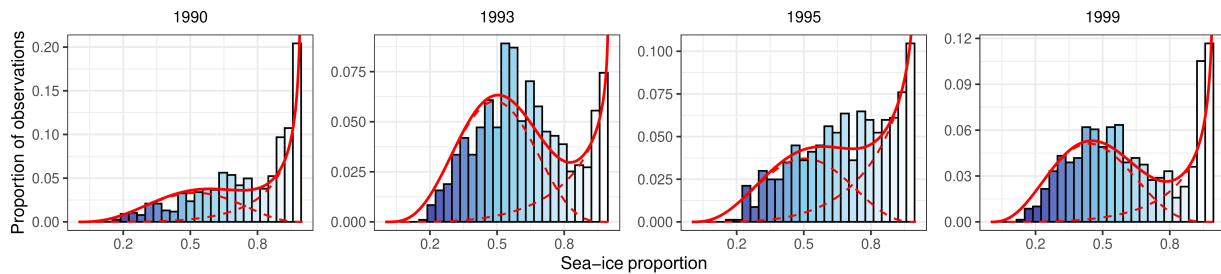
Figure S12: Arctic sea-ice data (first row) from September 1 for the years 1979, 1993, 1995, and 2023, together with corresponding predictions of sea-ice proportion and hidden states (second and third rows) from the fitted hidden Potts model described in Section 4 of the main text. Faint gray lines denote coastlines, with Greenland appearing at the bottom.



(a) Arctic sea-ice proportions from September 1, 1993. The left panel shows the full Arctic domain, with the gray box indicating the subdomain of interest shown in the middle panel, corresponding to the Canadian Arctic Archipelago west of Greenland. Faint gray lines denote coastlines, with Greenland appearing at the bottom. The right panels display histograms of sea-ice proportions restricted to the open interval  $(0, 1)$ , computed over the entire domain and over the subdomain of interest, respectively.



(b) Estimated parameters of the hidden Potts model for Arctic sea-ice proportion over time, and over both the full domain (solid lines) and the subdomain of interest (dashed lines). Headings above each panel give the model parameter.



(c) Histograms of observed Arctic sea-ice proportions in the subdomain of interest, restricted to the open interval  $(0, 1)$ , together with fitted Beta mixture densities for selected years (see Figure S9 for the corresponding plots over the entire domain). Red solid lines show the overall fitted mixture densities, and red dashed lines show the individual Beta components.

Figure S13: Evidence of spatial nonstationarity in the Arctic sea-ice proportions analyzed in Section 4 of the main text.

## References

- Barndorff-Nielsen, O. (1997). Normal inverse Gaussian distributions and stochastic volatility modelling. *Scandinavian Journal of Statistics*, 24:1–13.
- Blum, M. G. B. (2018). Regression approaches for ABC. In Sisson, S. A., Fan, Y., and Beaumont, M., editors, *Handbook of Approximate Bayesian Computation*, pages 71–85. Chapman & Hall/CRC Press, Boca Raton, FL.
- Blum, M. G. B. and François, O. (2010). Non-linear regression models for approximate Bayesian computation. *Statistics and Computing*, 20:63–73.
- Blum, M. G. B., Nunes, M. A., Prangle, D., and Sisson, S. A. (2013). A comparative review of dimension reduction methods in approximate Bayesian computation. *Statistical Science*, 28:189–208.
- Breiman, L. (1996). Bagging predictors. *Machine Learning*, 24:123–140.
- Brown, L. D. and Purves, R. (1973). Measurable selections of extrema. *The Annals of Statistics*, 1:902–912.
- Browne, R. P. and McNicholas, P. D. (2015). A mixture of generalized hyperbolic distributions. *The Canadian Journal of Statistics*, 43:176–198.
- Casella, G. and Berger, R. (2001). *Statistical Inference*, 2nd edition. Duxbury, Belmont, CA.
- Chan, K.-S. and Ledolter, J. (1995). Monte Carlo EM estimation for time series models involving counts. *Journal of the American Statistical Association*, 90:242–252.
- Cressie, N. (2022). Decisions, decisions, decisions in an uncertain environment. *Environmetrics*, 34:e2767.
- Csillery, K., François, O., and Blum, M. G. B. (2012). abc: an R package for approximate Bayesian computation (ABC). *Methods in Ecology and Evolution*.
- Dempster, A. P., Laird, N. M., and Rubin, D. B. (1977). Maximum likelihood from incomplete data via the EM algorithm. *Journal of the Royal Statistical Society B*, 39:1–38.
- Dumoulin, V. and Visin, F. (2016). A guide to convolution arithmetic for deep learning. <https://doi.org/10.48550/arXiv.1603.07285>.
- Elaydi, S. (2005). *An Introduction to Difference Equations*. Springer, New York, NY, 3rd edition.
- Fearnhead, P. and Prangle, D. (2012). Constructing summary statistics for approximate Bayesian computation: Semi-automatic approximate Bayesian computation. *Journal of the Royal Statistical Society B*, 74:419–474.
- Gerber, F. and Nychka, D. W. (2021). Fast covariance parameter estimation of spatial Gaussian process models using neural networks. *Stat*, 10:e382.
- Gneiting, T. and Schlather, M. (2004). Stochastic models that separate fractal dimension and the Hurst effect. *SIAM Review*, 46:269–282.
- Goodfellow, I., Bengio, Y., and Courville, A. (2016). *Deep Learning*. MIT Press, Cambridge, MA. <http://www.deeplearningbook.org>.
- Hansen, L. K. and Salamon, P. (1990). Neural network ensembles. *IEEE Transactions on Pattern Analysis and Machine Intelligence*, 12:993–1001.
- He, K., Zhang, X., Ren, S., and Sun, J. (2016). Deep residual learning for image recognition. In *Proceedings of the IEEE Conference on Computer Vision and Pattern Recognition (CVPR)*, pages 770–778.
- Ioffe, S. and Szegedy, C. (2015). Batch normalization: Accelerating deep network training by reducing internal covariate shift. In Bach, F. and Blei, D., editors, *Proceedings of the 32nd International Conference on Machine Learning*, volume 37 of *Proceedings of Machine Learning Research*, pages 448–456.

- Jamalizadeh, A. and Balakrishnan, N. (2019). Conditional distributions of multivariate normal mean-variance mixtures. *Statistics and Probability Letters*, 145:312–316.
- Joe, H. (1997). *Multivariate Models and Multivariate Dependence Concepts*. Chapman and Hall/CRC, New York, 1st edition.
- Ledford, A. and Tawn, J. (1996). Statistics for near independence in multivariate extreme values. *Biometrika*, 83:169–187.
- Lintusaari, J., Gutmann, M., Dutta, R., Kaski, S., and Corander, J. (2017). Fundamentals and recent developments in approximate Bayesian computation. *Systematic Biology*, 66:66–82.
- Matheron, G. (1987). Suffit-il, pour une covariance, d’être de type positif. *Sciences de la Terre, Série Informatique Géologique*, 26:51–66.
- McLachlan, G. J. and Krishnan, T. (2008). *The EM Algorithm and Extensions*, 2nd edition. Wiley, Hoboken, NJ.
- McNeil, A. J., Frey, R., and Embrechts, P. (2015). *Quantitative Risk Management*, revised edition. Princeton University Press, Princeton, NJ.
- Mestdagh, M., Verdonck, S., Meers, K., Loossens, T., and Tuerlinckx, F. (2019). Prepaid parameter estimation without likelihoods. *PLoS Computational Biology*, 15:e1007181.
- Nunes, M. A. and Prangle, D. (2016). abctools: An R package for tuning approximate Bayesian computation analyses. *The R Journal*, 7:189–205.
- Potts, R. B. (1952). Some generalized order-disorder transformations. *Mathematical Proceedings of the Cambridge Philosophical Society*, 48:106–109.
- Prause, K. (1999). *The Generalized Hyperbolic Model: Estimation, Financial Derivatives, and Risk Measures*. PhD thesis, Albert-Ludwigs-Universität Freiburg, Germany.
- Pritchard, J. K., Seielstad, M. T., Perez-Lezaun, A., and Feldman, M. W. (1999). Population growth of human Y chromosomes: a study of Y chromosome microsatellites. *Molecular Biology and Evolution*, 16:1791–1798.
- Richards, J., Sainsbury-Dale, M., Huser, R., and Zammit-Mangion, A. (2024). Neural Bayes estimators for censored inference with peaks-over-threshold models. *Journal of Machine Learning Research*, 25(390):1–49.
- Sainsbury-Dale, M., Zammit-Mangion, A., and Huser, R. (2024). Likelihood-free parameter estimation with neural Bayes estimators. *The American Statistician*, 78:1–14.
- Sainsbury-Dale, M., Zammit-Mangion, A., Richards, J., and Huser, R. (2025). Neural Bayes estimators for irregular spatial data using graph neural networks. *Journal of Computational and Graphical Statistics*, 34:1153–1168.
- Sisson, S. A., Fan, Y., and Beaumont, M. (2018). *Handbook of Approximate Bayesian Computation*. Chapman & Hall/CRC Press, Boca Raton, FL.
- Tavaré, S., Balding, D. J., Griffiths, R. C., and Donnelly, P. (1997). Inferring coalescence times from DNA sequence data. *Genetics*, 145:505–518.
- Wang, Z., Hasenauer, J., and Schälte, Y. (2024). Missing data in amortized simulation-based neural posterior estimation. *PLOS Computational Biology*, 20:e1012184.
- Wei, G. C. G. and Tanner, M. A. (1990). A Monte Carlo implementation of the EM algorithm and the poor man’s data augmentation algorithms. *Journal of the American Statistical Association*, 85:699–704.
- Wei, Y., Tang, Y., and McNicholas, P. D. (2019). Mixtures of generalized hyperbolic distributions and mixtures of skew-t distributions for model-based clustering with incomplete data. *Computational Statistics & Data Analysis*, 130:18–41.
- Wu, C. F. J. (1983). On the convergence properties of the EM algorithm. *The Annals of Statistics*, 11:95–103.

- Zammit-Mangion, A., Sainsbury-Dale, M., and Huser, R. (2025). Neural methods for amortized inference. *Annual Review of Statistics and Its Application*, 12:311–335.
- Zhang, Z., Huser, R., Opitz, T., and Wadsworth, J. (2022). Modeling spatial extremes using normal mean-variance mixtures. *Extremes*, 25:175–197.